2.5.2 Vibratory Ground Motion

NAPS COL 2.0-27-A
NAPS ESP VAR 2.0-4

The information needed to address DCD COL Item 2.0-27-A is included in SSAR Section 2.5.2, which is reproduced with the following variance and supplements.

This section provides a detailed description of vibratory ground motion assessments that were carried out for the Unit 3 site. The purpose of Section 2.5.2 is to determine the site-specific GMRS and eventually the Safe Shutdown Earthquake (SSE) at the site, as well as to provide structure Foundation Input Response Spectra (FIRS) from possible earthquakes that might occur in the site region and beyond. The GMRS is defined as the free-field horizontal and vertical ground motion response spectra at the site and must satisfy the requirements of 10 CFR 100.23. The SSE represents the design earthquake ground motion at the site and is the vibratory ground motion for which certain SSCs are designed to remain functional. Guidance on the development of these spectra is provided in NUREG-0800, SRP Sections 2.5.2 and 3.7.1, as well as the appropriate sections of Regulatory Guides (RG) referenced within these SRP sections.

Development of the ground motions begins with implementation of the provisions of RG 1.208. This guidance describes the acceptable methods to conduct geological, seismological, and geophysical investigations of the Unit 3 site and region around the site, identify and characterize seismic sources, perform a PSHA, perform site response analysis, and determine the GMRS and FIRS using the performance-based approach. Significant to the investigations and seismic hazard analyses presented in Section 2.5.2 is the publication of the CEUS SSC report by EPRI et al. (2012) (Reference 2.5-223). The CEUS SSC report includes several geological, seismological, and geophysical databases, including a catalog of CEUS earthquakes through 2008 and a fully detailed seismic source model for use in a CEUS PSHA.

Section 2.5.2.1 describes the seismicity of the site by providing detailed information on the CEUS SSC earthquake catalog, an update of this catalog through mid-December 2011, and historical significant site earthquakes, including the August 23, 2011 **M** 5.8 Mineral, Virginia earthquake. Section 2.5.2.2 describes the CEUS SSC report's seismic source characterization model for the central and eastern United States and the sources within the model that are used in the PSHA for Unit 3.

Section 2.5.2.3 presents the discussion of correlation of seismicity with seismic sources contributing to the seismic hazard of the site. Section 2.5.2.4 details the PSHA for Unit 3, resulting in hard rock ground motion hazard curves, the relative contribution by the various seismic sources, and UHRS. Section 2.5.2.5 describes the development of the site amplification factors that result from the transmission of the seismic waves through the site-specific geologic columns above hard rock and summarizes basic information about the seismic wave transmission characteristics of the Unit 3 site with reference to more detailed information in Section 2.5.4. Section 2.5.2.6 describes the development of the horizontal and vertical GMRS and FIRS for the Unit 3 site and structures. The derivation of the OBE is described in Section 3.7.1.

2.5.2.1 Seismicity

In the mid- to late-1980s the Electric Power Research Institute – Seismic Owners Group (EPRI-SOG) sponsored a detailed study of the geological, seismological, and geophysical information pertaining to the central and eastern United States (CEUS) in order to develop the databases, procedures, and seismic source characterization (SSC) necessary to perform PSHA (References 2.5-228, 2.5-247, 2.5-248, 2.5-249, and 2.5-249) of sufficient robust nature of the evaluation of earthquake ground motions and their uncertainties to address acceptability requirements of the NRC (Reference 2.5-226) for its evaluation of safe design of nuclear power plants.

Since the early 2000s several electric power utilities have been using the EPRI-SOG models and databases as a starting point to develop updated models and databases for PSHA analyses required for new nuclear units planned in the CEUS. One of the required database update activities had been updating the EPRI-SOG earthquake catalog, which covers through the end of 1984 (Reference 2.5-248).

In January 2012 the CEUS SSC Project published, in what is referred to here as the CEUS SSC Report (Reference 2.5-223), a newly developed regional SSC to replace the existing regional seismic source models, such as the EPRI-SOG SSC. The CEUS SSC Project was conducted from April 2008 to December 2011. The CEUS SSC Report includes a new historical and instrumental earthquake catalog with spatial coverage over a similar CEUS region as the EPRI-SOG catalog, an area of approximately latitudes 22.5°N to 53°N by longitudes 50°W to 110°W,

including earthquakes of the expected uniform moment magnitude E[**M**] 2.2 and larger from 1568 through the end of 2008. See Figure 2.5.2-201.

RG 1.208, the purpose of which is to provide guidance on the development of the site-specific GMRS, as prepared in Section 2.5.2.6, details the guidance of comprehensive geological, seismological, geophysical, and geotechnical engineering investigations of the site area and region that should be performed. An important purpose for the site-specific investigations is to determine whether there are any new data or interpretations that are not adequately incorporated into the existing PSHA databases. While the CEUS SSC Report was published in 2012, the seismicity characterization is based on data through 2008, warranting the review of more recent seismicity.

To evaluate the potential significance of any re-interpretation of past earthquakes and to consider the impact of more recent seismicity, including the 2011 **M** 5.8 Mineral, Virginia earthquake, the CEUS SSC earthquake catalog was reviewed and updated for the CEUS from 2009 through mid-December 2011.

2.5.2.1.1 Regional Earthquake Catalog Developed in the CEUS SSC Study

Two primary sources of information for the evaluation of earthquake ground motion hazard are, first, the historical and instrumental record of the occurrence of earthquakes (the earthquake catalog) and second, the geologic, geophysical, and geodetic evidence of not only past, pre-historic crustal deformation or event-specific after-effects, but also evidence of on-going, quantifiable, near-surface stresses. Given that the oldest historical records in an earthquake catalog are based on spatially and temporally sporadic written documentation of qualitative felt or damage effects, the latter geologic, geophysical, and geodetic evidence is critical since the occurrence rate or repeat times of major earthquakes is often longer than the temporal coverage of the earthquake catalog. Further, such evidence may more directly indicate the potential of maximum earthquake size (e.g., magnitude) of which a given tectonic structure or region may be capable. In tectonically active regions, such as the western United States (WUS), both of these elements are readily available and used in a PSHA. In stable continental regions (SCR) like the CEUS, the geologic, geophysical, and geodetic evidence of past earthquakes is not as widely available. The causative source

mechanisms and structures for the occurrence of damaging earthquakes are generally poorly understood, and the rates of crustal deformation are low such that surface and near-surface indications of stresses in the crust and the buildup and release of crustal strains are difficult to quantify. While the CEUS SSC Report identifies several tectonic structures showing evidence of repeated large magnitude earthquakes (RLME sources), as discussed in Section 2.5.2.2, these sources, while notable contributors to seismic hazard, are sparsely distributed throughout the CEUS (see Figure 2.5.2-218). Therefore, the catalog of past earthquakes that have occurred in the CEUS is a particularly important source of information for the quantification of future seismic hazards. Developing an earthquake catalog for the study region was an important focus of the CEUS SSC Project.

2.5.2.1.1.1 Goals for the CEUS SSC Earthquake Catalog Development

As detailed in the CEUS SSC Report, Chapter 3, the specific goals for the development of the CEUS SSC earthquake catalog included the following elements:

- Completeness,
- Uniformity of Catalog Processing, and
- Catalog Review

2.5.2.1.1.1.1 Completeness

The goal of compiling an earthquake catalog is to record the occurrence of all known earthquakes in the magnitude range considered important to the characterization of future earthquake hazards. Significant effort in the United States has been made toward this goal. The NCEER-91 CEUS earthquake catalog by Seeber and Armbruster (Reference 2.5-251), an update of the EPRI-SOG earthquake catalog, was the primary source for the CEUS earthquake catalog used by the U.S. Geological Survey (USGS) for its National Seismic Hazards Mapping Program (NSHMP) (References 2.5-252 and 2.5-253). Similarly, work by the Geological Survey of Canada (GSC) to develop an earthquake catalog for seismic hazard analysis (Reference 2.5-254) provides an equally important source catalog for earthquakes in the northern portion of the CEUS SSC study region. The CEUS SSC Project relied on the work underlying the USGS and GSC catalogs to form the backbone of the updated project earthquake catalog.

BASIS: NEW

The USGS and GSC catalogs each represent a synthesis of catalog information from many sources into simple one-line catalog entries of date, time, location, and selected estimate(s) of earthquake size. In that process, some information important to the use of the earthquake catalog for the CEUS SSC Project may not have been retained. Therefore, during the development of the CEUS SSC earthquake catalog an extensive review of original catalog sources was performed as part of the catalog compilation. In addition, numerous special studies of individual earthquakes, earthquake sequences, and specific geographic areas were reviewed and the information compiled as part of the CEUS SSC earthquake catalog development. A number of these studies included information on important parameters (e.g., moment magnitudes) that is not included in the more regional catalogs.

In the process of catalog compilation from multiple sources, close attention was paid to the inclusion of duplicate entries for some earthquakes, as well as the possible inclusion of nontectonic events (e.g., quarry blasts, collapses, and explosions) that had been purposely excluded from other catalogs.

2.5.2.1.1.1.2 Uniformity of Catalog Processing

An important goal of catalog compilation is to use an earthquake size measure that is consistent with the GMPEs that are used to compute seismic hazards. Most recent GMPEs applicable to the CEUS, such as EPRI (2004) (Reference 2.5-224), use the moment magnitude scale, **M**, as the earthquake size measure, and it is expected that the next generation of ground motion models will continue to use the moment magnitude scale. Unfortunately, however, this is not the magnitude scale that has been used for routine earthquake monitoring and catalog compilation in the CEUS. The recent practice for many seismic hazard analyses in the CEUS, including EPRI-SOG and NSHMP, has been to estimate earthquake occurrence rates in terms of body-wave magnitude, m_b, and then use magnitude conversion relationships to convert to **M** as part of the ground motion estimation. This magnitude conversion introduces an additional source of magnitude uncertainty, particularly since many of the catalog magnitude entries are themselves converted from other size measures, such as shaking intensity used for pre-instrumental earthquakes.

The EPRI-SOG project (Reference 2.5-248) developed techniques to produce a catalog with a uniform size measure that is appropriate for an

unbiased estimation of earthquake occurrence rates for use in a seismic hazard assessment. These techniques were used in the EPRI-SOG study to develop a uniform catalog of the m_b scale. Recent use of the EPRI-SOG SSC has been combined with a GMPE model based on **M** (i.e., Reference 2.5-224), requiring magnitude conversion within a PSHA. During the CEUS SSC Project, a goal of the catalog development efforts was to use the same techniques to produce a catalog of uniform **M** values that have properly accounted for the uncertainty in size estimation. As **M**-based GMPEs remain to be used in current PSHAs, development of **M**-based seismicity and source recurrence rates eliminates the need for magnitude conversion as part of the hazard calculation and avoids propagation of unnecessary conversion-associated uncertainty through the hazard analysis. To achieve this goal, the CEUS SSC Report presented the updated magnitude scale conversions, which are developed from a variety of earthquake size measures to moment magnitude. See CEUS SSC Report, Table 3.3-1.

An equally important task was to obtain the original size measures for catalog entries in order to use a direct conversion to moment magnitude, rather than introduce additional uncertainty by converting previously converted size estimates. Take for example in the GSC catalog where a number of the magnitudes are designated local magnitude, M_L, yet many of these earthquakes occurred in the pre-instrumental period. Examination of the magnitude entries suggests that they were, in fact, converted from maximum intensity, I_0, using the Gutenberg and Richter (1956) (Reference 2.5-255) relationship. Therefore, the original source for the catalog of intensity data was obtained References 2.5-256 and 2.5-257) and the I_0 values for these earthquakes were entered into the catalog in order to make a direct conversion from I_0 to **M**.

2.5.2.1.1.1.3 Catalog Review

An important element of the CEUS SSC earthquake catalog development was the review by seismologists with extensive knowledge and experience in catalog compilation. The result of the review contributed to enhance the methodologies used to develop the final CEUS SSC earthquake catalog. One result of the review was to recommend the use of original earthquake information sources as much as possible in general preference to relying only on catalog compilations, yet still recognizing that some compilations, like the CEUS SSC earthquake

catalog itself, have been developed with a high degree of seismological rigor already. Another notable result of the review was the recognition that potential differences in common magnitude scales (e.g., body-wave magnitude and duration magnitude) may exist due to differences in the approaches used by various organizations or agencies to calculate magnitude. This resulted in looking at magnitude conversion relations, which may be a function of time and/or location.

2.5.2.1.1.2 Development of the CEUS SSC Earthquake Catalog

The CEUS SSC earthquake catalog development consisted of four main steps:

- Compilation of the catalog,
- Assessment of a uniform size measure to apply to each earthquake,
- Identification of independent and dependent earthquakes (catalog declustering), and
- Assessment of the completeness of the catalog as a function of location, time, and earthquake size.

These four steps are discussed in the following sections.

2.5.2.1.1.2.1 Catalog Compilation

The compilation of the earthquake records for the CEUS SSC earthquake catalog comprised several types of sources as described below.

Continental-Scale Catalogs

These catalogs are primarily compilations of earthquake information from regional sources (see *Regional Catalogs* described below), as well as reporting information directly gathered or analyzed by a national organization itself, such as the USGS or the GSC. In these continental-scale compilations, the national organizations often receive information from a variety of regional sources, as well as information developed from their own resources (e.g., seismic recording stations), for a given earthquake. Some of the national organizations apply their staff seismologists to review the available information and evaluate the most accurate, consistent, and up-to-date information to present in their catalogs. This is the case for the catalogs from the USGS and the GSC. For the CEUS SSC earthquake catalog compilation a version of the USGS earthquake catalog created for the NSHMP was obtained from the USGS and updated through 2008 using the Preliminary Determination of

Epicenters (PDE) catalog from the National Earthquake Information Center (NEIC). Similarly, a version of the GSC catalog was obtained and updated through 2008 using the GSC's National Earthquake Database (NEDB) of Canada.

As is noted in the CEUS SSC Report, the Advanced National Seismic System (ANSS) catalog is also a continental-scale catalog, however, the level of review is not as complete and the amount of information is not as broad as with the USGS's NSHMP catalog.

Regional Catalogs

These catalogs are prepared by state geological surveys or universities. They are focused on a given local region of interest. While they often acquire primary information and perform the primary data analyses (e.g., determination of time, location, and magnitude), which is commonly passed along to the caretakers of the continental-scale catalogs, the individual caretaker of a regional catalog does not routinely compare their reports of earthquakes with other regional or continental-scale catalogs, and, therefore, do not have the opportunity for more in-depth quality assurance from information comparison, as is available to the caretakers of continental-scale catalogs.

The following regional catalogs were included in the CEUS SSC earthquake catalog compilation:

- Center for Earthquake Research and Information (CERI) catalog
- Saint Louis University (Nuttli, microearthquake, and moment magnitude catalogs)
- Lamont-Doherty Cooperative Seismographic Network catalog (LDO)
- Weston Observatory catalog (WES)
- Ohio Seismic Network catalog
- Department of Conservation and Natural Resources of Pennsylvania catalog
- Reinbold and Johnston (1987) (Reference 2.5-389)
- Oklahoma Geological Survey catalog (OKO)
- South Carolina Seismic Network (SCSN) catalog
- Southeastern United States (SUSN) catalog (Virginia Tech)

Catalogs from Special Studies

Several published studies were reviewed during the CEUS SSC Project that contained information on specific earthquakes in limited geographical areas, often providing seismic moment or moment magnitude values and revised locations and/or depths. Some of these studies were a source of original information considered in the continental-scale compiled catalogs, while others offered alternate information that could be considered in the assessment of magnitude uncertainties. Still others of these special studies assisted in indicating events of nontectonic origin.

Centroid Moment Tensor Catalogs

These earthquake catalogs, such as the Harvard Global Centroid Moment Tensor (GCMT) catalog and the Saint Louis University (SLU) North America Moment Tensor catalog, are limited catalogs of generally larger magnitude events wherein are presented the analyses of determining the earthquake source characteristics, i.e., the fault style (e.g., strike-slip, normal, reverse) and three-dimensional moments ("moment tensor") of the fault slip occurring during the earthquake. From the moment tensor analysis, a best estimate of the moment magnitude results. The moment magnitude determined in this fashion is generally considered as the most accurate measure of "magnitude" as can be determined for an earthquake, where magnitude is intended to represent the seismic energy associated with an earthquake. This latter observation is not only why the moment magnitude is the magnitude scale of choice in the CEUS SSC Report when defining a uniform magnitude, and converting all other magnitude scales to the moment magnitude scale, but also why the centroid moment tensor catalogs are worth considering for their direct reporting of moment magnitudes, while their date, time, location, and depth information is used only for correlating to other catalogs' information, which present the preferred data on date, time, location, and depth.

Moment magnitude estimates were also obtained by approximate means in the studies of Atkinson (2004a, 2004b) (References 2.5-258 and 2.5-259), Boatwright (1994) (Reference 2.5-260), and Moulis (2002) (Reference 2.5-261). These approximate moment magnitudes were corrected for minor biases, as discussed in the CEUS SSC Report, before using them to augment the CEUS SSC **M** data set.

Final Catalog Compilation

Part of the CEUS SSC Report database is the master compilation of all earthquake records, including the duplicates from multiple catalogs or studies reporting the same event. Among the duplicate records for each given event, it is necessary to assess a prioritization or preference order among the various catalog sources for specifying the earthquake parameters to be presented in the final catalog. Unless suggested otherwise by recent special studies, the date, time, location, and depth for a given event were taken preferably from the USGS or GSC catalogs, otherwise (for events not in USGS and GSC catalogs) this information was taken from the regional catalog closest to the event. As discussed below, the measures of magnitude for a given event as reported in multiple catalogs were considered in the assessment of the uniform moment magnitude and its uncertainty.

2.5.2.1.1.2.2 Development of a Uniform Moment Magnitude Earthquake Catalog

An important goal of the development of the CEUS SSC earthquake catalog was to provide an earthquake catalog that could be used to develop unbiased estimates of the recurrence of earthquakes as a function of magnitude using a magnitude scale that is consistent with modern GMPEs for the CEUS, which is the moment magnitude scale defined by Hanks and Kanamori (1979) (Reference 2.5-262). Because the size measures available for most of the earthquakes in the project catalog are different from this scale, a process for converting from a variety of magnitude and shaking intensity measures to moment magnitude was needed. In addition, it has been shown by Tinti and Mulargia (1985) (Reference 2.5-263) and EPRI (1988) (Reference 2.5-248) that uncertainty in the magnitudes reported in an earthquake catalog can lead to bias in the estimation of earthquake recurrence rates unless appropriate adjustments are applied.

The EPRI-SOG project (Reference 2.5-248) developed an approach for assigning a uniform magnitude measure to earthquakes in an earthquake catalog and producing unbiased recurrence parameters from that catalog. The EPRI-SOG approach was updated for application in the CEUS SSC Project.

The CEUS SSC Report presents the results of extensive analysis of the compiled earthquake catalog to develop conversion relationships for the magnitude scales presented in the various catalogs to moment

magnitude. CEUS SSC Report, Table 3.3-1, presents several conversion relationships to determine the best estimate moment magnitude E[**M**|X] and its standard deviation or measure of uncertainty σ[**M**|X] given the observed magnitude scale X. These magnitude conversion relationships are not only a function of magnitude scale, but also of epicentral location and whether the earthquake report is from the Canadian GSC or not.

If the reported magnitude is already a directly measured moment magnitude (e.g., see Section 2.5.2.1.1.2.1 on centroid moment tensor catalogs), there is uncertainty in that measure, as well. As presented in the CEUS SSC Report (Equation 3.3.1-5):

$$E[\mathbf{M}] = E[\mathbf{M}|\hat{\mathbf{M}}] = \hat{\mathbf{M}} - \beta\sigma^2[\mathbf{M}|\hat{\mathbf{M}}] \qquad (2.5.2.1\text{-}1)$$

where β is b*ln(10) and $\hat{\mathbf{M}}$ is a reported moment magnitude. The σ value for the reported moment magnitudes, which varies as a function of time period and has a value of 0.10 after 1984, and the *b*-value of 0.95, determined from the initial CEUS SSC Project analyses of the catalog, are discussed in the CEUS SSC Report, Chapter 3.

Duplicate records from different catalogs for the same event commonly report different magnitudes in value, as well as scale (e.g., m_b or **M**). Further, some catalogs report more than one measure of magnitude for a given earthquake. Considering the multiple measures of magnitude for a given event in a compiled catalog, the CEUS SSC Report uses the following formulation (CEUS SSC Report [Equations 3.3.1-9 and 3.3.1-10]) to assess the single best estimate uniform moment magnitude and its total uncertainty:

$$\sigma^2[\mathbf{M}] = \sigma^2[\mathbf{M}|\hat{\mathbf{X}}] = \{ \Sigma_i \{1 / \sigma^2[\mathbf{M}|\hat{X}_i]\} \}^{-1} \qquad (2.5.2.1\text{-}2)$$

$$E[\mathbf{M}] = E[\mathbf{M}|\hat{\mathbf{X}}]$$

$$= \{ \Sigma_i (\sigma^2[\mathbf{M}|\hat{\mathbf{X}}] / \sigma^2[\mathbf{M}|\hat{X}_i]) \times E[\mathbf{M}|\hat{X}_i] \}$$

$$+ (R-1)\beta\sigma^2[\mathbf{M}|\hat{\mathbf{X}}] \qquad (2.5.2.1\text{-}3)$$

where $\hat{X}_i$ is the i^{th} member of the vector $\hat{\mathbf{X}}$ of magnitudes of varying scale and $E[\mathbf{M}|\hat{X}_i]$ is an estimated moment magnitude from the relationships in CEUS SSC Report, Table 3.3-1, or Equation 2.5.2.1-1 for reported moment magnitude. R is the number of *original* and *independent* measures of magnitude $\hat{\mathbf{X}}$. That is, the vector $\hat{\mathbf{X}}$ of magnitudes should not include converted magnitudes or duplicates (as may occur when one source catalog reports a magnitude from another catalog). If one or more reported magnitudes are directly measured moment magnitudes, then

the application of Equations 2.5.2.1-2 and 2.5.2.1-3 is done only for the reported moment magnitudes (first adjusted per Equation 2.5.2.1-1), and other non-moment reported magnitudes (albeit, previously converted to moment magnitudes) are ignored. This latter procedure allows that directly determined moment magnitudes, though they may differ and represent uncertainties within those determinations, should not have their best estimates and uncertainties impacted or unduly biased by moment magnitudes developed from conversions from non-moment magnitude estimates.

Once the preferred and duplicate records of a given event have been used to evaluate uniform moment magnitude E[**M**] and its total uncertainty σ^2[**M**], the duplicate records are discarded.

It is noted that in the literature a reported moment magnitude $\mathbf{M}^{\wedge}$ (or just **M**) is commonly cited rather than the CEUS SSC Report-defined uniform moment magnitude, E[**M**], as given in Equation 2.5.2.1-1 or Equation 2.5.2.1-3. Therefore, '**M**' will often be cited in this FSAR for the common moment magnitude as given in the literature, as distinguished from the uniform moment magnitude value 'E[**M**]'.

A detailed discussion on the use of an earthquake catalog for earthquake recurrence rate or frequency-magnitude analysis is provided in the CEUS SSC Report, Chapter 3. As the typical processing entails counting numbers of earthquakes using bins of magnitude- and time-intervals, the CEUS SSC Report addresses the issue of the impact of uncertainties in magnitude values on the magnitude binning procedure.

EPRI (1988) (Reference 2.5-248) presented a methodology whereby an earthquake's best estimate of a given magnitude, m_b or "Emb," uses body-wave magnitudes, rather than moment magnitudes) is modified to a value referred to as m_b* or "Rmb", where the standard deviation of σ_{mb} or "Smb" is considered. EPRI (1988) uses m_b* magnitudes for earthquake recurrence rate analysis. The CEUS SSC Report reviews the EPRI (1988) methodology of adjusting the magnitudes, and demonstrates that better recurrence rate statistics can be developed by using a factor for adjusting the bin counts, rather than the magnitudes. Following the CEUS SSC Report, for each event the equivalent count factor N*, as defined in the CEUS SSC Report (Equation 3.3.1-12), is calculated:

$$N^* = exp\{\beta^2\sigma^2[\mathbf{M}|\mathbf{X}]/2\} \qquad (2.5.2.1\text{-}4)$$

For subsequent recurrence rate analysis, when earthquakes are counted as they are distributed among magnitude-interval and time-interval bins, each event counts as its N* value, rather than unity.

2.5.2.1.1.2.3 Identification of Independent and Dependent Earthquakes

The PSHA methodology, which is typically used to model the occurrence of distributed seismicity, is based on the Poisson model for the occurrence of independent earthquakes. Therefore, dependent earthquakes (foreshocks and aftershocks) must be identified and not included in the earthquake statistics generally used to develop estimates of earthquake recurrence rates for modeled distributed seismicity. This process is referred to as catalog declustering.

Identified dependent events are, however, valuable when considering postulated spatially and/or temporally clustered/episodic behavior of large magnitude earthquakes, such as at New Madrid that has potentially significant hazard implications. Many seismic sources, especially those within SCRs, display evidence of clustering through time such that the earthquake recurrence rates may be elevated for several seismic cycles during a cluster, followed by much longer time intervals. This behavior can be modeled by identifying two rates: the within-cluster rate and the out-of-cluster rate. The SSC model resulting from the CEUS SSC Project should be useful for engineering applications for the next 50 years or so. For this reason, it is important to assess whether the source is currently (i.e., over approximately the next 50 years) within or out of a cluster such that the within-cluster or out-of-cluster rate is applicable. This is an assessment made for the RLME sources in the CEUS SSC model, as discussed later.

Dependent events, along with the related mainshock event, are also valuable in assisting to image the rupture area of notable earthquakes, as discussed in Section 2.5.2.2.5.1 regarding the 2011 **M** 5.8 Mineral earthquake.

The CEUS SSC Report discusses multiple methods of earthquake catalog declustering. While the EPRI (1988) method was used in the declustering analysis for the CEUS SSC earthquake catalog, the CEUS SSC Report notes that similar results would have been obtained using the method of Gardner and Knopoff (1974) (Reference 2.5-264) without a significant difference in earthquake recurrence rates computed from the declustered catalog.

2.5.2.1.1.2.4 **Catalog Completeness**

For input to a PSHA the mean annual recurrence rate of the different possible size earthquakes must be evaluated for each seismic source feature or defined area. Except for distinct features such as the RLME seismic sources discussed in Section 2.5.2.2, where the recurrence rate is often established from geologic and paleoseismic evidence pre-dating the earthquake catalog, the recurrence rate of independent earthquakes generally follows a Poisson distribution, where the frequency of occurrence of different magnitude earthquakes follows the frequency-magnitude relationship of Gutenberg and Richter (1944) (Reference 2.5-265):

$$\mathrm{Log}_{10}\nu(\mathbf{M}) = a - b\,\mathbf{M} \qquad (2.5.2.1\text{-}5)$$

where $\nu(\mathbf{M})$ is the mean annual number of earthquakes of magnitude **M** and larger, and "*a*" and "*b*" are the log-linear regression coefficients or recurrence parameters for the frequency function determined by analysis of historical earthquakes associated with the given seismic source. The earthquake data used in the determination of recurrence parameters "*a*" and "*b*" will range between a given minimum magnitude (m_0) and maximum magnitude (Mmax).

In analyzing an earthquake catalog for the purpose of developing the recurrence parameters, it is necessary to recognize that the reporting of earthquakes is not perfect or complete through the duration of the available data. With current instrumentation within the CEUS the detectability of events of even small magnitude (e.g., 2s and 3s) is relatively high and the detectability of moderate size events (5 and greater) is effectively 100 percent. The detectability and reporting of earthquakes notably decreases, however, especially for small to moderate-size events, the older the event is within the earthquake catalog, particularly for time periods when seismic instrumentation did not exist and earthquake records are based on personal accounts or as sporadically recorded in newspapers and other written records. In assessing stable estimates of recurrence parameters ("*a*" and "*b*" in Equation 2.5.2.1-5), it is necessary to assess the completeness of the earthquake catalog to develop reliable estimates of those statistics. Only for that time-period portion of the catalog, as a function of magnitude, for which it can be reliably held that all events have been recorded (or the effect of expected missing events somehow compensated) – *Completeness* -- can Equation 2.5.2.1-5 be used, where the Poisson

statistics would have that independent earthquakes of a given magnitude or magnitude range would occur at a given rate, relatively constant over the time-period of completeness. The state of completeness is not only a function of the capability of effective or accurate earthquake recording by instrument or personal account, but also by the spatial distribution of the "recorders." Hence, the completeness is not only a function of the size and date of the event, but also a function of the demographics of location or region.

A common approach of defining the portion of the earthquake catalog that is complete has been the use of the general technique first proposed by Stepp (1972) (Reference 2.5-266). This approach evaluates the catalog completeness for specific magnitude ranges by starting at the present and moving back in time and counting the total number of earthquakes in the catalog in each magnitude interval. At each point in time when an earthquake in the specified magnitude interval occurred, the rate of earthquakes in the magnitude interval is computed by dividing the sum of the number of earthquakes from that point in time to the end of the catalog by the length in time from that point to the end of the catalog. Assuming that the rate of earthquakes is constant in time, plotting these values versus date for the complete portion of the catalog will show an approximately horizontal line representing a relatively constant rate for events in the specified magnitude range. Moving further back in time, eventually the plotted line will start to trend downward, indicating that not all earthquakes are being reported (again assuming stationarity in time of the true rate). The point at which this downward trend begins indicates the beginning of the complete period of catalog reporting for the specific magnitude interval. These plots are commonly referred to as "Stepp" plots, after their originator.

The mean annual rate of earthquakes occurring within a given magnitude interval, λ_i, is given as

$$\lambda_i = N_i^C / T_i^C \qquad (2.5.2.1\text{-}6)$$

where N_i^C is the number of earthquakes in magnitude interval i observed during the period of complete recording T_i^C in years (Reference 2.5-223), Equation 3.5-1). (Note: $\nu(\mathbf{M})$ in Equation 2.5.2.1-5 is a cumulative form of λ_i.) In the Stepp approach all earthquake data prior to the beginning of the complete period of catalog reporting for the specific magnitude interval are ignored.

The EPRI-SOG project developed an approach for incorporating the previously ignored catalog data in the partially complete period into the assessment of earthquake recurrence parameters. If a probability of detecting and reporting an earthquake as a function of magnitude and calendar time can be estimated, then the mean annual rate of earthquakes occurring within a given magnitude interval, λ_i, is given as

$$\lambda_i = \Sigma_j N_{ij} / \Sigma_j P_{ij}^D T_j \qquad (2.5.2.1\text{-}7)$$

where N_{ij} is the number of earthquakes in magnitude interval (i) observed during the period interval of recording T_j in years, and P_{ij}^D is the probability of detecting earthquakes in magnitude interval i observed during the period interval of recording T_j (Reference 2.5-223, Equation 3.5-4). If one assumes that the larger magnitudes are complete at present and imposes the constraints that P_{ij}^D should decrease more or less monotonically with increasing time into the past and should increase monotonically with magnitude at each point in time, then, again invoking stationarity, the parameters λ_i (or "*a*" and "*b*" of Equation 2.5.2.1-5) and P_{ij}^D can be estimated jointly through a maximum likelihood solution from the earthquake catalog data assuming a Poisson distribution of the earthquake data. In developing these estimates from its earthquake catalog, EPRI (1988) used no spatial smoothing on the rate parameter, and medium smoothing on *b*-value, and no prior on *b*-value.

Through analysis of the history of population growth and earthquake recording, EPRI (1988) defined 13 completeness regions covering most of the CEUS. These regions represent portions of the CEUS where catalog completeness as a function of time and magnitude is assessed to be sufficiently similar such that it can be treated as the same. For each of the 13 regions EPRI (1988) developed a single probability detection matrix of P_{ij}^D where no spatial smoothing on the rate parameter, medium smoothing on *b*-value, no prior on *b*-value where considered (see Volume 1, Part 1, Section 3.5, and Volume 1, Part 2, Section 4.5, of EPRI (1988)).

In looking at various issues of earthquake record coverage that differed from what was presented in the EPRI-SOG earthquake catalog, the CEUS SSC Report made modifications to the EPRI-SOG completeness regions, including adding a fourteenth region. See CEUS SSC Report, Figure 3.5-2, and Tables 3.5-1 through 3.5-3, for the *three* sets of matrices of probability of detection for each of the 14 regions, one set for each of the recurrence magnitude weighting cases, as discussed further

in Section 2.5.2.4.

2.5.2.1.1.3 The CEUS SSC Earthquake Catalog

The CEUS SSC project earthquake catalog, covering the period from 1568 through 2008, is tabulated in CEUS SSC Report, Table B-1, and shown here in Figure 2.5.2-201. As indicated in the CEUS SSC study, Chapter 3, this catalog contains 3,298 individual earthquakes of uniform moment magnitude E[**M**] 2.9 and larger within the entire CEUS SSC study area. Upon inspection of the catalog, however, the catalog actually includes 10,984 earthquakes of uniform moment magnitude E[**M**] 2.2 and larger. Table 2.5.2-201 presents additional statistical details of the published CEUS SSC earthquake catalog, including 159 of the 3,298 events of uniform moment magnitude E[**M**] 2.9 and larger that are within 200 miles of the North Anna 3 site.

2.5.2.1.2 Updated CEUS SSC Earthquake Catalog

Given that the **M** 5.8 August 23, 2011 Mineral earthquake occurred after the coverage period of the published CEUS SSC earthquake catalog, it was recognized that this event constituted significant “new data” that needed to be evaluated under Regulatory Position 1 of RG 1.208. Therefore, a chronological update of the CEUS SSC earthquake catalog for the time period of 2009 through mid-December 2011 was performed for a rectangular area encompassing the entire CEUS SSC study area. The same primary input data sources and analysis procedures as used in the published CEUS SSC Report, as specifically described in its *Chapter 3, Earthquake Catalog* and summarized above, were used in this update. As with the original CEUS SSC earthquake catalog, the focus of the earthquake catalog update was on events of uniform moment magnitude E[**M**] 2.2 and larger.

Table 2.5.2-201 presents statistics of the update to the original CEUS SSC earthquake catalog, as well as the total earthquake catalog, now including earthquakes from 1568 through mid-December 2011. The total updated earthquake catalog contains 3,772 individual earthquakes of uniform moment magnitude E[**M**] 2.9 and larger within the entire CEUS SSC study area, including 171 of these events that are within 200 miles of the North Anna 3 site. Table 2.5.2-202 is a tabulation of the 141 independent or mainshock earthquakes with uniform moment magnitude E[**M**] 2.9 and larger that are within 200 miles of the site.

Note that while Modified Mercalli Intensities (MMI), a standard measure of the qualitative site-specific effects of an earthquake, were considered in the development of the published CEUS SSC earthquake catalog, notably for the determination of corresponding magnitudes of historical, pre-instrumental earthquakes, the published CEUS SSC earthquake catalog did not include a tabulation of the maximum MMI values for the earthquakes. As maximum MMI values were not required for the determination of magnitude for the recent events from 2009 to mid-December 2011, maximum MMI was also not tabulated for the catalog update.

Figure 2.5.2-202 is a plot of the updated CEUS SSC earthquake catalog for the entire CEUS. Earthquakes shown are for independent or mainshock earthquakes with **M** ≥ 2.9. Figures 2.5.2-203 and 2.5.2-204 are similar plots focusing on the areas within approximately 322 km (200 miles) and 80 km (50 miles), respectively, of the site.

In the CEUS SSC Report the SLU North America Moment Tensor (NAMT) catalog was a primary source of reported moment magnitudes. CEUS SSC Report, Tables B-2 and B-3, list the moment magnitudes that were used in the development of correlation relationships to convert reported non-moment magnitudes to a best estimate of uniform moment magnitude. In Table B-2 the data from the SLU NAMT catalog are indicated with “WEB” in the ‘Source’ field. At the evaluations of the SLU data during both the CEUS SSC study and the CEUS SSC earthquake catalog update performed herein, the SLU web site had multiple ways of obtaining earthquake magnitudes, some of which were moment magnitudes, while others were some unspecified type magnitudes. During the process of updating the CEUS SSC earthquake catalog, it was determined that a few of the values of the moment magnitudes tabulated in the CEUS SSC Report were incorrect, primarily due to a brief period of manual processing of the earthquake data at SLU. Upon consultation with Dr. Robert Herrmann (2012) (Reference 2.5-267) at SLU, it was determined that the preferred manner by which to obtain the estimate of moment magnitude was to inquire of the site’s moment tensor “Mechanism Files,” rather than either of the tabulations of earthquakes, also available at the SLU Internet site. Table 2.5.2-203 compares the moment magnitudes in the CEUS SSC Report and the corresponding magnitudes obtained by investigating the individual “Mechanism Files.” In most cases the differences are small, resulting in negligible impact on

any of the analyses performed in the CEUS SSC Report. The one case where it is recommended that a correction is warranted is that of the April 7, 2008 **M** 3.86 earthquake in Texas, tabulated in the CEUS SSC Report, Table B-2, as **M^** 4.86. Given Equation 2.5.2.1-1, this event would have a uniform moment magnitude of E[**M**] 3.84.

2.5.2.1.3 Significant Site Earthquakes

RG 1.206, Part I, Subsection C.I.2.5.2.1 specifies that "for each earthquake, information, whenever available, on the epicenter coordinates, depth of focus, date, origin time, highest intensity, magnitude, seismic moment, source mechanism, source dimensions, distance from the site, and any strong-motion records, should be provided." This section presents available information on the **M** 5.8 (E[**M**] 5.71) Mineral earthquake that occurred on August 23, 2011 at 17:51 UTC at a distance of 8 km from Mineral, in Louisa County, Virginia with an epicenter location of 37.936° N, 77.933° W and a hypocentral depth of 6 ± 3.1 km (USGS, 2012) (Reference 2.5-268). Other large historical earthquakes that have occurred in the state of Virginia are also discussed. Finally, two sets of three-component ground motions recorded from accelerometers located in the North Anna Unit 1 structure are presented to provide strong-motion time histories from the **M** 5.8 Mineral earthquake.

Regional Seismicity

The **M** 5.8 Mineral earthquake epicentral region lies within the Appalachian Piedmont, about 130 km southwest of Washington, D.C., and within or near the Central Virginia Seismic Zone (CVSZ) (USGS, 2012). See Sections 2.5.1.1.4.d.1 and 2.5.2.2.3.1 and Figure 2.5.2-228. The mainshock hypocenter originated at 6.0 ± 3.1 km depth (Reference 2.5-268), with relatively large uncertainty stemming from the sparse P-wave recordings (Chapman, 2012) (Reference 2.5-235). The **M** 5.8 Mineral earthquake was the largest historical event in the region and the largest instrumentally recorded earthquake in eastern North America since the 1988 **M** 5.9 (E[**M**] 5.84) Saguenay, Canada earthquake (Cramer et al., 2012) (Reference 2.5-234). Seismicity in the region of the Mineral earthquake is attributed to the CVSZ, a previously recognized zone of seismicity that has produced numerous historical small and moderate earthquakes.

The largest earthquake in the CVSZ prior to the Mineral earthquake occurred in 1875 and has an estimated magnitude of about **M** 4.8 (E[**M**] 4.77) based on felt reports and reported damage (Reference 2.5-268). The most recent damaging earthquake prior to the Mineral earthquake was a magnitude **M** 4.5 (E[**M**] 4.33) on December 9, 2003 (Reference 2.5-268). Both of these prior earthquakes were located in Goochland County, Virginia, near the James River and south of the Mineral earthquake epicenter.

The Giles County (Virginia) seismic zone (GCVSZ), which is located in Giles County, southwestern Virginia, near the border with West Virginia, is another recognized seismic source by a concentration of small to moderate earthquakes. See Sections 2.5.1.1.4.d.2 and 2.5.2.2.3.3. The largest known earthquake to occur in this region is the 1897 **M** 5.9 (E[**M**] 5.91) Giles County event. The earthquake would have produced a Modified Mercalli Intensity (MMI) VIII in the epicentral area (Bollinger et al., 1992) (Reference 2.5-269) and MMI V at the site (Bollinger and Hopper, 1971) (Reference 2.5-270).

A preliminary estimate of about 0.7 Hz for earthquake corner frequency for the **M** 5.8 Mineral earthquake has been obtained from a strong-motion record, about 50 km from the mainshock epicenter (Reference 2.5-234). This corner frequency suggests a Brune stress drop of about 250 bars for the **M** 5.8 Mineral event (Reference 2.5-234).

Magnitude and Intensity

The moment magnitude for the Mineral earthquake was calculated as **M** 5.8 by Global Centroid-Moment-Tensor (CMT) solution, **M** 5.7 by U.S. Geological Survey-Saint Louis University (USGS-SLU) regional moment tensor solution, and **M** 5.8 by USGS W-phase CMT (Reference 2.5-268). The SLU moment tensor inversion (SLU, 2012) (Reference 2.5-271) yields an **M** 5.65 using the frequency band 0.01-0.03 Hz. This offset between the USGS and SLU moment magnitude measures is often observed for earthquakes, and may be due to the use of different velocity models (SLU, 2012).

According to the CEUS SSC uniform moment magnitude process, the reported moment magnitudes are assessed to have an uncertainty of 0.1 magnitude units. The Global CMT (referred to as “Harvard CMT” until the summer of 2006, when the CMT analyses were moved to Lamont-Doherty Earth Observatory (LDEO) of Columbia University),

W-phase CMT, and SLU's moment tensor solution are considered independent measures of the reported moment magnitude of the Mineral earthquake. Thus, following the CEUS SSC procedure for uniform magnitude, this event is assigned a best estimate uniform moment magnitude E[**M**] 5.71 in the updated earthquake catalog incorporating a magnitude uncertainty of 0.1 units into the reported moment magnitudes, as discussed in Section 2.5.2.1.1.2. However, the E[**M**] 5.71 given in the updated earthquake catalog is often attributed as **M** 5.8 in the literature, which is the largest reported moment magnitude for this earthquake.

Earthquakes in the CEUS, although less frequent than in the WUS, are typically felt over a much broader region. The **M** 5.8 Mineral earthquake caused moderate damage in the epicentral region, although felt intensity at close distances (less than 40 km) was less than predicted by Atkinson and Wald (2007) (Reference 2.5-272) relations (Assatourians and Atkinson, 2011) (Reference 2.5-273). Intensities for the **M** 5.8 Mineral earthquake were approximately one unit lower than those for the 1988 **M** 5.9 Saguenay earthquake at distances less than 40 km, but attenuated more slowly with increasing distance due to the different focal depths of events (Reference 2.5-273).

The **M** 5.8 Mineral earthquake shaking was widely felt through several major metropolitan areas, including the greater Washington, D.C. region, Philadelphia, and parts of New York State. The overall felt extent of the earthquake was significant, with perceptible shaking reported as far west as Minnesota and as far south as Florida. To the northeast it was felt as far as Fredericton, New Brunswick, Canada (Hough, 2012) (Reference 2.5-274). The felt extent was significantly larger than that of the 1897 Giles County, Virginia, earthquake (Bollinger and Hopper, 1971 (Reference 2.5-270); Nuttli et al., 1979 (Reference 2.5-275); Bollinger and Wheeler, 1983 (Reference 2.5-276); Hough, 2012).

Dependent Events and Clusters

Previously unrecognized from the surface, a series of aftershocks highlighted the rupture plane of the earthquake in the subsurface (see Figure 2.5.1-203). Aftershocks ranged in depth from about 1 to 7.5 km and included events up to **M** 3.9 (E[**M**] 3.91) (Horton et al., 2012) (Reference 2.5-232). Walsh et al. (2012) (Reference 2.5-277) suggest that aftershocks of the Mineral earthquake, as well as other intraplate earthquakes, could endure decades to a century, as opposed to only a few years in more tectonically active margins.

The majority of aftershocks defined a concave-up planar surface (Reference 2.5-232), while several smaller clusters of aftershocks were located up to about 10 km from the primary cluster. Horton et al. (2012) describe the rupture surface as an approximately 10-km-long plane oriented N30°E, dipping 46°SE plane that extends from about 7.5 km to 1 km depth, while Chapman (2012) determined a plane striking N29°E and dipping 51°SE based on the aftershock sequences recorded by the portable instruments.

The orientation of the rupture plane based on aftershocks is in close agreement with orientations suggested by focal mechanisms of the mainshock event.

Focal Mechanisms

The Global and USGS moment tensor solutions as well as the pattern of aftershocks for the Mineral earthquake define a rupture plane striking approximately N26°-30°E, and dipping 50°-57°SE. For instance, the mainshock event relocated in the primary cluster has a focal mechanism solution determined from waveform inversion that shows a nodal plane striking N28°E and dipping 50°SE with a rake angle of 113 degrees and mostly reverse motion (Reference 2.5-232). Chapman (2012) determined the rupture plane to be striking N29°E, dipping 51°SE from early aftershocks in the sequence. The USGS has also used a method to perform fast source parameter inversions for moderate to large earthquakes using the W-phase, a very long-period phase starting right after the P-wave arrival (Kanamori and Rivera, 2008) (Reference 2.5-278). Since W-phase inversion method covers the frequency band which has not been covered by the existing regional and global inversion methods, W-phase solutions provide important additional information on long-period characteristics of earthquakes. Table 2.5.2-204 lists the summary of focal mechanisms of the mainshock event. The focal mechanism solutions indicate a primarily reverse sense of slip on a north or northeast-striking plane within the CVSZ region of diffuse seismicity.

Source Rupture Dimension

Based on reconnaissance performed by other researchers immediately following the earthquake and Dominion's field reconnaissance of the epicentral region, it was concluded that the **M** 5.8 Mineral earthquake did not produce any discernible rupture or deformation at the ground surface. No evidence of surface rupture, surface fault features, or geomorphic

expression of surface rupture or coseismic surface tectonic deformation exists for the **M** 5.8 Mineral earthquake.

In order to best represent the approximate rupture plane or fault that produced the Mineral earthquake, the aftershock information was used to develop a representation of the possible rupture plane and its up-dip projection to the surface:

- The mainshock event has a focal mechanism determined from waveform inversion that shows a nodal plane striking N28°E and dipping 50°SE with a rake angle of 113° and mostly reverse motion (Reference 2.5-232).
- The early aftershocks define a plane striking N29°E and dipping 51 degrees to the southeast (Reference 2.5-235).
- Given the regional trend of the geology and aftershock distribution, the fault plane has a strike of N28°E and a dip of 55° based on the Saint Louis University regional CMT solution (Shao, et al., 2012) (Reference 2.5-240).

These interpretations as well as trend of aftershocks represent an approximate depiction of the rupture plane and the area where any surface rupture would likely be located (see Figure 2.5.1-203). The subtle differences in strike and dip estimated by seismologists are considered as inherent uncertainty in the aftershock location calculations.

Propagation of the rupture plane was complex, exhibiting three distinct slip events—a smaller and deeper initiation event followed by two larger and shallower events (Reference 2.5-235).

Strong-Motion Records

The **M** 5.8 Mineral earthquake occurred about 18 km southwest from the North Anna site. This seismic event was widely felt through the CEUS region and the two strong-motion instruments located at the North Anna Unit 1 containment mat foundation (Reference 2.5-386): Elevation 217 ft, about 54 ft below plant grade) and containment operating deck (Elevation 291 ft, about 20 ft above plant grade) triggered and recorded this earthquake (Reference 2.5-386). These North Anna Unit 1 power plant records are the closest available strong motion recordings of the **M** 5.8 Mineral earthquake. Following this earthquake, the strong ground-motion records from the two-instrument locations were retrieved and processed by Kinemetrics (Kinemetrics, 2011) (Reference 2.5-279). As part of this processing, the acceleration time histories were bandpass filtered with

ramps between frequencies of 0.04 – 0.1 Hz and 43 - 45 Hz. These time histories consist of 3,520 spectral acceleration ground-motion data points in units of cm/sec^2 with an equal time step of 0.005 sec. Peak ground accelerations in units of "g" from the corrected time histories are:

Containment Mat: Channel 1 (L (Longitudinal) = E/W, East-West direction)	0.109g
Containment Mat: Channel 2 (V (Vertical) = UP, Vertical direction)	0.118g
Containment Mat: Channel 3 (T (Transverse) = S/N, South-North direction)	0.264g
Containment 291: Channel 1 (L (Longitudinal) = W/E, West-East direction)	0.163g
Containment 291: Channel 2 (V (Vertical) = UP, Vertical direction)	0.284g
Containment 291: Channel 3 (T (Transverse) = N/S, North-South direction)	0.400g

The resulting acceleration, velocity and displacement time histories for each component of the recorded motions are shown in Figures 2.5.2-205 through 2.5.2-210. Reference 2.5-386 concludes that when comparisons are made between the time histories of the containment mat foundation and containment operating deck records, it is apparent that both sets of recordings are affected by the structure and should not be considered equivalent to free-field recordings.

The Center for Engineering Strong-Motion Data (CESMD) was established by the USGS and the California Geological Survey (CGS) to provide a single access point for earthquake strong-motion records and station metadata from the CGS California Strong-Motion Instrumentation Program, the USGS National Engineering Strong-Motion Program, and the US Advanced National Seismic System (ANSS). The Center provides uniformly processed U.S. strong-motion data for earthquake engineering applications at www.strongmotioncenter.org. Table 2.5.2-205 lists the peak ground-motion data recorded from different stations for the **M** 5.8 Mineral, Virginia earthquake (CESMD, 2012) (Reference 2.5-280).

At short periods (PGA, 0.2s), ground motions agreed well with eastern ground-motion prediction equations, but were less than expected at longer periods (1.0s) (Cramer et al., 2012) (Reference 2.5-234).

2.5.2.2 Geologic and Tectonic Characteristics of the Site and Region

This section describes the new SSC for the CEUS and the sources within the CEUS SSC model that are used in the PSHA for the Unit 3 site. As described in Section 2.5.1, a comprehensive review of available geological, seismological, and geophysical data has been performed for the site region, as well as for portions of seismic sources that extend beyond the site region. Detailed descriptions of known geologic structures are provided in Section 2.5.1.

As described in RG 1.208, the seismic sources used in a PSHA may be identified based on existing databases and models, with the provision that new information relevant to a seismic source must be evaluated and incorporated as appropriate (Section 2.5.2.4). The starting point for the Unit 3 PSHA is the regional seismic source model developed by the CEUS SSC Project, which was published in 2012. The CEUS SSC model is the most recent seismic source characterization specifically designed for PSHAs of nuclear facilities, replacing the EPRI-SOG model (References 2.5-228, 2.5-247, 2.5-248, 2.5-249, and 2.5-250) and the Lawrence Livermore National Laboratory model (Bernreuter et al., 1989) (Reference 2.5-229). The CEUS SSC model also incorporates new data gathered during the most recent iteration of the USGS NSHMP.

The CEUS SSC model was developed using Senior Seismic Hazard Analysis Committee (SSHAC) Study Level 3 methodology (SSHAC, 1997 (Reference 2.5-281); Hanks et al., 2009 (Reference 2.5-282); Kammerer and Ake, 2012 (Reference 2.5-283)), ensuring that uncertainty is represented in a manner consistent with NRC regulatory guidance. Toward this end, scientists involved in the development of the NSHMP, the most recent regional seismic source characterization at the time, were included in the evaluation process of the CEUS SSC model.

2.5.2.2.1 Overview of CEUS SSC

The CEUS SSC model was created to provide a regionally consistent model of seismic hazard for nuclear facilities throughout the CEUS. The CEUS SSC model focuses on regionally significant elements, with the understanding that site-specific PSHAs would need to refine the CEUS SSC model with site-specific and updated data as necessary.

In the CEUS SSC model, the spatial and temporal distribution of future earthquakes is modeled by two types of seismic sources. The first type is

a distributed seismicity source, which is based on observed seismicity. These sources cover the entire CEUS region. The second type is a RLME source, which is based on the paleo- and historical earthquake record. The RLME sources cover the much more localized phenomenon of repeated large magnitude earthquakes at specific locations. While notably considering distinct tectonic characteristics, the CEUS SSC model places less importance on specific discrete or localized tectonic features, which were emphasized in the older EPRI-SOG model (References 2.5-228, 2.5-247, 2.5-248, 2.5-249, and 2.5-250).

Distributed seismicity sources are defined in the CEUS SSC model according to two conceptual approaches (Figure 2.5.2-211). The first approach smoothly varies seismicity rates throughout the entire CEUS; distributed seismicity sources are only differentiated by maximum magnitude (Mmax) potential. These sources are modeled as “Mmax Zones” (Section 2.5.2.2.2). Figure 2.5.2-212 shows the locations and extents of the Mmax zones and Figure 2.5.2-213 shows the logic tree for the Mmax zones. The second approach to distributed seismicity sources considers a wider array of seismotectonic properties in order to define distributed seismicity sources. These sources are modeled as “Seismotectonic Zones” (Section 2.5.2.2.3). Figures 2.5.2-214 and 2.5.2-215 show the location and extent of the seismotectonic zones and Figures 2.4-216 and 2.5.2-217 show the logic tree for the seismotectonic zones. In each model alternative, RLME sources are independently assessed and added to the hazard of the distributed seismicity sources. Section 2.5.2.2.4 provides additional discussion of the RLME sources.

Table 2.5.2-206 lists all distributed seismic sources defined in the CEUS SSC model, and Table 2.5.2-207 provides a list of seismotectonic zones as they correspond (spatially) to the larger Mmax zones. Figure 2.5.2-218 shows the locations of all RLME sources in the CEUS SSC model.

2.5.2.2.1.1 CEUS SSC Methodology

The CEUS SSC model was created following SSHAC Level 3 guidelines (References 2.5.2-281, 2.5.2-282, and 2.5.2-283), ensuring that uncertainty is represented in a manner consistent with RG 1.208. The SSHAC process calls for a Technical Integration (TI) Team, headed by a TI Lead, to evaluate and integrate all available data, models, and methods into the hazard model. These evaluation and integration steps

are performed with the aid of the informed technical community, members of which serve as resource and proponent experts for the TI Team. Technical assessment and regulatory adherence is reviewed throughout the course of the project by the Participatory Peer Review Panel (PPRP). The intended result of the SSHAC process is to create a hazard model that represents the center, body, and range of technically defensible interpretations of the informed technical community.

As stated above, the CEUS SSC model accounts for the likely spatial and temporal distribution of future earthquakes using observed seismicity and the paleo-earthquake record. Specifically, the model depends on the theory that the spatial pattern of small to moderate magnitude earthquakes is indicative of the future locations of moderate to large magnitude earthquakes. This idea is generally accepted by the scientific community, and thus forms the basis for the spatial model of distributed seismicity sources in the CEUS SSC model. Similarly, the average rate and a periodicity of future earthquakes is also governed by the temporal distribution of earthquakes in the instrumental and historical catalog.

2.5.2.2.1.2 CEUS SSC Earthquake Recurrence Rate

The earthquake recurrence rate within each distributed seismicity source is assessed by dividing each source into a number of ¼° to ½° cells. The rate and *b*-value in each cell is calculated using the likelihood function of the data in that cell (which addresses catalog completeness), along with penalty functions that smooth out large variations in rate and *b*-value between cells. Earthquakes associated with RLME sources are excluded from these calculations. The full earthquake recurrence calculation in each zone produces the following results:

- The recurrence rate of earthquakes of moment magnitude (**M**) > m_0 (where m_0 = 2.9 is the lowest magnitude considered in the recurrence analysis) per equatorial degree
- The *b*-value, expressed in log base-10 units
- The area of each cell in equatorial degrees

This is a vastly simplified overview of the method for calculating and smoothing earthquake recurrence rates in distributed seismicity sources. A complete discussion of the smoothing approach is provided in the CEUS SSC Report, Section 5.3.2.

The calculation of earthquake recurrence rates in RLME sources is more straightforward, since RLME sources tend to have a more narrowly

defined Mmax distribution and geographical extent. Earthquake occurrence rates for RLME sources are based on data in the paleo- and historical earthquake record, and modeled using either a Poisson model or a renewal model. In the Poisson model, the time between RLME earthquakes is modeled by an exponential distribution with a standard deviation that equals the mean earthquake recurrence interval. This model is favored for RLME sources that exhibit a higher degree of aperiodic RLME occurrence. The renewal model is better suited to RLME sources in which RLME earthquakes appear to be more periodic. The time between RLME earthquakes in this model is based on the Brownian Passage Time (BPT) model, which represents the physical process of strain buildup and release (Ellsworth et al., 1999 (Reference 2.5-284); Matthews et al., 2002 (Reference 2.5-285)). Full details related to the estimation of earthquake recurrence in RLME sources is provided in the CEUS SSC Report, Section 5.3.3.

2.5.2.2.1.3 CEUS SSC Maximum Magnitude

The Mmax potential in the CEUS SSC distributed seismicity sources is assessed through two alternative approaches. In the Bayesian approach, a prior Mmax distribution (or, in some cases, two prior Mmax distributions) is determined by comparison of each respective seismic source with analogous world-wide SCR (Johnston et al., 1994) (Reference 2.5-286). This prior distribution is then updated based on site-specific observations; the updated prior distribution is called a likelihood function. The prior distribution and the likelihood function are convolved to create a posterior Mmax distribution for use in the hazard analysis, truncated at **M** 5.5 and **M** 8.25.

In the Kijko (2004) (Reference 2.5-287) approach, Mmax is based solely on the observed seismicity. The CEUS SSC model utilizes two weighted alternatives from Kijko (2004): the K-S estimator, which is a truncated exponential distribution, and the K-S-B estimator, which includes uncertainty in the *b*-value. Kijko (2004) also includes a third estimator for Mmax. This third estimator, however, is not included in the CEUS SSC as a weighted alternative for the distributed seismicity sources since it is based on characteristic earthquake behavior. Earthquakes of this type are modeled by RLME sources in the CEUS SSC, as described below. Mmax distributions computed according to the Kijko (2004) approach are truncated at **M** 5.5 and **M** 8.25. A complete description of the process for assessing Mmax is provided in the CEUS SSC Report, Section 5.2.

Whereas the instrumental and historical record of small-to-moderate earthquakes is used to determine hazard in the distributed seismicity sources, historical and pre-historical data in some places point to the repeated occurrence of large-magnitude (**M** ≥ 6.5) earthquakes. Where data are sufficient, these zones are modeled as RLME sources, and earthquakes associated with these zones are excluded from the calculation of Mmax in the host distributed seismicity source. The distribution of magnitudes used to model the characteristic earthquake size in RLME sources is narrower than that in the distributed seismicity sources, and is based on the amount and quality of data available for each RLME.

2.5.2.2.2 CEUS SSC Mmax Zones Included in the North Anna PSHA

In the CEUS SSC model, Mmax zones are sources of distributed seismicity distinguished from one another solely by differences in potential maximum earthquake magnitude. Based on a statistical analysis of the global SCR database (Johnston et al., 1994 (Reference 2.5-286); Schulte and Mooney, 2005 (Reference 2.5-288)), alternative sets of Mmax zones are considered in the CEUS SSC. In the first alternative, which is given a slightly stronger weight, the eastern U.S. is divided into two zones of unique prior Mmax distributions as described in Sections 2.5.2.2.2.1 and 2.5.2.2.2.2). In the second alternative, the seismic hazard of the entire CEUS region is modeled as a single Mmax zone with a single prior distribution as described in Section 2.5.2.2.2.3. In both alternatives, Mmax and recurrence are determined according to the methods described in Section 2.5.2.2.1.1. The full logic tree for the Mmax zones model alternative is shown in Figure 2.5.2-213.

All Mmax zones defined in the CEUS SSC model are included in the hazard calculation for the North Anna site, truncated at a distance from the site of approximately 1,000 km (see Figures 2.5.2-212 and 2.5.2-219). Maximum magnitude distributions and expected future rupture characteristics for Mmax zones are described in Tables 2.5.2-208 and 2.5.2-209.

2.5.2.2.2.1 MESE (wide and narrow)

As discussed in Section 2.5.1, rifting of the African and North American plates created a series of Mesozoic basins trending parallel to the Appalachian orogenic belt. Those portions of the CEUS exhibiting such Mesozoic-and-younger extension (MESE) are included in the MESE

Mmax zone (Figure 2.5.2-212). Although Mesozoic basins are known to exist in the modern-day Piedmont, Blue Ridge, Coastal Plain, and Continental Shelf physiographic provinces, the western termination of Mesozoic extension is poorly constrained. To account for this uncertainty, two alternatives for the MESE Mmax zone are modeled: a “narrow” MESE (MESE-N), which only includes the portion of the CEUS that exhibits clear Mesozoic-and-younger extension, and a “wide” MESE (MESE-W) that extends further west to capture areas of more questionable Mesozoic-and-younger extension (see Figure 2.5.2-212). The MESE-N zone is the more heavily weighted alternative due to the fact that evidence supporting this alternative is more technically defensible.

The largest historical earthquake in both the MESE-N and MESE-W zones that is not associated with an RLME source is the 1732 E[**M**] 6.25 St. Lawrence region earthquake (Reference 2.5-223). Modeled Mmax values and weights for the MESE-N and MESE-W zones are listed in Table 2.5.2-208. A full description of the MESE-N and MESE-W zones is provided in the CEUS SSC Report, Sections 6.2, 6.3, and 6.4.

2.5.2.2.2.2 NMESE (wide and narrow)

The portion of the CEUS that is not interpreted to have experienced Mesozoic-and-younger extension (NMESE) is modeled by the NMESE Mmax zone. As is the case for the MESE, the NMESE is modeled by “narrow” and “wide” alternatives (see Figure 2.5.2-213). These alternatives, however, are labeled according to their corresponding MESE zone. The result is that the NMESE-N zone is actually wider than the NMESE-W zone, since the “-N” and “-W” designators for the NMESE refer to the width of the MESE zone (see Figure 2.5.2-212).

The largest historical earthquakes in the NMESE-N and NMESE-W zones that are not associated with an RLME source are, respectively, the 1897 E[**M**] 5.91 Giles County, Virginia earthquake and the 1909 E[**M**] 5.72 earthquake of eastern Montana (Reference 2.5-223). Modeled Mmax values and weights for the NMESE-N and NMESE-W zones are listed in Table 2.5.2-208. A full description of the NMESE-N and NMESE–W zones is provided in the CEUS SSC Report, Sections 6.2, 6.3, and 6.4.

2.5.2.2.2.3 Study Region

The statistical analysis conducted for the CEUS SSC model concluded that there is only a marginally significant probability the MESE and NMESE could be characterized by unique prior distributions. As such, an alternative model in which the entire study region is treated as a single Mmax zone, labeled as the Study Region zone (see Figure 2.5.2-212). This is indicated on the Mmax Zones logic tree as the "No" branch of the "Separation of Mesozoic Extended and Non-extended" node, which is assigned a weight of 0.4 (see Figure 2.5.2-213).

The largest historical earthquake attributed to the Study Region Mmax zone that is not associated with an RLME source is the 1732 E[**M**] 6.25 St. Lawrence region earthquake (Reference 2.5-223). Modeled Mmax values and weights for the Study Region zone are listed in Table 2.5.2-208.

2.5.2.2.3 CEUS SSC Seismotectonic Zones Included in the North Anna PSHA

In contrast to the Mmax zones, seismotectonic zones in the CEUS SSC model are distinguished from one another based on a variety of crustal properties and characteristics (e.g., tectonic history, structural grain, seismicity rates, and Mmax; see Figures 2.5.2-214 and 2.5.2-215). The uncertainty related to the location of zone boundaries is only considered for a few of the seismotectonic zones, with the assumption that site-specific studies will examine zone boundaries in more detail as necessary. In all seismotectonic zones, recurrence rate and Mmax are calculated according to the procedures detailed in Sections 2.5.2.2.1.2 and 2.5.2.2.1.3. The full logic tree for the seismotectonic zones model alternative is shown in Figures 2.5.2-216 and 2.5.2-217.

The seismotectonic zones included in the hazard calculation for the North Anna 3 site are the Extended Continental Crust-Atlantic Margin (ECC-AM), Atlantic Highly Extended Crust (AHEX), Paleozoic Extended Crust Narrow (PEZ-N) and Paleozoic Extended Crust Wide (PEZ-W), Midcontinent-Craton (Mid) model alternatives MidC-A though MidC-D, St. Lawrence Rift (SLR), and Illinois Basin Extended Basement (IBEB) zones Each zone is truncated at a distance of 1,000 km from the site.

2.5.2.2.3.1 ECC-AM

The ECC-AM seismotectonic zone encompasses the portions of the Piedmont, Coastal Plain, and Continental Shelf physiographic provinces

that have experienced Mesozoic-and-younger extension (see Figure 2.5.2-220). The rationale for defining this zone is primarily based on the observation that all **M**>7 earthquakes in SCR crust occur within Mesozoic-and-younger extended crust (Reference 2.5-286). In addition, the continental crust outside the ECC-AM is characterized by a different structural grain and reactivation history, suggesting a difference in future earthquake rupture characteristics. In the vicinity of the site, the boundaries of the ECC-AM zone are the Piedmont gravity anomaly to the west, the western boundary of the East Coast Magnetic Anomaly (ECMA) to the east, and the Brunswick magnetic anomaly to the south as depicted in Figure 2.5.2-221.

The primary structural feature of the ECC-AM zone is an east-dipping Paleozoic basal thrust that juxtaposes sheared Appalachian terranes against the underlying North American craton (see SSAR Figures 2.5-2 and 2.5-8). The Appalachian terranes host a number of Paleozoic thrust faults that have been reactivated during Mesozoic extension. Possible Pleistocene activity has been proposed for the Everona-Mountain Run fault system based on faulted gravel deposits of questionable age (e.g., Prowell, 1988 (Reference 2.5-289); Manspeizer et al., 1989 (Reference 2.5-290); Crone and Wheeler, 2000 (Reference 2.5-291)), however, no faults within the ECC-AM show direct evidence for Quaternary activity. Expected future earthquake characteristics within the ECC-AM zone are summarized in Table 2.5.2-210.

Seismicity within the ECC-AM zone is spatially variable. For example, in the region of the site, notable clusters of earthquakes occur in central Virginia (Central Virginia seismic zone, see Section 2.5.1.1.4.d.1), and Charleston, South Carolina (see Section 2.5.1.1.4.d.3) (See Figure 2.5.2-222). The largest non-RLME historical earthquake to have occurred within the ECC-AM zone is the 1755 E[**M**] 6.10 Cape Ann, Massachusetts earthquake. Given location uncertainty for this event, however, it was assigned in the CEUS SSC Report a 60 percent probability of having occurred within the ECC-AM, leaving a 40 percent probability that the largest earthquake within the ECC-AM is instead the June 11, 1638 E[**M**] 5.32 earthquake (Reference 2.5-223). The recent 2011 E[**M**] 5.71 Mineral earthquake occurred after the development of the CEUS SSC earthquake catalog. This earthquake in 2011 now represents the second largest earthquake in the ECC-AM that is not associated with an RLME source. Further discussion of this earthquake is included in

Section 2.5.2.1, and its impact on Mmax and earthquake rate assessments is discussed in Section 2.5.2.4. Mmax values and weights for the ECC-AM zone as originally modeled by EPRI et al. (2012) (Reference 2.5-223) are listed in Table 2.5.2-211. Revisions to the ECC-AM Mmax distribution based on the Mineral earthquake are indicated in a footnote to Table 2.5.2-211.

2.5.2.2.3.2 AHEX

The phase of Mesozoic extension affecting the continental crust of the ECC-AM occurred to a greater extent in the adjacent mafic oceanic crust; this thinned oceanic crust is represented as the AHEX seismotectonic zone. The greater degree of extension in this zone has produced crust that is 15-30 km thick, thinner than the 35-40 km thickness of the ECC-AM. Although seismological data within the AHEX are too sparse to directly assess seismogenic thickness, the observation of thinner crust is taken to indicate that seismogenic thickness is correspondingly thinner. This is expected to result in a significant difference in future earthquake rupture characteristics between the ECC-AM and AHEX zones (see Table 2.5.2-210). In addition, the AHEX zone can be compositionally distinguished from the ECC-AM due to the introduction of large amounts of basalt during extension of the AHEX zone.

The AHEX zone lies entirely offshore (see Figure 2.5.2-220), roughly paralleling the continental shelf. The boundary between the ECC-AM zone and the AHEX zone is the ECMA (see Figure 2.5.2-221), which has been shown to be spatially correlated with the easternmost extent of continental crust using seismic reflection data (e.g., LASE Study Group, 1986 (Reference 2.5-292), Austin et al., 1990 (Reference 2.5-293)).

The largest historical earthquake in the AHEX zone is the September 24, 1996 E[**M**] 2.89 earthquake (Reference 2.5-223). Due to the sparse seismicity of the AHEX zone, the Kijko (2004) (Reference 2.5-287) methods of Mmax calculation (which depend on observed seismicity) are not used in the calculation of Mmax. Modeled Mmax values and weights for the AHEX zone are listed in Table 2.5.2-211.

2.5.2.2.3.3 PEZ (wide and narrow)

As described in Section 2.5.1, the African and North American plates experienced several phases of rifting and collision. The Mesozoic phase of rifting and associated continental extension discussed above partially overprinted structures formed during a more extensive phase of late

Proterozoic to early Paleozoic rifting (during the opening of the Iapetus Ocean). The portion of the craton containing all known and inferred normal faulting associated with the opening of the Iapetus Ocean is the Iapetan rifted margin (IRM) (Wheeler, 1995) (Reference 2.5-294). The western boundary of the IRM is poorly defined, since Paleozoic rift structures irregularly decrease in size and abundance to the west.

In the CEUS SSC model, the IRM is divided into three seismotectonic zones: the Northern Appalachian (NAP), SLR, and Paleozoic Extended Crust (PEZ) zones (see Figures 2.5.2-214 and 2.5.2-215). The PEZ zone is the portion of the IRM abutting against the ECC-AM zone. The boundary between the PEZ and ECC-AM zones is marked by the Piedmont gravity gradient (see Figure 2.5.2-221). Due to the uncertainty associated with the western boundary of the IRM, two alternative geometries of the PEZ zone are modeled in the CEUS SSC. In the PEZ Narrow (PEZ-N) geometry, the western boundary of the zone is formed by the Birmingham basement fault system of Alabama and the New York-Alabama lineament. This zone geometry encompasses the most well-defined set of Iapetan faults and rift sediments in the North American craton, and is heavily favored in the CEUS SSC model. The PEZ Wide (PEZ-W) geometry includes more tentative evidence of Iapetan rifting, and extends to the Rome trough of Kentucky and West Virginia. Expected future earthquake characteristics for both zones are summarized in Table 2.5.2-210.

In the region of the site, concentrated zones of seismicity of the PEZ zones occur in the Eastern Tennessee seismic zone (Section 2.5.1.1.4.d.3) and in the GCVSZ (Section 2.5.1.1.4.d.2) (See Figure 2.5.2-222). The GCVSZ produced the 1897 Giles County earthquake (MMI = VIII, m_b = 5.7, E[**M**] 5.91), the largest observed earthquake in the PEZ seismotectonic zones (Reference 2.5-223). Modeled Mmax values and weights for the PEZ-N and PEZ-W zones are listed in Table 2.5.2-211.

2.5.2.2.3.4 MidC

The portion of the CEUS SSC model that did not experience Mesozoic-and-younger extension is represented by the MidC seismotectonic zone (see Figure 2.5.2-220). The seismotectonic character of this zone is instead shaped by Paleoproterozoic plate collisions that formed the core of the North American continent. These collisions resulted in deeply buried Precambrian crustal structures that

overlie a thick, strong, and compositionally depleted lithosphere (i.e., lithosphere from which certain dense minerals have been extracted via partial melting, resulting in a relatively buoyant, thick, and anhydrous composition). The absence of Mesozoic-and-younger extension, as described by Johnston et al. (1994) (Reference 2.5-286) and in Section 2.5.2.2.3.1, is expected to lower the Mmax potential of the MidC seismotectonic zone. In addition, Mooney and Ritsema (2009) (Reference 2.5-295) show that high lithospheric S-wave velocities (which serve as a proxy for high lithospheric strength) are correlated with lower Mmax potential. The MidC is further differentiated from other midcontinental sources based on the expectation that neighboring zones will have different future earthquake rupture characteristics (Table 2.5.2-210), in part due to differences in structural grain.

The northern and western boundaries of the MidC zone terminate at the CEUS study region boundary (see Figures 2.5.2-214 and 2.5.2-215). The location of the southern and eastern boundaries of the MidC zone, however, vary based on the alternative geometries of neighboring seismotectonic zones, which results in four alternative MidC zone geometries. These model alternatives are labeled MidC-A, MidC-B, MidC-C, and MidC-D (see Figures 2.5.2-214 and 2.5.2-215). Although only MidC-A and MidC-B intersect the 200-mile site region, all four model alternatives are included in the baseline hazard calculation (see Figure 2.5.2-220).

As is the case throughout the CEUS region, seismicity in the MidC seismotectonic zone is spatially variable. Although several concentrated areas of seismicity occur in the MidC zone (e.g., the Anna, Ohio seismic zone (Figure 2.5.2-222) and the Northeast Ohio seismic zone), there is not enough evidence to suggest that any of these areas produce RLMEs. The largest earthquake in this zone that is not associated with an RLME source is the 1909 E[**M**] 5.72 earthquake of eastern Montana (Reference 2.5-223). Modeled Mmax values and weights for all MidC seismotectonic zones are listed in Table 2.5.2-211.

2.5.2.2.3.5 St. Lawrence Rift

The SLR zone is one of three seismotectonic zones that constitute the IRM (see Section 2.5.2.2.3.3). The SLR is therefore primarily defined as that portion of the crust that was rifted during the opening of the Iapetus Ocean. However, crust in the SLR is differentiated from the rest of the IRM by evidence for multiple phases of reactivation (Tremblay et al.,

2003 (Reference 2.5-296); Lemieux et al., 2003 (Reference 2.5-297); Rocher et al., 2003 (Reference 2.5-298); Rimando and Benn, 2005 (Reference 2.5-299)), and a history of moderate to large magnitude earthquakes.

The SLR seismotectonic zone encompasses several prominent Iapetan grabens and areas of rift-related volcanic intrusions. At its closest approach, the SLR seismotectonic zone extends to within approximately 590 km of the site (see Figure 2.5.2-214). Sensitivity calculations to assess hazard contributions from distant sources, however, indicate that this source contributes 0.5 percent of the total 1 Hz hazard at the 10^{-4} hazard level. When combined with contributions from two other distant sources (IBEB and Wabash Valley), these three zones exceed 1 percent of the total hazard.

Seismicity rates vary throughout the SLR. The ubiquitous distribution of moderate to large magnitude earthquakes, when coupled with paleoseismic data, suggests that the entire SLR seismotectonic zone has the potential to produce moderate to large magnitude earthquakes. The largest non-RLME earthquake magnitude within this zone is the September 16, 1732 E[**M**] 6.25 event (Reference 2.5-223). Modeled Mmax values for the SLR seismotectonic zone are provided in Table 2.5.2-211.

2.5.2.2.3.6 Illinois Basin Extended Basement

The IBEB seismotectonic zone models seismicity associated with the Illinois basin, which is an area of structural complexity within the midcontinent (McBride et al., 2007) (Reference 2.5-300). The primary rationale for defining this zone is the observation of an elevated rate of instrumental seismicity compared to the neighboring craton, as well as evidence for moderate-magnitude earthquakes in the paleoearthquake record. Additionally, the structural complexity of the IBEB zone suggests that its crust is distinct from the crust in neighboring zones.

The boundaries of the IBEB zone are based on the oval shape of the Illinois basin and the spatial distribution of underlying Precambrian basement structures. The extent of these basement structures, however, is poorly constrained. At its closest approach, the IBEB zone extends to within approximately 700 km of the site (see Figure 2.4-214). Sensitivity calculations to assess hazard contributions from distant sources indicate that this source contributes 0.2 percent of the total 1 Hz hazard at the

10^{-4} hazard level. When combined with contributions from two other distant sources (SLR and Wabash Valley), these three zones exceed 1 percent of the total hazard.

Seismicity within the IBEB zone is concentrated at its southern end, adjacent to the Reelfoot rift. Although McBride et al. (2007) (Reference 2.5-300) note that seismicity tends not to be clearly associated with mapped structures in the IBEB zone, the location of some moderate-magnitude earthquakes suggests that Precambrian basement faults and Paleozoic faults are being reactivated. The largest historical non-RLME event in the IBEB seismotectonic zone is the September 27, 1891 E[**M**] 5.52 earthquake (Reference 2.5-223). Paleoliquefaction studies, however, suggest that the IBEB zone has experienced one approximately **M** 6.3 event and three approximately **M** 6.2 events (Reference 2.5-223). Modeled Mmax values for this seismotectonic zone are provided in Table 2.5.2-211.

2.5.2.2.4 CEUS SSC RLME Sources Included in the North Anna PSHA

In several places throughout the CEUS, historical and paleoearthquake records point to the repeated occurrence of large-magnitude (**M**≥6.5) earthquakes in specific locations (see Figure 2.5.2-218). Due to the amount of strain accumulation needed to generate a large magnitude earthquake, these events are most often interpreted from the paleoearthquake record. This inherently results in a bias in the location of RLMEs throughout the model, as the spatial coverage of the paleoearthquake record is more limited than that of the historical record. This limitation is recognized in the CEUS SSC model, and is accounted for by allowing significant earthquake potential in the distributed seismicity sources.

The only RLME sources that contribute significantly to hazard at the site are Charleston, New Madrid, and Wabash Valley sources. Each of these sources is described in detail below.

2.5.2.2.4.1 Charleston

The largest historical earthquake in the eastern U.S. occurred in Charleston, South Carolina in 1886. Estimates of the magnitude of this earthquake are based on liquefaction data and isoseismal area regressions, and vary from the high-6 to mid-7 range (Reference 2.5-223). In addition, a number of geologic investigations

have documented evidence for large pre-1886 earthquakes in the Charleston, South Carolina area based on sand blows and paleoliquefaction features (e.g., Obermeier et al., 1989 (Reference 2.5-301); Weems and Obermeier, 1990 (Reference 2.5-302); Amick et al., 1990a (Reference 2.5-303), 1990b (Reference 2.5-304); Talwani and Schaeffer, 2001 (Reference 2.5-305); Talwani et al., 2008 (Reference 2.5-306)). Based on the quality and quantity of the available data, Charleston is modeled as an RLME source in the CEUS SSC model. At its closest approach, the Charleston RLME source is approximately 430 km from the site (see Figures 2.5.2-222 and 2.5.2-223).

No tectonic features have been conclusively correlated with the 1886 earthquake. In addition, although a number of faults have been postulated in the Charleston area, none have been shown to be tectonically active. In order to account for the spatial uncertainty associated with Charleston RLME source, three alternative geometries are modeled (see Figures 2.5.2-223, 2.5.2-224, and 2.5.2-225). The Charleston Local geometry encompasses the area with the densest concentration of liquefaction associated with the 1886 earthquake and prehistoric earthquakes, the meizoseismal area of the 1886 earthquake, and the majority of local tectonic features. This alternative is the most heavily weighted of the three. The Charleston Narrow geometry is based on the location and orientation of postulated faults and tectonic features in the Charleston area, resulting in a relatively narrow, north-northeast oriented source geometry. The Charleston Regional geometry encompasses the Local and Narrow zones, along with outlying paleoliquefaction sites and other tectonic features. In all cases, future earthquakes are modeled as occurring on *pseudo*faults with the properties listed in Table 2.5.2-210.

Geologic and geomorphic studies have suggested that the seismic activity of the Charleston RLME source since the mid-Holocene may not be indicative of the long-term recurrence rate (e.g., Chapman and Beale, 2008, 2010 (References 2.5-307 and 2.5-308)). Models of temporal clustering used to account for this uncertainty are discussed in detail in the CEUS SSC Report, Section 5.1.2, and further uncertainties associated with the earthquake recurrence rate are discussed in the CEUS SSC Report, Section 6.1.2.5.

The CEUS SSC earthquake catalog assigns E[**M**] 6.90 to the 1886 Charleston earthquake. Geotechnical studies in the Charleston, South Carolina area suggest that prehistoric large earthquakes were in the high-5 to high-7 range (e.g., Hu et al., 2002a, 2002b (References 2.5-309 and 2.5-310); Leon et al., 2005 (Reference 2.5-311); Gassman et al., 2009 (Reference 2.5-312)). Based on the assumption that future earthquakes in the Charleston RLME source will be similar to previous large earthquakes in the Charleston area, the CEUS SSC model assigns Mmax values of between **M** 6.7 and **M** 7.5 (see Table 2.5.2-212).

2.5.2.2.4.2 New Madrid Fault System

The three largest historical earthquakes in the CEUS region all occurred in the New Madrid area. These earthquakes occurred on December 16, 1811, January 23, 1812, and February 7, 1812, and a great deal of uncertainty exists regarding their exact magnitudes. In addition, a number of paleoliquefaction studies document multiple major prehistoric earthquakes in the New Madrid area (e.g., Saucier, 1991 (Reference 2.5-313); Tuttle and Schweig, 2001 (Reference 2.5-314); Tuttle et al., 2002 (Reference 2.5-315); Tuttle et al., 2005 (Reference 2.5-316)). Based on these observations, the CEUS SSC model defines the New Madrid fault system (NMFS) as an RLME to account for large prehistoric earthquakes and the three large events that occurred in 1811-1812. At its closest approach, this RLME is approximately 970 km from the site (see Figure 2.5.2-218).

Modern seismic activity within the New Madrid area closely aligns with the three fault segments that constitute the NMFS (also occasionally referred to as “Reelfoot Rift Central Fault System” in CEUS SSC Report) (see Figure 2.5.2-223). These individual fault segments (New Madrid North, New Madrid South, and Reelfoot Thrust) have been associated with the earthquakes of the 1811-1812 sequence (see discussion in the CEUS SSC Report, Section 6.1.5, and sources therein). Consequently, the geometry of the NMFS RLME source is narrowly defined, with alternative geometries for long and short interpretations of the New Madrid North fault and the Reelfoot thrust (see Figures 2.5.2-226 and 2.5.2-227). Alternative geometries for the New Madrid South fault either combine the Blytheville arch with the Bootheel lineament or the Blytheville fault zone (see Figure 2.5.2-226).

Seismic reflection data (e.g., Schweig and Ellis, 1994 (Reference 2.5-317); Van Arsdale, 2000 (Reference 2.5-318)) and

geomorphic observations (e.g., Holbrook et al., 2006) (Reference 2.5-319) suggest that the Holocene Epoch represents a period of temporally clustered earthquake activity along the NMFS that is not representative of the long-term rate of activity. Additionally, geodetic studies suggest that the present rate of strain accumulation is much too small to account for the Holocene rate of paleoseismicity (Calais et al., 2005 (Reference 2.5-320); Smalley et al., 2005 (Reference 2.5-321)). To account for uncertainty in the future rate of earthquakes in the NMFS RLME, the CEUS SSC model allows for alternatives (at very low weights) in which some or all of the fault segments of the NMFS are inactive. A detailed discussion of the recurrence of large earthquakes in the NMFS RLME source is presented in CEUS SSC Report, Section 6.1.5.4.

The Mmax distribution for the NMFS RLME source is based on the estimated magnitudes of the earthquakes in the 1811-1812 sequence. The CEUS SSC model equally weights the estimates from Bakun and Hopper (2004) (Reference 2.5-322), Johnston (2004, personal communication, as cited in Reference 2.5-223)), and Hough and Page (2011) (Reference 2.5-323), which are **M** 7.2 to **M** 7.8, **M** 7.5 to **M** 7.9, and **M** 6.5 to **M** 6.9, respectively. The resulting Mmax distribution for the NMFS RLME source in the CEUS SSC model ranges from **M** 6.7 to **M** 7.9 (see Table 2.5.2-213).

All other uncertainties identified in the NMFS logic tree (see Figure 2.5.2-227) are included in the North Anna 3 site hazard calculation exactly as detailed in the CEUS SSC Report, with the exception of seismogenic depth, which is simplified from the distribution listed in Table 2.5.2-210 to a single value of 15 km. Given the distance of the NMFS RLME source to the site, this simplification is judged to be adequate for the Unit 3 PSHA.

2.5.2.2.4.3 **Wabash Valley**

Liquefaction features within the southern Illinois basin provide evidence for at least eight Holocene to latest Pleistocene earthquakes, which are estimated to be between approximately **M** 6 and **M** 7.8 (Obermeier et al., 1991 (Reference 2.5-324); Munson et al., 1997 (Reference 2.5-325); Pond and Martin, 1997 (Reference 2.5-326); Obermeier, 1998 (Reference 2.5-327); McNulty and Obermeier, 1999 (Reference 2.5-328); Tuttle et al., 1999 (Reference 2.5-329)). The proximity of the two largest paleoearthquakes (referred to in the literature as “Vincennes” and “Skelton”) to the strongest historical events in the Wabash Valley area

suggests that this is a source of repeating large-magnitude earthquakes. The Wabash Valley area is therefore modeled as an RLME source in the CEUS SSC model.

At its closest approach, this RLME source extends to within approximately 780 km of the site (see Figure 2.5.2-218). Sensitivity calculations to assess hazard contributions from distant RLME sources, however, found that this source contributes 0.4 percent of the total 1 Hz hazard at the 10^{-4} hazard level. When combined with contributions from two other distant sources (SLR and IBEB), these three zones exceed 1 percent of the total hazard.

The tectonic features responsible for large-magnitude earthquakes in Wabash Valley are not known. The geometry of the Wabash Valley RLME therefore captures a range of potentially causative structures, neotectonic deformation, and inferred energy centers for the two largest paleoearthquakes in the region. Further uncertainty specified by the CEUS SSC Report related to the style, orientation, and focal depth of Wabash Valley earthquakes is detailed in Table 2.5.2-210. For the Unit 3 PSHA, earthquakes within the Wabash Valley source are represented as point sources using the EPRI (2004) (Reference 2.5-224) correction factors for rupture distance.

Estimates of the magnitudes of the Vincennes and Skelton paleoearthquakes range from **M** 7.0-7.8 and **M** 6.3-7.3, respectively (see the CEUS SSC Report, Section 6.1.9.3). The difference in magnitude between these two paleoearthquakes is assumed to reflect both aleatory uncertainty and epistemic uncertainty in the estimation of the characteristic Wabash Valley RLME magnitude. As a result, the modeled maximum magnitude for this RLME source is broadly distributed from **M** 6.75 to **M** 7.5 (see Table 2.5.2-214).

2.5.2.2.5 Post-CEUS SSC Studies

This section describes geologic and seismic investigations of the site region and provides information that can be used to evaluate and potentially update the CEUS SSC model relevant to the Unit 3 PSHA. Specifically, these studies include ongoing investigations of the 2011 Mineral earthquake that occurred in or near the CVSZ and the geologic investigations of the ETSZ.

2.5.2.2.5.1 Investigations of the 2011 Mineral Earthquake

The **M** 5.8 Mineral earthquake, as described in Sections 2.5.1.1.7 and 2.5.2.1.3, occurred southwest of the Unit 3 site and near the town of Mineral (Figure 2.5.2-228). A series of aftershocks highlighted the rupture plane of the Mineral earthquake, which was previously unrecognized at the surface or in the subsurface (see Figure 2.5.1-203). Aftershocks ranged in depth from 1 to 7.5 km and included events up to **M** 3.9 (Horton et al., 2012 (Reference 2.5-232); VTSO, 2012 (Reference 2.5-330)). Walsh et al. (2011) (Reference 2.5-331) suggest that aftershocks of the Mineral earthquake, as well as other intraplate earthquakes, could last up to 100 years, as opposed to only a few years in more tectonically active margins (e.g., Southern California).

The majority of 2011 Mineral earthquake aftershock hypocenters defined a concave-up, curvi-planar surface (References 2.5-232 and 2.5-235), while several smaller clouds of aftershocks were located up to about 10 km from the primary cloud (see Figure 2.5.1-203) (References 2.5-232 and 2.5-330). The strike of the 10-km-long primary aftershock plane that best fits these aftershock locations is oriented approximately north-northeast with a moderate dip of about 45 degrees to the east (Ellsworth et al., 2011 (Reference 2.5-332); Horton et al., 2012 (Reference 2.5-232); Chapman, 2012 (Reference 2.5-235); SLU, 2012 (Reference 2.5-241)). Propagation of the rupture was complex, exhibiting three distinct slip events: a smaller and deeper initiation event, followed by two larger and shallower events (Reference 2.5-235). Focal mechanisms of the mainshock indicate a primarily reverse sense of slip (Reference 2.5-268).

The earthquake caused moderate damage in the epicentral region, although felt intensity at close distances (less than 100 km) was less than predicted by Atkinson and Wald (2007) (Reference 2.5-272) relations (Assatourians and Atkinson, 2011) (Reference 2.5-273). Ground motions at larger distances were in relatively close agreement with the Atkinson and Wald (2007) relations, and the earthquake was felt by more people than any other earthquake in U.S. history (Carter et al., 2012) (Reference 2.5-233). At short periods (0.2 sec), ground motions agreed well with eastern ground motion prediction equations, but were less than expected at longer periods (1.0 sec) (Reference 2.5-234).

Geologic evidence of the 2011 Mineral earthquake was sparse, although some coseismic features were observed. Rock falls were identified over

a wide region covering most of mountainous Virginia and parts of Maryland and West Virginia (EERI, 2011 (Reference 2.5-333); GEER, 2011 (Reference 2.5-334); Carter et al., 2012). Four sand boils (two definite, one likely, and one questionable) were observed in two locations that lie within the approximate vertical surface projection of the rupture plane (EERI, 2011; GEER, 2011 (Reference 2.5-334); Green and Lasley, 2012 (Reference 2.5-243)).

Despite targeted searches in the field, the EERI (2011), GEER (2011), and investigations performed for this project did not identify surface rupture associated with the 2011 Mineral earthquake (Sections 2.5.1.1.7 and 2.5.3.4). In addition to field reconnaissance, geomorphic analyses were performed for this project that utilized high-resolution light detection and ranging (lidar) elevation data. These geomorphic analyses included stream profile analyses, and interpretation of several lidar-derived data sets. The analyses revealed no signs of surface rupture, and only questionable evidence that could be interpreted as related to tectonic deformation. The consensus results of these investigations suggest that the Mineral earthquake occurred on a previously unrecognized structure, the dimensions of which are not observable at the ground surface or well defined by evidence beyond the distribution of aftershock hypocenters recorded following the Mineral earthquake.

Therefore, it is appropriate to evaluate the 2011 Mineral earthquake within the CEUS SSC model framework to determine whether the event alters the magnitude and recurrence distributions in the host zones (ECC-AM, MESE-N, MESE-W, and Study Region). Sensitivity analyses were performed for both Mmax and earthquake recurrence in these zones, resulting in modification of certain Mmax and recurrence parameters for distributed seismicity zones, as described in Section 2.5.2.4. Earthquakes in background sources (such as ECC-AM) are modeled conceptually as finite ruptures on randomly located faults with random orientations, and the correct distance is calculated to those ruptures. Thus the model includes (as one of many possibilities) an earthquake such as the Mineral earthquake, both at its location and at all other possible locations within each background source. The 2011 Mineral earthquake is not included as an RLME source in the Unit 3 PSHA, since, by definition, RLME sources are locations of repeated (more than one) large-magnitude (**M** ≥6.5) earthquakes in the historical or paleoseismic record.

2.5.2.2.5.2 Geologic Investigations of the Eastern Tennessee Seismic Zone

At its nearest point, seismicity associated with the ETSZ is approximately 500 km from the site (see Figure 2.5.2-222). The ETSZ can be identified as a narrow trend of concentrated seismicity east of the New York-Alabama magnetic lineament (Chapman et al., 2002) (Reference 2.5-335). However, in spite of the high rate of seismic activity, the largest historical earthquake in the region is magnitude 4.6 (magnitude scale unspecified) (References 2.5-335 and 2.5-336).

The most recent geologic studies of the ETSZ either post-date the CEUS SSC model or were published during development of the CEUS SSC model. These studies suggest that the ETSZ may have produced large prehistoric earthquakes. Vaughn et al. (2010) (Reference 2.5-337) find evidence of minor surface faulting, fracturing, and disrupted features in terrace alluvium, along with minor paleoliquefaction, northeast of Knoxville, Tennessee. Similarly, the study of Douglas Reservoir documents fracture systems and sandy intrusions in terrace deposits that they interpret as paleoseismic in origin, although the significance of these features is unclear (Reference 2.5-336). Howard et al. (2011) (Reference 2.5-338) and Warrell et al. (2012) (Reference 2.5-339) document fractures, small faults, and displacements in Quaternary alluvium along Douglas Reservoir that they suggest resulted from earthquakes with magnitudes greater than 6.0 and 6.5 (magnitude scale unspecified).

While these recent studies strengthen the argument that the ETSZ has experienced at least one moderate-sized earthquake in the late Quaternary, they do not quantify parameters (e.g., recurrence interval, magnitude) necessary to demonstrate that the ETSZ produces repeating large-magnitude events. As such, the ETSZ is modeled within the MESE Mmax zone and the PEZ seismotectonic zone using smooth seismicity. No RLME source is defined for the ETSZ.

2.5.2.3 Correlation of Seismicity with Seismic Sources

The CEUS SSC earthquake catalog includes earthquakes in the CEUS from 1568 through the end of 2008, and its development is discussed in Section 2.5.2.1. As described in that section, the catalog has been updated for Unit 3 to include events through mid-December 2011, including the 2011 Mineral earthquake (see Figure 2.5.2-202). The complete CEUS SSC earthquake catalog comprises 10,984 earthquakes

of uniform moment magnitude E[**M**] 2.2 and larger, including 3,298 events added during the update of the earthquake catalog as described in Section 2.5.2.1. The complete catalog and the updated events include dependent events and earthquakes with E[**M**] ≥ 2.2. For rate calculations, the dependent and small events are removed, but patterns of seismicity are better illustrated when these events are included (e.g., as shown in Figures 2.5.2-212, 2.5.2-219, 2.5.2-220, 2.5.2-222, 2.5.2-223, and 2.5.2-226). Over 80 percent of the independent earthquakes in the CEUS SSC earthquake catalog with E[**M**] ≥ 2.9 are contained in the 2008 NSHMP earthquake catalog (Reference 2.5-253), with remaining events gathered from special studies, and local and regional catalogs (Reference 2.5-223).

The uncertainty in the horizontal location of earthquakes included in the CEUS SSC earthquake catalog is the result of a combination of standard errors for instrumentally recorded earthquakes from the various catalog sources and estimates based on accounts of shaking intensity. In general, location uncertainties have improved through time, with horizontal uncertainties up to 50 km for less well-documented events in the earliest part of the catalog, to as little as 1-2 km for well-recorded events in the most recent part of the catalog (see CEUS SSC Report, Appendix B).

Earthquake depths are reported in the updated CEUS SSC earthquake catalog based on data from source catalogs, or depths documented in a variety of published sources. Many of the earthquake depths represent fixed crustal depths for either shallow or deep events. For example, the NEIC catalog uses fixed depths of 10 km for shallow events and 33 km for deep events (cf. Reference 2.5-223). Additionally, many earthquakes in the CEUS SSC earthquake catalog are assigned a depth of 0 km when no data are available to provide a basis for an estimate. This is most common in the earlier years of the catalog. Alternative depth estimates are presented if more than one value was reported in source catalogs or published literature, however, depth uncertainties are not provided in the CEUS SSC earthquake catalog. Despite these horizontal and depth location uncertainties, gross regional patterns of seismicity are preserved and partially form the basis for defining some CEUS SSC seismic sources.

As described in Section 2.5.2.2, the CEUS SSC source model defines three types of seismic sources: Mmax zones, zones of repeated

large-magnitude earthquakes (RLMEs), and seismotectonic zones. Mmax zones are defined on expected differences in Mmax potential and are broad zones that are not defined on the basis of geologic structures or the spatial distribution of seismicity. The discussion of correlation of seismicity with seismic sources presented in this section is limited to seismotectonic zones and RLME sources significant to the site (Sections 2.5.2.2.3 and 2.5.2.2.4, respectively).

There are no RLME sources within the 200-mile radius site region (see Figure 2.5.2-218) but, as described in Section 2.5.2.2.4, the Charleston, South Carolina, NMFS, and Wabash Valley RLMEs are included in the Unit 3 PSHA. At its nearest point, the Charleston RLME is located approximately 430 km south of the site. The NMFS and Wabash Valley RLMEs are located approximately 970 km and 780 km west of the site, respectively. The correlation of seismicity with these two RLMEs is described in the following text.

Charleston - The Charleston RLME, as described in Section 2.5.2.2.4.1, represents the Charleston seismic zone, the source for the largest recorded earthquake in the eastern U.S., the 1886 Charleston E[**M**] 6.90 earthquake (see Figure 2.5.2-223). The Charleston seismic zone is characterized by sparse seismicity (in comparison to the Eastern Tennessee or New Madrid seismic zones) that is tightly concentrated, but lacking prominent linear trends. There is no evidence that indicates a correlation of well-documented prehistoric large earthquakes or historical earthquakes with a discrete structure. Therefore, three alternative zones are hypothesized for the Charleston RLME that are based on locations of posited fault sources, damage, felt intensity, and/or density of liquefaction features. Theorized fault sources, spaced about 10 km apart, are modeled throughout the zones, and are based on the rupture strikes listed in Table 2.5.2-210. This approach accounts for uncertainty in the location, extent, and existence of faulting, reflecting the poor understanding of the correlation of earthquakes with structures in the Charleston seismic zone.

New Madrid Fault System - The NMFS RLME lies within the broader New Madrid seismic zone and represents the source of the three largest historical earthquakes in the CEUS region, and several prehistoric large earthquakes in 1811 and 1812 (E[**M**] 7.60, 7.50, and 7.80) (see Figure 2.5.2-226). A number of faults have been identified in the New Madrid seismic zone. The NMFS RLME comprises three main fault

sources, each with two alternative geometries to reflect uncertainty in their extent and/or location. The spatial distribution of seismicity defines clear, highly concentrated trends of earthquakes along these faults as seen on Figure 2.5.2-226. Seismicity also occurs away from these faults, defining a roughly 250 x 400 km concentration of earthquakes from the Marianna zone near the southern end, extending northeast along the Mississippi River to just south of northwest-trending basement structures in Illinois (see Figure 2.5.2-223). Earthquakes within this broader concentration of seismicity are commonly associated with faults comprising the Reelfoot Rift system.

Wabash Valley - The Wabash Valley RLME is designed to model large-magnitude earthquakes in the southern Illinois basin, as documented in the paleoseismic record (Section 2.5.2.2.4.3). No causative tectonic features, however, have been associated with these paleoearthquakes. This is illustrated in Figure 2.5.2-223 by the spatial distribution of historical earthquakes within this RLME source, which reveals a broadly distributed cloud of earthquakes that do not cluster along potentially causative structures. It is for this reason that the Wabash Valley RLME source geometry broadly encompasses a number of tectonic structures and neotectonic deformation in the southern Illinois basin (Section 2.5.2.2.4.3).

The seismotectonic zones are based on varying geologic and geophysical characteristics, as well as possible future rupture characteristics, such as style of faulting, seismogenic thickness, and/or rupture orientation (see Figures 2.5.2-214 and 2.5.2-215) (Reference 2.5-223). The following sections contain descriptions of the correlation of seismicity with seismotectonic zones in the CEUS SSC model located within the site region.

Extended Continental Crust – Atlantic Margin (ECC-AM) - As discussed in Section 2.5.2.2.3.1, the ECC-AM seismotectonic zone is defined primarily on the basis of Mesozoic rift-related extension. Seismicity within the ECC-AM is spatially variable, ranging from very diffuse to spatially concentrated. As seen in Figure 2.5.2-220, higher concentrations of seismicity are observed near the southern end of the ECC-AM in South Carolina, as well as along the Atlantic Coast from New Jersey northward. Additionally, the ECC-AM encompasses the CVSZ, an area with an elevated rate of generally small-magnitude seismicity (see Figure 2.5.2-222). Seismicity is generally shallow within the CVSZ, and

interpreted to occur on Paleozoic and Mesozoic faults that lie above the Appalachian detachment (Keller et al., 1985 (Reference 2.5-362); de Witt and Bayer, 1986 (Reference 2.5-363)). An area of elevated concentration of seismicity with similar characteristics occurs in the New York-Philadelphia region. These areas lack evidence for repeated, large-magnitude earthquakes and discrete faults associated with seismicity are not mapped at the surface. Thus, these seismic zones do not meet the CEUS SSC criteria for inclusion as RLMEs. Outside of these more prominent zones of seismicity, earthquakes in the ECC-AM do not appear to correlate with known geologic structures or define linear trends.

The largest observed earthquake possibly within the ECC-AM seismotectonic zone is the 1755 Cape Ann, Massachusetts E[**M**] 6.10 earthquake. Due to the uncertainty associated with the horizontal location of the Cape Ann earthquake, it is assigned a 60 percent probability of having occurred within the ECC-AM and 40 percent probability of having occurred within the Northern Appalachian seismotectonic zone (NAP) (Reference 2.5-223). When the Cape Ann earthquake is considered to have occurred in the NAP, the 2011 Mineral E[**M**] 5.71 earthquake is the largest event in the ECC-AM.

The 2011 Mineral earthquake and associated aftershocks occurred within the ECC-AM on a previously unknown structure, oriented similar to many of the thrust faults in the region. As discussed in Section 2.5.2.2.5.1, the aftershocks defined a southeast-dipping, northeast-striking rupture plane that extends from about 7.5 to 1.0 km depth (References 2.5-232 and 2.5-235). Information in the technical community does not exist for this structure that would justify addition of an RLME to the CEUS SSC model. The CEUS SSC earthquake catalog was updated to include post-2008 seismicity, including the 2011 Mineral earthquake, which resulted in local increases in the rate of seismicity in ECC-AM when rates (*a*-values) were calculated using the updated earthquake catalog.

Paleozoic Extended Crust - The PEZ seismotectonic zone represents the western portion of the Iapetus rifted margin (IRM) and includes narrow (PEZ-N) and wide (PEZ-W) alternative geometries, as discussed in Section 2.5.2.2.3.3. Seismicity within the zone is spatially variable, ranging from diffuse to concentrated, occasionally defining trends. Relatively high concentrations of seismicity are observed between Lake Ontario and Lake Erie (PEZ-W only) and at the southern end of the PEZ

zone in Alabama. Additionally, the PEZ encompasses several well-studied areas of elevated seismicity including the ETSZ and the GCVSZ (see Figure 2.5.2-229). Earthquakes within the ETSZ are generally deep, spatially associated with or limited in extent by geophysical anomalies including the Alabama-New York lineament, and define several northeast-oriented linear trends. Several studies have posited a variety of possible structures and processes associated with earthquakes in the ETSZ, including reactivated basement faults (Reference 2.5-335), depositional anisotropies (Steltenpohl et al., 2010) (Reference 2.5-364), and heterogeneity in crustal strength (Reference 2.5-343).

The GCVSZ (see Figure 2.5.2-222) is similarly characterized by deep seismicity that defines a northeast-oriented, steeply southeast-dipping tabular zone. This zone of seismicity lies beneath the Appalachian detachment in Precambrian basement (Bollinger and Wheeler, 1983 (Reference 2.5-276); 1988 (Reference 2.5-365)) and, therefore, the deep seismicity is not reflected in the geology of overlying thrust sheets. Several small-displacement faults and folds have been identified at the ground surface in terrace sands within the GCVSZ (e.g., Law et al., 1993 (Reference 2.5-366)). Whether this surface deformation is related to deep seismicity, or other processes such as karst development and collapse in underlying carbonate rocks, is unclear (e.g., Chapman and Krimgold, 1994 (Reference 2.5-367); Law et al. 1994 (Reference 2.5-368), 1997 (Reference 2.5-369)). The GCVSZ hosted the largest earthquake observed in the PEZ, the 1897 Giles County, Virginia E[**M**] 5.91 earthquake.

Atlantic Highly Extended Crust - The AHEX seismotectonic zone represents the highly extended transition between extended and thick continental crust and thin oceanic crust. The zone is defined primarily on the basis of its shallow seismogenic thickness. Only five earthquakes from the updated CEUS SSC earthquake catalog lie within the AHEX, and seismicity is sparse throughout the zone (see Figure 2.5.2-220). Therefore, trends in seismicity are not readily apparent, despite the presence of large faults inferred from geophysical data. The largest earthquake observed within the AHEX is the 1996 E[**M**] 2.89 earthquake located approximately 310 km off the coast of New Jersey.

Midcontinent-Craton Zone - The MidC seismotectonic zone comprises crust that has not been significantly deformed by Phanerozoic orogens.

Seismicity of the MidC zone is generally diffuse with a few areas of spatially concentrated seismicity including the Anna (Ohio), northeast Ohio, and Nemaha Ridge-Humboldt fault (Oklahoma, Kansas, and Nebraska) seismic zones (see Figure 2.5.2-229). Seismicity within the Anna seismic zone is spatially concentrated and tenuously associated with basement faults that comprise the Fort Wayne rift. A paleoseismic investigation by Obermeier (1995) (Reference 2.5-370) indicates a lack of large-magnitude, repeated earthquakes for several thousand years in the Anna seismic zone. Seismicity within the northeast Ohio seismic zone is defined by a northeast-trending zone of earthquakes. A 1986 E[**M**] 4.65 earthquake and aftershock sequence within the zone has been associated with northeast-trending geophysical anomalies (e.g., Seeber and Armbruster, 1993 (Reference 2.5-371); Dineva et al., 2004 (Reference 2.5-346)). In a paleoseismic investigation, however, Obermeier (1995) found a lack of evidence for large, repeated earthquakes in the zone. Seismicity within the Nemaha Ridge-Humboldt fault seismic zone is questionably associated with basement structures that are sub-parallel and west of the Proterozoic Midcontinent rift system (e.g., Wheeler and Crone, 2001 (Reference 2.5-372); Niemi et al., 2004 (Reference 2.5-373)). Outside of the seismic zones described above, spatially concentrated areas of seismicity within the MidC zone are observed in central Oklahoma and northern Alabama, and along the Nebraska-South Dakota border (see Figure 2.5.2-229).

St. Lawrence Rift Zone - The SLR seismotectonic zone encompasses crust that was deformed during two rifting episodes in the Proterozoic and Mesozoic. The zone contains several historically significant earthquakes including the 1935 Timiskaming E[**M**] 6.02 and 1988 Saguenay E[**M**] 5.84 events. Larger earthquakes have occurred within the SLR zone (E[**M**] ≥ 6.5), but they are characterized as the Charlevoix RLME. Seismicity within the SLR zone is spatially variable, ranging from diffuse to concentrated (see Figure 2.5.2-229). Earthquake depths range from shallow (less than 5 km) to deep (up to 32 km), with moderate depths most common. Higher concentrations of seismicity are observed trending not only in the northeast along the St. Lawrence River but also northwest along the Quebec-Ontario border (see Figure 2.5.2-229). These zones converge to the south in an area of concentrated seismicity that extends into the Adirondack Mountains. Several structures, for example faults within the Saguenay and Ottawa-Bonnechere grabens, have been identified as potentially seismogenic structures in previous

studies (e.g., Adams and Basham, 1991 (Reference 2.5-374); Lamontagne and Ranalli, 1997 (Reference 2.5-375)). Seismicity within the SLR seismotectonic zone is often associated with these grabens and other structures that share similar orientations.

Illinois Basin Extended Basement Zone (IBEB) - The IBEB zone encompasses faults within Precambrian basement and the Paleozoic Illinois Basin as well as a zone of liquefaction features thought to be associated with four moderate events (approximately **M** 6.20 to 6.30). The largest event to have occurred in the IBEB zone was the 1898 E[**M**] 5.5 event in southern Illinois. Larger earthquakes have occurred in the zone (E[**M**] ≥ 6.5), but they are characterized by the Wabash Valley RLME. Seismicity is sparse in the northern part of the IBEB zone, increasing regularly to the south (see Figure 2.5.2-229). Hypocentral depths range from shallow (less than 5 km) to deep (up to 27 km), with shallower earthquakes slightly more common. Earthquakes do not define linear trends or areas of concentrated seismicity. Seismicity is relatively evenly distributed and dense compared with surrounding regions not characterized as RLME sources. Several structures and processes have been posited as sources of earthquakes in the IBEB zone, but they remain poorly understood.

2.5.2.4 Probabilistic Seismic Hazard Analysis and Controlling Earthquakes

This section details the PSHA for Unit 3. In accordance with the guidance of RG 1.206 and RG 1.208, Section 2.5.2.4.1 describes the starting point for the PSHA, which is the 2012 CEUS SSC Report. Relevant new geologic and seismic information that post-dates completion of the CEUS SSC model is discussed in Section 2.5.2.4.2. Related updates to the CEUS SSC model based on this new information are discussed in Section 2.5.2.4.3. GMPEs used in the PSHA are detailed in Section 2.5.2.4.4. The results of the PSHA, including mean and fractile seismic hazard curves, the relative contribution of individual seismic sources, uniform hazard response spectra, and details on the controlling earthquakes are presented in Section 2.5.2.4.5.

2.5.2.4.1 CEUS SSC Model Implementation

The CEUS SSC model is the starting point used for probabilistic seismic hazard calculations at Unit 3. As discussed in Section 2.5.2.2, the CEUS SSC model is the most recent seismic source characterization

specifically designed for PSHAs of nuclear facilities, developed using the SSHAC Study Level 3 methodology (References 2.5-281, 2.5-282, and 2.5-283) to ensure that uncertainty is represented in a manner consistent with NRC regulations.

For Unit 3, seismic hazard was calculated using source parameters from the CEUS SSC model. Simplifications to the CEUS SSC model were made for this calculation, and included:

- The exclusion of distributed seismicity sources and RLME sources that do not contribute significantly to hazard at the site (Section 2.5.2.2, Tables 2.5.2-206 and 2.5.2-210).
- The truncation of seismicity within distributed seismicity sources at 1,000 km from the site (Sections 2.5.2.2.2 and 2.5.2.2.3).
- Collapsing seismogenic depth in the New Madrid RLME logic tree to a single value of 15 km (with a corresponding weight of 1.0) (Section 2.5.2.2.4.2).
- The exclusion of sense of slip (described as a future rupture characteristic in the CEUS SSC Report, Table 5.4-2; Table 2.5.2-210), since current GMPEs (EPRI, 2004; 2006 do not consider this parameter.
- Rupture strike and dip (described as a future rupture characteristic in the CEUS SSC Report, Table 5.4-2; Table 2.5.2-210) were included for the Charleston and New Madrid RLME sources, but were not considered for other sources. A sensitivity study performed for the CEUS SSC model (Reference 2.5-223, p. 9-8) demonstrated that representing earthquakes as point sources, using EPRI (2004) correction factors for rupture distance, is an acceptable approximation.
- Depth distributions (described as a future rupture characteristic in the CEUS SSC Report, Table 5.4-2; Table 2.5.2-210) were collapsed to a single value for background sources.

Further modifications to the CEUS SSC model motivated by the updated earthquake catalog and site investigations are discussed in detail below.

2.5.2.4.2 New Information and New Seismic Source Characterizations

Sources of new information that potentially require updates to the CEUS SSC model include the updated earthquake catalog

(Section 2.5.2.1) and geologic investigations of the site.

The published CEUS SSC earthquake catalog extends through 2008. For the Unit 3 PSHA, this catalog was updated through mid-December of 2011, as described in Section 2.5.2.1. As discussed in Section 2.5.2.3, the most prominent effect of updating the earthquake catalog through 2011 is the incorporation of the 2011 Mineral earthquake. The Mineral earthquake is the largest instrumentally recorded earthquake in eastern North America since the 1988 E[**M**] 5.84 Saguenay earthquake. Most researchers attribute the 2011 Mineral earthquake to the CVSZ (e.g., References 2.5-232, 2.5-235, 2.5-332, 2.5-376, and 2.5-377).

In response to the Mineral earthquake, a SSHAC Level 2 investigation of the Mineral earthquake epicentral area was performed. This investigation included field reconnaissance, geomorphic analysis of lidar data, solicitation of expert opinions, and a review of recently published literature. As discussed in Section 2.5.1.1.7, the consensus result of these investigations was that the Mineral earthquake did not exhibit evidence of surface rupture. As discussed in Section 2.5.2.2.5.1, a potentially causative structure for the Mineral earthquake is proposed in recent literature. This recent literature does not, however, provide specifications or constraints on seismic source parameters such as slip-rate, recurrence, and Mmax. Therefore, the most appropriate way to incorporate the Mineral earthquake source in the PSHA is with distributed seismicity (background) zones. The updated seismicity catalog, which includes the Mineral earthquake, provides the basis to include updated seismicity rates to the host zones (ECC-AM, MESE-N, MESE-W, and Study Region) and a slight increase in the Mmax distribution to the ECC-AM zone. Experts contacted as part of the project SSHAC Level 2 assessment that investigated the issue of whether the Mineral earthquake rupture should be included as a new fault source all recommended against modifying the model in this fashion.

There are no additional or new regional seismic sources appropriate for use in a nuclear PSHA that would require a seismic source supplementation to the recent CEUS SSC model.

2.5.2.4.3 Updated Seismic Source Parameters

Based on the new information discussed in Section 2.5.2.4.2, earthquake recurrence rates, maximum magnitudes, and geometries are updated for CEUS SSC sources as described below.

2.5.2.4.3.1 Earthquake Recurrence Rates

Earthquake recurrence rates were recalculated using the updated earthquake catalog, following the CEUS SSC methodology. The earthquake recurrence assessment found that for those sources hosting the Mineral earthquake, the updated earthquake catalog resulted in small and localized increase on the rates per unit area and *b*-values for cells in the vicinity of the site, as compared to the original CEUS SSC values. Earthquake recurrence rates were also recalculated for most of the remaining zones that are within 1,000 km of the site. The only sources for which recurrence rates were not recalculated were NMESE-W, AHEX, MidC-C, MidC-D, and IBEB, since the very small number of new earthquakes of E[**M**] 2.9 or larger in these zones (within 1,000 km of the site) were judged to be insignificant to hazard. Based on visual inspection of plots showing seismicity and source zones, the portions of these background sources within 1,000 km of the site included either no new earthquakes (AHEX and IBEB) or only two new earthquakes (NMESE-W, MidC-C, and MidC-D) of E[**M**] 2.9 and larger.

2.5.2.4.3.2 Maximum Magnitudes

Maximum magnitude values were recalculated using the updated earthquake catalog, following the CEUS SSC methodology. The only earthquake in the updated earthquake catalog that exceeds the previously recognized historical Mmax for a source zone is the 2011 Mineral earthquake. Of the four source zones from the CEUS SSC that represent host zones to the Mineral earthquake, only the ECC-AM seismotectonic zone required a recalculated update to the Mmax distribution. The other three host zones sufficiently exceeded the magnitude of the Mineral earthquake and therefore did not require any revision. Section 2.5.2.2.5.1 provides additional discussion of the 2011 Mineral earthquake.

The lowest value on the five-point Mmax distribution for the ECC-AM seismotectonic source zone was E[**M**] 6.0 (Reference 2.5-223). The E[**M**] 5.71 Mineral earthquake is the largest event to occur within the ECC-AM, with the possible exception of the 1755 E[**M**] 6.1 Cape Ann, MA event. However, given the uncertainty in the location of the Cape Ann earthquake, it was assigned in the CEUS SSC model a 60 percent probability of having occurred within ECC-AM seismotectonic zone and a 40 percent probability that it occurred within the adjacent NAP seismotectonic zone (Reference 2.5-223). On the Mmax zones branch of

the CEUS SSC logic tree, the Mineral earthquake occurred within the MESE-W, MESE-N, and Study Region Mmax zones. The lowest value of the five-point Mmax distributions for these three zones is E[**M**] 6.4-6.5, well above the Mineral earthquake magnitude of E[**M**] 5.71.

The Mmax assessment resulted in a minor revision to the lower bound of the Mmax distribution for ECC-AM seismotectonic source zone (see Table 2.5.2-215). No other Mmax values are affected in zones that hosted the Mineral earthquake. Had the E[**M**] 6.1 Cape Ann event occurred with a 100 percent probability in the ECC-AM, then there would have been no modification to any Mmax value. The occurrence of the Mineral earthquake shifts the lower part of the distribution to the right, enough to shift the lowest magnitude in the discretized distribution (weight 0.101; associated with the intersection between the curve and the lowest horizontal line) from **M** 6.0 to 6.1. One could even argue that this 0.1 unit shift is an artifact of the one-decimal round-off and that the true difference would be on the order of 0.02 magnitude units if one used two decimals to characterize the discretized magnitude distributions.

2.5.2.4.4 Ground Motion Prediction Equations

Ground motions were estimated using hard-rock GMPEs from EPRI (2004) with aleatory uncertainties from EPRI (2006). These equations were developed for hard-rock conditions (shear-wave velocities V_S of 9200 ft/s). Separate sets of equations are used for “general, non-rift” sources typical of the CEUS, and for “non-general rift” sources, such as the Charleston seismic zone and the New Madrid seismic zone. These GMPEs were developed following a SSHAC (1997) (Reference 2.5-281) Level 3 process and are well-documented regarding the underlying models, parameters, and weights assigned to alternative interpretations. For “general, non-rift” sources, 9 alternative equations are used with weights. For “non-general rift” sources, 12 alternative equations are used with weights. For each equation, 6 alternative logarithmic standard deviations are used with weights to quantify aleatory uncertainty are used. The mid-Continent equations were not used from EPRI (2004), because the site lies well within the mid-Continent region specified therein.

Ground motions are available for 7 spectral frequencies from EPRI (2004). These spectral frequencies are PGA (equivalent to 100 Hz), 25 Hz, 10 Hz, 5 Hz, 2.5 Hz, 1 Hz, and 0.5 Hz. All ground motion equations represent spectral acceleration at 5 percent of critical

damping, and this damping applies to all spectral amplitude results presented here.

2.5.2.4.5 Updated Probabilistic Seismic Hazard Analysis and Deaggregation

The following sections describe the updated PSHA and the deaggregation results for the site.

2.5.2.4.5.1 Seismic Sources

The analysis here is an updated calculation of rock seismic hazard using the CEUS SSC seismic source characterizations, the EPRI (2004) ground motion model with the revised sigmas of EPRI (2006), and updated seismicity files that include the effect of recent seismicity on background sources. The cumulative absolute velocity (CAV) filter is not applied in this calculation and no site amplification factors are used, so the results are consistent with hard-rock conditions (shear-wave velocities of 9200 ft/s). The methodology for seismic hazard calculations is well established in the technical literature (e.g., McGuire, 2004 (Reference 2.5-378)).

Seismic source inputs to the hazard calculations consist of background sources (large regions representing earthquakes not associated with specific tectonic structures, i.e., Mmax Zones and Seismotectonic Zones) and RLME sources (those representing the potential occurrence of Repeated Large Magnitude Earthquakes). Specific background sources that are documented in the CEUS SSC Report and that are included in the hazard calculations consist of the following:

Atlantic Highly Extended Crust (AHEX)

Extended Continental Crust-Atlantic Margin (ECC-AM)*

Mesozoic Extended-wide (MESE-W)*

Mesozoic Extended-narrow (MESE-N)*

Non-Mesozoic Extended-narrow (NMESE-N)*

Non-Mesozoic Extended-wide (NMESE-W)

Paleozoic Extended Crust-narrow (PEZ-N)*

Paleozoic Extended Crust-wide (PEZ-W)*

Study Region (Study_R)*

Midcontinent-Craton (MiDC-A)*

Midcontinent-Craton (MiDC-B)*

Midcontinent-Craton (MiDC-C)

Midcontinent-Craton (MiDC-D)

Illinois Basin Extended Basement (IBEB)

St. Lawrence Rift (SLR)*

* indicates seismicity file was updated, as discussed below.

This list represents all background sources that lie within 322 km (200 miles) of the site, which is consistent with the recommendation in RG 1.208, Section 1.1.1 regarding the identification of seismic sources. BEB and SLR are well beyond this 322 km (200 miles) distance but were included because sensitivity studies indicated that the hazard from these two sources, when combined with the hazard from the Wabash Valley RLME, amounts to 1 percent of total hazard at the 10^{-4} amplitude for 1 Hz spectral acceleration. Sources are truncated so that only distributed seismicity within 1,000 km is considered in the analysis. All background sources are represented with gridded seismicity at 5 km depth consisting of 24 sets of rates and *b*-value parameters for each source. These parameters consist of 8 equally likely realizations of parameters (Reference 2.5-223, pages 5-35 and 5-36) for each of three smoothing models (Reference 2.5-223, page 5-37 and cases A, B, and E in Table 5.3.2-1). Each background source also has a distribution of maximum magnitude (Reference 2.5-223, Tables 6.3.2-1 and 7.4.2-1) with a minimum magnitude of 5.0. All magnitudes in this calculation are moment magnitudes (**M**).

For background sources identified with an asterisk in the above list, seismicity parameters were recalculated using an updated earthquake catalog, because the earthquake catalog from the CEUS SSC study included earthquakes only through 2008. This catalog was updated using the same procedures documented in the CEUS SSC Report, to identify earthquakes occurring in the CEUS between January 1, 2009, and mid-December, 2011 (see Section 2.5.2.1). Updated rate- and *b*-value files were calculated for the 24 cases described above, using the same spatial smoothing assumptions, for each background source. In addition, the Mmax distribution for each background source was examined and compared to additional earthquakes that occurred in that source, to determine if the Mmax distribution should be modified based on the additional seismicity. With the exception of the seismotectonic zone

ECC-AM, as discussed earlier, it was determined that the original Mmax distributions of all background sources remain valid.

RLMEs represent additional sources of seismic hazard that are added to the hazard from the background sources discussed above. RLME sources that are included in the hazard calculations consist of the following:

- Charleston—regional source
- Charleston—local source
- Charleston—narrow source
- New Madrid fault system—Reelfoot Thrust (cluster model)
- New Madrid fault system—New Madrid North fault (cluster model)
- New Madrid fault system—New Madrid South fault (cluster model)
- Reelfoot Thrust alone
- Wabash Valley

These RLME sources have distributions representing the frequency of occurrence of large earthquakes, and the potential sizes of those earthquakes. In the CEUS SSC Report the Charleston magnitudes and annual frequencies are documented in Section 6.1.2.4 and Tables 6.1.2-4 and 6.1.2-5. The NMFS includes a model of earthquake clusters and the frequency of occurrence of those clusters, wherein all three New Madrid faults cause earthquakes in a short period of time (effectively simultaneously). In the CEUS SSC Report the magnitudes and annual frequencies of the NMFS earthquakes are documented in Section 6.1.5.3 and Tables 6.1.5-5 through 6.1.5-7.

In the CEUS SSC Report, Section 6.1.5.1, the NMFS cluster model is given a weight of 0.9. A second model is that the NMFS cluster is in a period of quiescence (not in a cluster sequence), but that the Reelfoot Thrust alone is active (weight of 0.05). A third model is that all faults are quiescent and the NMFS does not produce large earthquakes (weight of 0.05). A discussion of the cluster model, as well as the alternatives, can be found in the CEUS SSC Report, Section 6.1.5.1.

The Wabash Valley RLME is approximately 800 km from the site and only contributes ~0.4 percent to the total hazard at 1 Hz spectral amplitude corresponding to 10^{-4}. However, this hazard, when combined with the contributions from distant background sources IBEB and SLR, exceeds 1 percent of total hazard at this amplitude. (Contributions at higher

spectral frequencies, and at lower annual frequencies of exceedance, would be lower). Therefore the Wabash Valley RLME is included in the analysis. Magnitudes and annual frequencies for this RLME are documented in the CEUS SSC Report, Section 6.1.9.3 and Table 6.1.9-2.

Other RLMEs (e.g., the Eastern Rift Margin, Marianna, and Commerce) are much farther from the site, have lower annual frequencies, and/or lower characteristic magnitudes, and, therefore, would contribute even less hazard. These RLMEs would not exceed 1 percent of total hazard and were not included in the analysis.

Seismic source characteristics relevant to seismic hazard described in the CEUS SSC Report were modeled, including the correlation of the activity of seismic sources, as represented in logic trees published therein. This applies to both the background sources and RLME sources.

The 9 general, non-rift mid-Continent ground motion models from EPRI (2004) were applied to background sources, and the 12 non-general rift mid-Continent ground motion models from EPRI (2004) were applied to the Charleston, NMFS, and Wabash Valley sources. For the background sources the point source (epicenter) to rupture adjustment ("random epicenters" model) from EPRI (2004) was implemented. For the Charleston and NMFS sources, earthquake sources were explicitly modeled as ruptures on faults, so the point source to rupture adjustment was not used. The correlation of ground motion equations between background (general, non-rift) sources and RLME (non-general, rift) sources was modeled, as described in EPRI (2004).

2.5.2.4.5.2 Seismic Hazard Results

Mean and fractile rock hazard curves for 7 frequencies (0.5, 1, 2.5, 5, 10, 25 Hz and PGA) are shown in Figures 2.5.2-230 through 2.5.2-236. The contributions to rock hazard from the background, Charleston, New Madrid and Wabash Valley for 1 Hz and 10 Hz are plotted in Figures 2.5.2-237 and 2.5.2-238. Contributions to 1 Hz and 10 Hz hazard by individual background sources are plotted in Figures 2.5.2-239 and 2.5.2-240. Contributions to 1 Hz and 10 Hz hazard for individual Charleston sources are plotted in Figures 2.5.2-241 and 2.5.2-242.

Sensitivity of 1 Hz and 10 Hz rock hazard to the 9 EPRI GMPE used for background sources are plotted in Figures 2.5.2-243 and 2.5.2-244. Similar plots showing the 12 GMPEs used with the Charleston, NMFS, and Wabash Valley RLMEs are shown in Figures 2.5.2-245

and 2.5.2-246. Note for these plots that seismic hazard curves are not weighted by the weights assigned to each GMPE. Note also that all seismic sources are included in the hazard curves for each plot, so that (for example) a seismic hazard curve for GMPE #1 for background sources includes the mean hazard from the associated RLME GMPEs.

The total median hazard curve and the median hazard curves from the background, Charleston, New Madrid and Wabash Valley sources are plotted in Figures 2.5.2-247 and 2.5.2-248 for 1 Hz and 10 Hz, respectively. Note that median hazard curves from each source do not sum to the total median hazard curve (the sum of the medians of two random variables does not equal the median of the sum of those random variables, except under special conditions).

Figure 2.5.2-249 plots mean total hazard curves for the 7 spectral frequencies at which hazard calculations were conducted. The individual hazard curves are documented in digital form in Table 2.5.2-216.

The 10^{-4}, 10^{-5}, and 10^{-6} UHRS amplitudes are reported in Table 2.5.2-217.

2.5.2.4.5.3 Deaggregation and Uniform Hazard Response Spectra

Deaggregation of seismic hazard is calculated by determining the contribution by magnitude **M** and distance R, grouping the contributions by **M** and R bin. The contributions are calculated for individual seismic sources and are aggregated for all sources. The deaggregations are calculated by spectral frequency and by mean annual frequency of exceedance (MAFE) (10^{-4}, 10^{-5}, and 10^{-6}), using the amplitudes indicated in Table 2.5.2-217.

The deaggregation and the determination of the controlling magnitudes and distances follow the methodology presented in RG 1.208. Specifically, log-distance is used in the calculation of the controlling distances and linear-magnitude is used in calculating the controlling magnitudes. If a substantial portion (> 5 percent) of the low frequency hazard (average of 1 and 2.5 Hz) is from distant sources (> 100 km), the controlling magnitude and distance are determined only from contributions from hazard at distances greater than 100 km.

Low-frequency (LF) and high-frequency (HF) deaggregation plots for each MAFE are shown in Figures 2.5.2-250 through 2.5.2-255. The LF plot represents the average deaggregation of the 1 and 2.5 Hz spectral acceleration hazard; the HF plot represents the average deaggregation

of the 5 and 10 Hz spectral acceleration hazard. Note that the 569 km bin (average site to fault distance for the Local Charleston source) primarily represents hazard from the Charleston RLME, and the 1,051 km bin (weighted average distance from all NMFS fault geometries) primarily represents hazard from the New Madrid RLME. However, a small amount of hazard in each of these bins comes from the Wabash Valley RLME and/or distant events in background zones. Local events dominate at both high and low frequencies at all hazard levels, although New Madrid and Charleston contribute 11 percent and 4.7 percent, respectively, to the low frequency 10^{-4} MAFE. For a MAFE of 10^{-6}, the total contribution of LF hazard for distances R >100 km is less than 5 percent, so the controlling magnitude and distance are calculated for all distances, following RG 1.208.

Table 2.5.2-218 shows the controlling earthquake magnitudes and distances for mean annual frequencies of exceedance (MAFEs) of 10^{-4}, 10^{-5}, and 10^{-6} hazard levels at spectral frequencies of 1 and 2.5 Hz (low frequency) and 5 and 10 Hz (high frequency).

HF and LF response spectra for MAFEs of 10^{-4}, 10^{-5} and 10^{-6} are plotted in Figure 2.5.2-256 and tabulated in Table 2.5.2-219. These spectra were developed following the guidelines in RG 1.208. The starting points were the 10^{-4}, 10^{-5}, and 10^{-6} spectral amplitudes for the 7 spectral frequencies at which hazards were calculated, as shown in Table 2.5.2-216. In between these spectral frequencies, HF and LF spectra were constructed by interpolation, adopting the CEUS rock spectral shapes published in Reference 2.5-385. To apply these spectral shapes, the high-frequency magnitude and distance were used for 2.5 Hz and higher spectral frequencies, and the low-frequency magnitude and distance were used for 2.5 Hz and lower spectral frequencies. For spectral frequencies below 0.5 Hz, 1/T scaling was assumed (where T is spectral period). This is consistent with requirements for seismic building codes (e.g., Building Seismic Safety Council, 2009 (Reference 2.5-379)).

Finally, envelopes of HF and LF response spectra anchored to mean spectral amplitudes for MAFEs of 10^{-4}, 10^{-5}, and 10^{-6} were also created by selecting the maximum of the HF and LF spectra for each of the mean annual frequencies of exceedance. These envelopes represent UHRS and are plotted in Figure 2.5.2-257. Median UHRS were also constructed by scaling the same spectral shapes to median spectral amplitudes at each of the 7 spectral frequencies at which hazard calculations were

made. These median UHRS are plotted in Figure 2.5.2-258.

2.5.2.5 Seismic Wave Transmission Characteristics of the Site

The UHRS described in Section 2.5.2.4 are defined on hard rock. Hard rock is characterized with a minimum shear-wave velocity (V_S) of 9,200 fps, which at the site is located between 155 ft and 165 ft below the ground surface at Elevation 290 ft (all elevations are rounded to whole numbers for the purpose of site response analyses). All elevations in this section are based on the North American Vertical Datum of 1988 (NAVD88). This section describes the development of the site amplification factors and soil UHRS that result from the transmission of the seismic waves through the site-specific geologic columns above hard rock, referred to as "soil columns" thereafter. The site amplification factors are used in determination of the GMRS and Performance Based Surface Response Spectra (PBSRS) for the site, and of the Foundation Input Response Spectra (FIRS) for each Seismic Category I (SC-I) structure. As described in Section 2.5.4, different base case soil columns are developed for the Reactor Building/Fuel Building (RB/FB), Control Building (CB) and Fire Water Support Complex (FWSC) locations. The amplification factors and their corresponding UHRS at the foundation elevations for each SC-I building are calculated using their respective soil columns. The amplification factors and UHRS corresponding to the GMRS are calculated using the RB/FB soil column since this soil column is developed using the information obtained from the V_S measurements from all boreholes in the power block area and is considered applicable to this entire area. Furthermore, at each elevation, the design response spectra (DRS) obtained from RB/FB soil column and CB soil column are enveloped, as discussed in Section 2.5.2.6, to calculate the RB/FB FIRS, CB FIRS as well as the GMRS and PBSRS. The effect of variability in material properties of the soil columns is included by randomizing over the range of low-strain dynamic properties and layer thicknesses extending from the finished ground surface to randomized hard rock depths, and randomizing over the range of shear modulus reduction and damping curves, where applicable.

The development of the site amplification factors and soil UHRS for each soil column is performed in the following steps:

1. The model of the base case soil column (referred to as the best estimate (BE) profile) is developed using site-specific geotechnical and geophysical data from the finished surface at Elevation 290 ft to the hard rock, as described in Section 2.5.2.5.1. A different model for BE shear-wave velocity profiles is developed for each of the RB/FB, CB, and FWSC locations. The RB/FB model for BE shear-wave velocity profile is determined from log-mean of profiles 1 and 2, as defined in Section 2.5.4.7 which are determined using the V_S measurements from all boreholes in the power block area. The CB and FWSC BE profiles are determined using the V_S data from Borehole B-909 which is the closest V_S measurement to these buildings and is more consistent with the RQD information obtained from the other boreholes within the footprint of these buildings. The difference between the BE profiles for the CB and FWSC are limited to the thickness of each soil/rock layer, and the details for their development are described in Section 2.5.4.7. These models provide the BE representation for evaluation of the dynamic behavior of subsurface site materials under seismic loading.

2. For each BE soil column, a set of 60 simulated profiles is generated by using the BE soil column, and developing a probabilistic model that includes the uncertainties in the soil and rock shear-wave velocities, shear modulus reduction and damping curves, soil and rock layer thicknesses, depth to the hard rock boundary ($V_S \geq 9{,}200$ fps), and correlation between the velocities in adjacent layers in the site-specific soil column as described in Section 2.5.2.5.2.

3. For each set of simulated profiles, the 10^{-4} and 10^{-5} annual-frequency-of-exceedance LF and HF hard rock spectra of Section 2.5.2.4 are used as input at the base of the simulated profiles to calculate the dynamic response of the considered soil columns for each realization of the 60 simulated profiles. For this purpose, an equivalent-linear site-response formulation is used together with Random Vibration Theory (RVT), and the mean site response is calculated. Input time histories for the site response

analysis are not required for the frequency-domain RVT approach. This step is repeated for each of the four input motions (10^{-4} and 10^{-5} annual frequencies, HF and LF spectra).

The GMRS horizon is defined at Elevation 224 ft which corresponds to the deepest excavation at the site and lies on competent material ($V_S \geq 1000$ fps). Due to the linear (strain-independent) characteristics of the considered soil column below the GMRS horizon, there are no confining effects from the soils above. The calculation of the GMRS as a free field geologic outcrop and its corresponding amplification factors is carried out by removing the layers above the GMRS horizon per requirements of DC/COL-ISG-17 (Reference 2.5-380).

The bottom of foundation for RB/FB structure (Elevation 224 ft, refer to Section 2.5.4) is used as the FIRS elevation for the RB/FB. Amplification factors and their corresponding soil UHRS are calculated for this building to obtain both full column outcrop FIRS and partial column outcrop FIRS which are appropriate for the SSI analysis of the RB/FB structure as fully embedded and as partially embedded (only considering embedment in rock), respectively. The amplification factors corresponding to the full column outcrop FIRS include the effects of down-coming waves from the soil and rock layers above the FIRS elevation to the finished grade; while the amplification factors corresponding to the partial column outcrop FIRS only include the effects of down-coming waves from the rock layers above the FIRS elevation. In the case of the amplification factors corresponding to the partial column outcrop FIRS, the effects of soil layers above the FIRS horizon on the nonlinear properties of the rock layers below in terms of both the confining pressure and the soil column frequency are considered through a truncated soil column response (TSCR) analysis consistent with the requirements of DC/COL-ISG-17. Such effects are included by definition in the amplification factor calculation corresponding to the full column outcrop FIRS.

The bottom of foundation for CB structure (Elevation 241 ft, refer to Section 2.5.4) is used as the FIRS elevation for the CB. Similar to the RB/FB, amplification factors and their corresponding UHRS are calculated for this building to obtain both full column outcrop FIRS and partial column outcrop FIRS which are appropriate for its SSI analysis as a fully embedded structure and as a partially embedded structure (only considering embedment in rock), respectively.

The bottom of foundation for FWSC structure (Elevation 282 ft, refer to Section 2.5.4) is used as the FIRS elevation for the FWSC. Amplification factors and their corresponding UHRS are calculated for this building to obtain the geologic outcrop FIRS which are appropriate for its SSI analysis as a surface-founded structure. A TSCR analysis consistent with the requirements of DC/COL-ISG-17 is carried out to include the effects of soil layers above the FIRS horizon on the nonlinear properties of the rock layers below in terms of both confining pressure and soil column frequency.

Details of the implementation of these steps are described in the following sections. The resulting site-specific amplification factors are used to amplify the hard rock spectra of Section 2.5.2.4 to develop the UHRS at the GMRS horizon and at finished grade, as well as at the FIRS horizons for each of the RB/FB, CB, and FWSC structures, as described in Section 2.5.2.5.4.

2.5.2.5.1 Base Case Site-Specific Soil Columns and Uncertainties

Section 2.5.4.7 describes the subsurface shear wave velocity and related material property information for the site. Three different base case soil columns (also referred to as the BE soil columns) are developed for the RB/FB, CB and FWSC locations and discussed in the following sections.

2.5.2.5.1.1 RB/FB Best Estimate Soil Column

The RB/FB BE soil column is developed based on the provided data in the power block area which is characteristic of the entire site. For this reason this soil column is used in the development of the GMRS and PBSRS as well as the FIRS for RB/FB structure. Above Elevation 273 ft to the finished grade at Elevation 290 ft, the BE profile for the RB/FB structure includes Saprolite layers denoted as Zone IIA and Zone IIB. Below Elevation 273 ft, the BE profile entirely consists of in-situ Zone III, Zone III-IV and Zone IV rock material and is determined from the logarithmic-mean of profiles 1 and 2, as defined in Section 2.5.4.7. The hard rock material with $V_S \geq 9{,}200$ fps is specified at BE depth of 155 ft (Elevation 135 ft) for the soil column. As described in Section 2.5.4.2, the in-situ saprolite, and Zone III rock are each assigned a set of strain-dependent property curves (shear modulus degradation and damping), while Zone III-IV rock, and Zone IV rock are assigned linear properties (strain-independent shear modulus and damping). The shear-wave velocity profile for the BE RB/FB soil column is presented in

Figure 2.5.2-259.

The standard deviation for V_S for in-situ rock below Elevation 273 ft is obtained from the results of the boreholes B-901, B-907, and B-909 described in Section 2.5.4.7. Note that the mean used in the calculation of the logarithmic standard deviation (log-SD) is obtained from the same three boring data. Alternatively, the log-SD may be estimated from the two lower bound and upper bound profiles (Profiles 1 and 2 in Section 2.5.4.7) by assuming that they are each one standard deviation away from their mean (average). Based on the results calculated from both approaches, log-SD for rock above the assumed bedrock (Elevation 135 ft) ranging from 0.1 to 0.4 is adopted at different depths. For the in-situ saprolite, the average shear wave velocity values are reported in Section 2.5.4.7 as well as the lower bound and upper bound V_S values. The standard deviation for each saprolite layer is estimated as the average difference between the reported average values, and the lower and upper bounds. The logarithmic-mean and the log-SD are calculated from the average and standard deviation values assuming a logarithmic normal distribution for V_S. The calculated Log-SD ranges from 0.28 to 0.49. Accordingly, for the saprolite layers, a log-SD of 0.4 is adopted and used in the soil profile simulations. The hard rock is assigned a shear-wave velocity of 9,200 ft/s with no uncertainty, i.e., log-SD=0. The calculated and adopted values of the log-SD used in the simulation are presented in Figure 2.5.2-260.

For the in-situ rock layers, maximum and minimum rock stratum thicknesses are obtained from borehole data within the power block area (Section 2.5.4.7). Where the maximum and minimum thickness values are not available, the maximum and minimum thicknesses are estimated by an approximate 20 percent increase and decrease from the BE thickness value, respectively. Sensitivity studies confirm that the site response analysis results are not sensitive to the assumed range of variation of in-situ rock thicknesses.

2.5.2.5.1.2 CB Best Estimate Soil Column

As described in Section 2.5.4.7, the CB soil column is developed based on the V_S measurements obtained from borehole B-909 which is located within the footprint of the CB. These V_S values are interpreted as the BE or logarithmic-mean shear-wave velocities. The layer thickness variations for the CB profile are based on the RQD data obtained from 4 borings in the close vicinity of the CB footprint. Below the finished grade, these

borings show layers of Zone IIA (Saprolite), Zone IIB (Saprolite), and Zone III (weathered rock) supported on Zone III-IV and Zone IV rock material. The hard rock material with $V_S \geq 9{,}200$ fps is specified at BE depth of 165 ft (Elevation 125 ft) for this soil column. As described in Section 2.5.4.2, the in-situ saprolite, and Zone III rock are each assigned a set of strain-dependent property curves (shear modulus degradation and damping), while Zone III-IV rock, and Zone IV rock are assigned linear properties (strain-independent shear modulus and damping). The shear-wave velocity profile for the CB BE soil column is presented in Figure 2.5.2-259.

Similar to the RB/FB profile described above, the V_S standard deviation values for saprolite and rock layers of CB are estimated as the average difference between the reported average values, and the lower and upper bounds and used to calculate consistent V_S logarithmic-mean and log-SD. The calculated and adopted values of the log-SD used in the simulation of the CB soil column are presented in Figure 2.5.2-261. In the case of in-situ Zone III-IV (moderately to slightly weathered rock) and Zone IV rock (parent rock) layers, where the maximum and minimum thickness values are not available, the maximum and minimum thicknesses are estimated by an approximate 20 percent increase and decrease from the BE value, respectively.

2.5.2.5.1.3 FWSC Best Estimate Soil Column

As described in Section 2.5.4.7 the FWSC soil column is developed based on the V_S measurements obtained from borehole B-909 which is located less than 50 ft from the edge of the footprint of the FWSC. These V_S values are interpreted as the BE or logarithmic-mean shear-wave velocities. The layer thickness variations for the FWSC profile based on the RQD data obtained from 4 borings in the close vicinity of the FWSC footprint. Below finished grade, these borings show layers of Zone IIA (Saprolite), Zone IIB (Saprolite), and Zone III (weathered rock) supported on Zone III-IV and Zone IV rock material. The hard rock material with $V_S \geq 9{,}200$ fps is specified at BE depth of 164 ft (Elevation 126 ft) for this soil column. As described in Section 2.5.4.2 and similar to the RB/FB and CB soil columns, the in-situ saprolite, and Zone III rock are each assigned a set of strain-dependent property curves (shear modulus degradation and damping), while Zone III-IV rock, and Zone IV rock are assigned linear properties (strain-independent shear modulus and damping). The shear-wave velocity profile for the FWSC BE soil column

is presented in Figure 2.5.2-262.

Similar to the RB/FB and CB profiles described above, the V_S standard deviation values for saprolite and rock layers of FWSC are estimated as the average difference between the reported average values, and the lower and upper bounds and used to calculate consistent V_S logarithmic-mean and log-SD. The calculated and adopted values of the log-SD used in the simulation of the FWSC soil column are presented in Figure 2.5.2-263. In the case of in-situ Zone III-IV (moderately to slightly weathered rock) and Zone IV rock (parent rock) layers, where the maximum and minimum thickness values are not available, the maximum and minimum thicknesses are estimated by an approximate 20 percent increase and decrease from the BE value, respectively.

For all three soil columns considered, the Poisson's ratios and unit weights identified for Saprolite (Zone IIA and IIB) and Zone III, Zone III-IV, and Zone IV rock in Section 2.5.4.7 are adopted for their corresponding material in the BE profile.

The input rock motions for site amplification analyses are specified at the bottom of the site-specific soil columns, below which the half-space is modeled with shear-wave velocity of 9,200 fps and a damping ratio of 1 percent, i.e., hard rock.

As described in Section 2.5.2.5.2, the properties for each layer in the soil columns are randomized to account for the inherent natural variability, as well as the (epistemic) uncertainty associated with the variation of shear modulus, damping ratios, and layer thicknesses. Therefore, the actual site response analysis comprised a range of properties for each layer, and in particular, a range of shear moduli, damping ratios and layer thicknesses which address the subsurface variability below the GMRS elevation observed in the geotechnical investigation of the site.

2.5.2.5.2 Capturing Site-Specific Geologic Column Properties, Uncertainties, and Correlations

The computer program SPS (Reference 2.5-211) is used to generate site-specific simulated (randomized) soil profiles to represent the dynamic properties of each soil column while considering the uncertainty associated with each of these properties. The generation of the low-strain simulated soil profiles uses the input BE properties defined in Section 2.5.2.5.1 and their associated uncertainties. The uncertainty is expressed in terms of statistical distribution, standard deviation (SD), and

correlation among engineering parameters. A soil or rock “stratum” is defined in the simulation program as a layer having the same V_S and strain-dependent property curves. For each soil column, the boundaries between different strata are defined using the BE V_S profiles defined in Section 2.5.2.5.1.

Correlation coefficients between natural logarithm of V_S in adjacent strata are calculated based on generic studies using the inter-layer correlation model described in Reference 2.5-381. The resulting inter-layer correlation values are used as guidelines, in addition to the site-specific information, to define the inter-layer correlation values to be used as input for simulation.

Figure 2.5.2-264 presents the set of 60 shear-wave velocity simulated profiles before including thickness variation, i.e., based on the BE thicknesses provided for each soil layer for the RB/FB soil column. Note that the logarithmic-average (simulated median) profile closely matches the input BE profile. Maximum and minimum bounds of twice the log-SD around the BE are imposed to prevent unrealistic shear-wave velocity realizations. Figure 2.5.2-265 presents the set of 60 shear-wave velocity simulated profiles for the RB/FB soil column, including thickness variation. Note that while the simulated median profile matches the input BE profile, it shows smoother transitions between the consecutive strata, which are the result of the combination of shear-wave velocity and thickness variation in the simulated profiles. Figures 2.5.2-267 and 2.5.2-268 show similar plots for the 60 simulated profiles of the CB soil column and Figures 2.5.2-270 and 2.5.2-271 show the same information for the FWSC soil column.

For the purpose of site response analysis, half-space bedrock, where the input hard rock motion is applied, is defined by a shear-wave velocity of 9,200 fps. In all three soil column sets, the Zone III-IV and IV strata are assigned strain-independent damping ratios, based on BE damping ratio of 1 percent with a log-SD of 0.6. This amounts to damping values with one standard deviation range of 0.55 percent to 1.8 percent. The resulting low-strain damping ratio profiles are presented in Figure 2.5.2-266 for the RB/FB soil column, in Figure 2.5.2-269 for the CB soil column, and in Figure 2.5.2-272 for the FWSC soil column.

As described in Section 2.5.4.2, the in-situ saprolite and Zone III rock are each assigned a set of strain-dependent property curves (shear modulus degradation and damping). As an example of the simulated shear

modulus reduction and damping ratio curves, Figure 2.5.2-273 presents the simulated strain-dependent property curves for the top Zone IIA (saprolite) stratum of the RB/FB soil column (referred to as Saprolite1). In these plots, the BE and simulated median are compared, as well as the input log-standard deviation (Input SD) and simulated log-standard deviation (Simulated SD). Maximum and minimum bounds of twice the log-SD around the BE are imposed on the strain-dependent property curves. Note that damping curves, in Figure 2.5.2-273, are truncated at a maximum of 15 percent as required by SRP Section 3.7.1, which explains the discrepancy between input and simulated properties once that upper limit is reached. The damping truncation at 15 percent is a conservative measure with respect to the subsequent use of the curves in site response analysis.

These sets of 60 random profiles, consisting of V_S versus depth, depth to hard rock, damping ratio and shear-modulus degradation curves, are used to calculate and quantify site response and its uncertainty, as described in the following sections.

The V_{S30} for each soil profile is calculated as the average (based on the shear-wave travel time) shear-wave velocity in the top 100 ft (approximately the top 30 meters) below elevations where vertical response spectra are required. These V_{S30} values are presented in Table 2.5.2-220 and are used in Section 2.5.2.6.2 for the determination of V/H ratios.

2.5.2.5.3 Site Response Analysis

Site response analysis is conducted using the program P-SHAKE (Reference 2.5-222), which uses a procedure based on Random Vibration Theory (RVT) with the following assumptions:

- Vertically propagating shear waves are the dominant contributor to site response.
- An equivalent-linear formulation of nonlinearity is appropriate for the characterization of site response.

These are the same assumptions that are implemented in the SHAKE program (Reference 2.5-382). With respect to RVT implementation, the major steps used in P-SHAKE are as follows:

1. The input motion is provided in terms of an acceleration response spectrum (ARS) and associated spectral damping instead of spectrum-compatible acceleration time histories. The input ARS is converted to an acceleration power spectral density (PSD) using an iterative RVT based procedure with the peak factor function.

2. From the frequency domain computation (following SHAKE approach), the transfer function for shear strain in each layer of the profile is obtained and convolved with the PSD of input motion to get the PSD and the maximum strain in each layer. The effective strain is obtained from the maximum strain and is used to obtain new properties (shear modulus and damping) for the next iteration.

3. The iterations are repeated until the convergence limit set by the analyst is reached in all layers.

4. Once the final frequency domain solution is obtained, the ARS at each layer interface can be computed from the PSD of the solution using the RVT based procedure with the peak factor function.

The site-response analysis procedure, as described above, requires the following additional parameters:

- **Strong-motion duration** - The RVT methodology requires this parameter, but results are not sensitive to it. These are calculated from the mean magnitudes and distances from the deaggregation. NUREG/CR-6728, Table 3-2 (Reference 2.5-385) provides strong motion duration values as a function of magnitude and distance pairs. Accordingly, strong motion durations were assigned for each of the cases considered (10^{-4} and 10^{-5} annual frequencies, HF and LF smooth spectra) and are presented in Table 2.5.2-221.
- **Effective strain ratio** - An additional parameter required for P-SHAKE is the effective strain ratio (equivalent uniform strain divided by maximum strain), which is calculated as a function of earthquake magnitude, as shown in Equation 2.5.2.5-1 (Reference 2.5-383). The resulting effective strain ratios used in site response analysis are reported in Table 2.5.2-221.

Effective Strain Ratio = (**M**-1)/10 (2.5.2.5-1)

The site response analyses are carried out for each of the RB/FB, CB, and FWSC soil columns. The results of the site response analyses are used to calculate UHRS which are used in determination of the GMRS, full column and partial column outcrop FIRS for RB/FB structure, full column and partial column outcrop FIRS for CB structure, and geologic outcrop FIRS for FWSC structure. As discussed earlier, as a conservative measure, the GMRS, RB/FB FIRS and CB FIRS are calculated at their respective elevations using envelope of DRS calculated in RB/FB and CB soil columns (refer to Section 2.5.2.6). The FWSC FIRS is calculated using FWSC soil column. The site response analysis results for each soil column are summarized in the following sections.

2.5.2.5.3.1 Site Response Analysis for the RB/FB Soil Column

As discussed earlier, the RB/FB soil column results are used in determination of the GMRS (at Elevation 224 ft), full column and partial column outcrop FIRS for RB/FB (at Elevation 224 ft) and full column and partial column outcrop FIRS for CB (at Elevation 241 ft). Accordingly, three sets of analyses are conducted using this soil column:

1. Full column analysis, in which the rock LF and HF at two hazard levels (10^{-4} and 10^{-5}) presented in Section 2.5.2.4 are applied at bedrock with V_S exceeding 9,200 fps and propagated through the set of 60 simulated profiles to calculate the responses and strain compatible soil properties corresponding to each simulated profile and each input ground motion. The full column outcrop acceleration response spectra (ARS) for each input ground motion are calculated as the mean of the 60 ARS results at Elevations 224 ft and 241 ft including the effects of down-coming waves from the soil and rock layers above to the finished grade using the strain compatible soil properties. The mean ARS at the finished grade (Elevation 290 ft - denoted as FG) are also calculated in this analysis for each input ground motion.

2. Partial column analysis, which uses the truncated strain compatible soil layers obtained from the full column analyses after removing the saprolite layers which exist above the foundation elevations. On the best estimate basis, the saprolite layers correspond to 17 ft on top of RB/FB soil column and 25 ft on top of the CB soil column. The

partial column outcrop ARS are obtained as the mean of 60 ARS results at Elevations 224 ft and 241 ft by propagating the rock ground motions through the set of 60 truncated strain compatible soil profiles. These ARS include the effects of down-coming waves from the soil and rock layers above to the top of Zone III rock.

3. TSCR analysis, which uses the truncated strain compatible soil layers obtained from the full column analyses after removing all layers above the GMRS horizon (Elevation 224 ft). The geologic outcrop ARS are obtained as the mean of 60 ARS results at top of the truncated soil columns (Elevation 224 ft) by propagating the rock ground motions through the set of 60 truncated soil profiles. Note that since the rock profile below the GMRS horizon entirely consists of Zone III-IV and Zone IV rock material which behave linearly (constant damping ratio and shear modulus), there are no confining effects from soils above.

The LF and HF input hard rock spectra at 10^{-4} and 10^{-5} annual frequencies are presented in Figure 2.5.2-274. The hard rock spectra are applied at bedrock having a shear wave velocity of 9,200 fps, and are propagated upward from bedrock to the considered horizons, through the set of 60 simulated and truncated profiles, representing the site-specific conditions using the computer program P-SHAKE. The mean amplification factors for each elevation are calculated as the ratio of the calculated mean ARS at that elevation to their corresponding input hard rock spectrum.

For the full column analysis of the RB/FB soil column, the log-mean (median) strains induced in the soil layers corresponding to the 4 input ground motions (HF and LF at 10^{-4} and 10^{-5} hazard levels) are presented in Figure 2.5.2-275. Note that the strains increase with depth within the saprolite soil strata. A sudden drop in strain amplitudes occurs at the interface with the first rock layer and the rock layers below the foundation have very small strain amplitudes which agrees with the underlying assumption that the Zone III-IV and Zone IV rock below the foundation level remain elastic when subject to the input ground motion. Figure 2.5.2-276 presents the log-mean low strain and strain compatible shear wave velocity profiles for each input ground motion to identify the amount of softening (shear modulus reduction) that occurs in the soil column. Note that the reductions are only applicable to the nonlinear material in the analysis, i.e., the saprolite layers and Zone III rock. The

reductions observed in the shear wave velocity profiles are consistent with the strain profiles presented earlier. Figure 2.5.2-277 presents the log-mean damping ratio profiles corresponding to the 4 input ground motions as well as the low-strain damping profile. The increases in damping ratio are only applicable to the nonlinear material in the analysis and are consistent with the strain profiles presented earlier.

For the full column analysis, Figures 2.5.2-278 and 2.5.2-279 present the mean amplification functions for the RB/FB soil column set at the FG, Elevation 290 ft, at the bottom of foundation elevation for RB/FB (Elevation 224 ft, denoted as RB-FB BoF) and at the bottom of foundation elevation for CB (Elevation 241 ft, denoted as CB BoF) at the 10^{-4} and 10^{-5} hazard levels, respectively. While the foundation level amplification is essentially the same for the 10^{-4} and 10^{-5} hazard levels, the ground surface amplification function amplitudes are somewhat less for the 10^{-5} hazard level and at a lower frequency due to more saprolite nonlinearity at 10^{-5} hazard level compared to the 10^{-4} hazard level. Figures 2.5.2-280 and 2.5.2-281 present the mean full column outcrop ARS for the RB/FB soil column set due to the LF and HF motions at the 10^{-4} and 10^{-5} hazard levels, respectively, along with the corresponding rock motions. Note that the response at finished grade at 10^{-4} hazard level is significantly higher than the bottom of foundation (BoF) level responses suggesting significant amplification of the ground motion in the saprolite layers.

Similarly for the partial column analysis of RB/FB soil column, Figures 2.5.2-282 and 2.5.2-283 present the amplification functions at the bottom of foundation elevations for RB/FB and CB at the 10^{-4} and 10^{-5} hazard levels, respectively. Figures 2.5.2-284 and 2.5.2-285 present the mean partial column outcrop ARS at the same elevations due to the LF and HF motions at the 10^{-4} and 10^{-5} hazard levels, respectively, along with the corresponding rock motions.

For the TSCR analysis of RB/FB soil column, Figures 2.5.2-286 and 2.5.2-287 present the amplification functions at the GMRS elevation (Elevation 224 ft) at the 10^{-4} and 10^{-5} hazard levels, respectively. Figures 2.5.2-288 and 2.5.2-289 present the mean geologic outcrop ARS at the same elevation due to the LF and HF motions at the 10^{-4} and 10^{-5} hazard levels, respectively, along with the corresponding rock motions.

2.5.2.5.3.2 Site Response Analysis for the CB Soil Column

Similar to the RB/FB soil column, the CB soil column results are also used in determination of the GMRS (at Elevation 224 ft), full column and partial column outcrop FIRS for RB/FB (at Elevation 224 ft) and full column and partial column outcrop FIRS for CB (at Elevation 241 ft). Accordingly, three sets of analyses (full column analysis, partial column analysis, and TSCR analyses) are conducted using the CB soil column following the same methodology as was described above for the RB/FB soil column.

Similar to the RB/FB soil column, the strain compatible properties for the CB soil column are calculated from the full soil column analyses and used to propagate the 4 input ground motions (HF and LF at 10^{-4} and 10^{-5} hazard levels) to determine the full column outcrop ARS and partial column outcrop ARS and their corresponding amplification functions at Elevation 241 ft and full column outcrop ARS, partial column outcrop ARS, as well as the geologic outcrop ARS and their corresponding amplification functions at Elevation 224 ft. As an example of these results the full column outcrop ARS at 10^{-4} and 10^{-5} hazard levels are presented in Figures 2.5.2-290 and 2.5.2-291.

2.5.2.5.3.3 Site Response Analysis for the FWSC Soil Column

The FWSC soil column results are used in determination of the geologic outcrop FIRS for FWSC (at Elevation 282 ft). Accordingly, a TSCR analysis is carried out for this soil column in which the top 8 ft of saprolite layers are removed from the strain compatible soil profiles and the geologic outcrop ARS and their corresponding amplification factors are determined at the top of the truncated soil column (Elevation 282 ft). As an example of these results the geologic column outcrop ARS at 10^{-4} and 10^{-5} hazard levels are presented in Figures 2.5.2-292 and 2.5.2-293.

2.5.2.5.4 Horizontal Uniform Hazard Response Spectra at the GMRS Horizon

This section presents the horizontal 10^{-4} and 10^{-5} UHRS at the GMRS and FIRS horizons as well as the finished grade in each considered soil column. The UHRS at each hazard level are obtained by enveloping its corresponding HF and LF mean spectra obtained at that elevation.

For the RB/FB soil column, Figures 2.5.2-294, 2.5.2-295, and 2.5.2-296 show the 10^{-4} and 10^{-5} horizontal UHRS obtained from enveloping the LF and HF full column outcrop ARS discussed in Section 2.5.2.5.3.1 at

Elevations 224 ft (BoF for RB/FB), 241 ft (BoF for CB), and 290 ft (finished grade), respectively. Similarly, Figures 2.5.2-297 and 2.5.2-298 provide the 10^{-4} and 10^{-5} horizontal UHRS obtained from enveloping the LF and HF partial column outcrop ARS discussed in Section 2.5.2.5.3.1 at Elevations 224 ft (BoF for RB/FB) and 241 ft (BoF for CB). At last for this soil column, Figure 2.5.2-299 provides the 10^{-4} and 10^{-5} horizontal UHRS obtained from enveloping the LF and HF geologic outcrop ARS discussed in Section 2.5.2.5.3.1 at Elevation 224 ft (GMRS horizon).

For the CB soil column, Figures 2.5.2-300, 2.5.2-301, and 2.5.2-302 show the 10^{-4} and 10^{-5} horizontal UHRS obtained from enveloping the LF and HF full column outcrop ARS discussed in Section 2.5.2.5.3.2 at Elevations 224 ft (BoF for RB/FB), 241 ft (BoF for CB), and 290 ft (finished grade), respectively. Similarly, Figures 2.5.2-303 and 2.5.2-304 provide the 10^{-4} and 10^{-5} horizontal UHRS obtained from enveloping the LF and HF partial column outcrop ARS discussed in Section 2.5.2.5.3.2 at Elevations 224 ft (BoF for RB/FB) and 241 ft (BoF for CB), respectively. At last for this soil column, Figure 2.5.2-305 provides the 10^{-4} and 10^{-5} horizontal UHRS obtained from enveloping the LF and HF geologic outcrop ARS discussed in Section 2.5.2.5.3.2 at Elevation 224 ft (GMRS horizon).

Finally, for the FWSC soil column, Figure 2.5.2-306 shows the 10^{-4} and 10^{-5} horizontal UHRS obtained from enveloping the LF and HF geologic outcrop ARS discussed in Section 2.5.2.5.3.3 for the FWSC soil column at Elevation 282 ft (BoF for the FWSC).

Note that the above figures also present the design response spectra (DRS) corresponding to each considered horizon which is calculated using the 10^{-4} and 10^{-5} UHRS, as discussed in Section 2.5.2.6.1.

2.5.2.6 Design Response Spectra

In Section 2.5.2.5 the results of site response analyses are presented for input to the development of six design response spectra (DRS): five different foundation input response spectra (FIRS) and the GMRS, as presented in this section:

- RB/FB Full Column Outcrop FIRS
- CB Full Column Outcrop FIRS
- RB/FB Partial Column Outcrop FIRS
- CB Full Partial Outcrop FIRS

- PBSRS for RB/FB and CB
- FWSC Geologic Outcrop FIRS
- GMRS

2.5.2.6.1 Horizontal DRS

Whether it is a FIRS or the GMRS, the horizontal DRS are developed following the RG 1.208 performance-based procedure for the assessment of a site-specific seismic design ground motion, satisfying the requirements of 10 CFR 100.23, paragraphs (c), (d)(1), and (d)(2), and leading to the establishment of an SSE to satisfy the design requirements of 10 CFR 50, Appendix S. The steps necessary to develop the design ground motions are described in NUREG-0800, Chapter 2, Site Characteristics and Site Parameters, and Chapter 3, Design of Structures, Components, Equipment and Systems.

The performance-based, site-specific design earthquake ground motion is developed using the method presented in RG 1.208, Section B, which is analogous to the development of the ASCE/SEI Standard 43-05 (ASCE/SEI, 2005 (Reference 2.5-384) DRS that achieves the annual first onset of significant inelastic deformation (FOSID) target performance goal with a performance factor (P_F) of 10^{-5}, and hazard exceedance probability (H_D) of 10^{-4}, described in ASCE/SEI Standard 43-05, Chapters 1 and 2. To meet the performance goal, the performance-based methodology specifies the two parameters A_R and DF:

$$A_R(f) = UHRS_{sH}(f\,|10^{-5})/UHRS_{sH}(f\,|10^{-4}) \qquad (2.5.2.6\text{-}1)$$

where $A_R(f)$ represents the slope of the site-specific hazard curve for a given spectral frequency f between hazard levels of mean annual frequencies of exceedance (MAFE) of 10^{-4} and 10^{-5}, estimated from the structure-, soil column-, and horizon-specific, horizontal UHRS, $UHRS_{sH}(f\,|MAFE)$, presented in Section 2.5.2.5; and

$$DF(f) = Max\{1.0,\ 0.6\,[A_R(f)]^{0.8}\} \qquad (2.5.2.6\text{-}2)$$

where the design factor $DF(f)$ was developed to meet the performance goal, as presented in ASCE/SEI Standard 43-05.

Given $A_R(f)$ and $DF(f)$, the horizontal $DRS_H(f)$ is given by

$$DRS_H(f) = DF(f) \times UHRS_{sH}(f\,|10^{-4}) \text{ for } A_R(f) \le 4.2 \qquad (2.5.2.6\text{-}3a)$$

$$= 0.45 \times UHRS_{sH}(f\,|10^{-5}) \text{ for } A_R(f) > 4.2 \qquad (2.5.2.6\text{-}3b)$$

Equation 2.5.2.6-3a is based on the assumption that the hazard curves are approximated by a power law equation (i.e., linear on a log-log plot) in the range of 10^{-4} and 10^{-5}. As presented in RG 1.208, if A_R is greater than 4.2, then this assumption is not valid and in these cases, it is acceptable to use a value equal to 45 percent of the mean 10^{-5} UHRS, given in Equation 2.5.2.6-3b.

2.5.2.6.1.1 RB/FB Full Column Outcrop Horizontal FIRS

Figure 2.5.2-294 shows the plot of the $UHRS_{sH}(f\,|10^{-4})$ and $UHRS_{sH}(f\,|10^{-5})$ for the RB/FB full column outcrop at the elevation of 224 ft. The same figure shows the corresponding DRS, as developed in application of Equations 2.5.2.6-1 through 2.5.2.6-3.

Similarly, Figure 2.5.2-300 shows the plot of the $UHRS_{sH}(f\,|10^{-4})$ and $UHRS_{sH}(f\,|10^{-5})$ for the CB full column outcrop at the same elevation of 224 ft. The same figure shows the corresponding DRS, as developed in application of Equations 2.5.2.6-1 through 2.5.2.6-3.

Given the proximity of the RB/FB and CB structures and consideration of marginal conservatism, the RB/FB Full Column Outcrop Horizontal FIRS, as shown in Figure 2.5.2-307 and tabulated in Table 2.5.2-222, is the envelope of the two DRS shown in Figures 2.5.2-294 and 2.5.2-300.

2.5.2.6.1.2 CB Full Column Outcrop Horizontal FIRS

Figure 2.5.2-301 shows the plot of the $UHRS_{sH}(f\,|10^{-4})$ and $UHRS_{sH}(f\,|10^{-5})$ for the CB full column outcrop at the elevation of 241 ft. The same figure shows the corresponding DRS, as developed in application of Equations 2.5.2.6-1 through 2.5.2.6-3.

Similarly, Figure 2.5.2-295 shows the plot of the $UHRS_{sH}(f\,|10^{-4})$ and $UHRS_{sH}(f\,|10^{-5})$ for the RB/FB full column outcrop at the same elevation of 241 ft. The same figure shows the corresponding DRS, as developed in application of Equations 2.5.2.6-1 through 2.5.2.6-3.

Given the proximity of the CB and RB/FB structures and consideration of marginal conservatism, the CB Full Column Outcrop Horizontal FIRS, as shown in Figure 2.5.2-308 and tabulated in Table 2.5.2-223, is the envelope of the two DRS shown in Figures 2.5.2-295 and 2.5.2-301.

2.5.2.6.1.3 RB/FB Partial Column Outcrop Horizontal FIRS

Figure 2.5.2-297 shows the plot of the $UHRS_{sH}(f\,|10^{-4})$ and $UHRS_{sH}(f\,|10^{-5})$ for the RB/FB partial column outcrop at the elevation of 224 ft. The same figure shows the corresponding DRS, as developed in

application of Equations 2.5.2.6-1 through 2.5.2.6-3.

Similarly, Figure 2.5.2-303 shows the plot of the $UHRS_{sH}(f\,|10^{-4})$ and $UHRS_{sH}(f\,|10^{-5})$ for the CB partial column outcrop at the same elevation of 224 ft. The same figure shows the corresponding DRS, as developed in application of Equations 2.5.2.6-1 through 2.5.2.6-3.

Given the proximity of the RB/FB and CB structures and consideration of marginal conservatism, the RB/FB Partial Column Outcrop Horizontal FIRS, as shown in Figure 2.5.2-309 and tabulated in Table 2.5.2-224, is the envelope of the two DRS shown in Figures 2.5.2-297 and 2.5.2-303.

2.5.2.6.1.4 CB Partial Outcrop Horizontal FIRS

Figure 2.5.2-304 shows the plot of the $UHRS_{sH}(f\,|10^{-4})$ and $UHRS_{sH}(f\,|10^{-5})$ for the CB partial column outcrop at the elevation of 241 ft. The same figure shows the corresponding DRS, as developed in application of Equations 2.5.2.6-1 through 2.5.2.6-3.

Similarly, Figure 2.5.2-298 shows the plot of the $UHRS_{sH}(f\,|10^{-4})$ and $UHRS_{sH}(f\,|10^{-5})$ for the RB/FB partial column outcrop at the same elevation of 241 ft. The same figure shows the corresponding DRS, as developed in application of Equations 2.5.2.6-1 through 2.5.2.6-3.

Given the proximity of the CB and RB/FB structures and consideration of marginal conservatism, the CB Partial Column Outcrop Horizontal FIRS, as shown in Figure 2.5.2-310 and tabulated in Table 2.5.2-225, is the envelope of the two DRS shown in Figures 2.5.2-298 and 2.5.2-304.

2.5.2.6.1.5 Horizontal PBSRS for RB/FB and CB

Figure 2.5.2-296 shows the plot of the $UHRS_{sH}(f\,|10^{-4})$ and $UHRS_{sH}(f\,|10^{-5})$ for the RB/FB full column outcrop at the finished grade elevation of 290 ft. The same figure shows the corresponding DRS, as developed in application of Equations 2.5.2.6-1 through 2.5.2.6-3.

Similarly, Figure 2.5.2-302 shows the plot of the $UHRS_{sH}(f\,|10^{-4})$ and $UHRS_{sH}(f\,|10^{-5})$ for the CB full column outcrop at the same finished grade elevation of 290 ft. The same figure shows the corresponding DRS, as developed in application of Equations 2.5.2.6-1 through 2.5.2.6-3.

Given the proximity of the RB/FB and CB structures and consideration of marginal conservatism, the PBSRS for RB/FB and CB, as shown in Figure 2.5.2-311 and tabulated in Table 2.5.2-226, is the envelope of the two DRS shown in Figures 2.5.2-296 and 2.5.2-302.

2.5.2.6.1.6 FWSC Geologic Outcrop Horizontal FIRS

Figure 2.5.2-306 shows the plot of the $UHRS_{sH}(f\,|10^{-4})$ and $UHRS_{sH}(f\,|10^{-5})$ for the FWSC geologic outcrop at the elevation of 282 ft. The same figure shows the corresponding DRS, as developed in application of Equations 2.5.2.6-1 through 2.5.2.6-3. This DRS is the FWSC Geologic Outcrop Horizontal FIRS, as shown in Figure 2.5.2-312 and tabulated in Table 2.5.2-227.

2.5.2.6.1.7 Horizontal GMRS

Figure 2.5.2-299 shows the plot of the $UHRS_{sH}(f\,|10^{-4})$ and $UHRS_{sH}(f\,|10^{-5})$ for the RB/FB geologic outcrop at the elevation of 224 ft. The same figure shows the corresponding DRS, as developed in application of Equations 2.5.2.6-1 through 2.5.2.6-3.

Similarly, Figure 2.5.2-305 shows the plot of the $UHRS_{sH}(f\,|10^{-4})$ and $UHRS_{sH}(f\,|10^{-5})$ for the CB geologic outcrop at the same elevation of 224 ft. The same figure shows the corresponding DRS, as developed in application of Equations 2.5.2.6-1 through 2.5.2.6-3.

Given the proximity of the RB/FB and CB structures and consideration of marginal conservatism, the GMRS, as shown in Figure 2.5.2-313 and tabulated in Table 2.5.2-228, is the envelope of the two DRS shown in Figures 2.5.2-299 and 2.5.2-305.

2.5.2.6.2 Vertical DRS

As presented in RG 1.208, a vertical response spectrum is developed by combining the appropriate horizontal response spectrum and the most up-to-date V/H response spectral ratios appropriate for the site. That is,

$$DRS_V(f) = DRS_H(f) \times V/H(f) \qquad (2.5.2.6\text{-}4)$$

While appropriate V/H ratios for CEUS rock and soil sites are best determined from the most up-to-date attenuation relations, there are currently, however, no CEUS GMPEs that predict vertical ground motions. Again, as presented in RG 1.208, for CEUS rock sites—with V_{S30} of at least 9,200 ft/s—appropriate V/H ratios are provided in Reference 2.5-385. For CEUS soil sites, NUREG/CR-6728, Appendix J (Reference 2.5-385) outlines a procedure to determine a WUS-to-CEUS transfer function that may be used to modify the WUS V/H ratios.

Appendix J of the NUREG describes a procedure by which V/H functions can be estimated for CEUS sites where there is little empirical data. The NUREG procedure is to consider the wealth of empirical horizontal and

vertical ground motion data for WUS, as well as known differences in relevant crustal characterizations of WUS and CEUS, as a guide for developing transfer functions that can be used to scale accepted CEUS V/H functions for application to a given CEUS location. As discussed in the NUREG, this approach was used to develop the NUREG-recommended hard rock CEUS V/H functions (Reference 2.5-385, Figure 4-39 and Table 4-5). Since the Unit 3 site is not a hard rock site (i.e., explicitly, shear-wave velocity of 9,200 ft/s), then the effects of lower shear-wave velocity on V/H should be considered.

The following equation indicates an implementation of the NUREG procedure used here:

$$V/H_{CEUS,soil} = V/H_{CEUS,rock} \times f\,(\text{rock-to-soil}) \times f\,(\text{WUS-to-CEUS}) \qquad (2.5.2.6\text{-}5)$$

where:

$V/H_{CEUS,rock}$ = the appropriate hard rock CEUS V/H from the NUREG

f (rock-to-soil) = transfer function for converting rock V/H to soil V/H

f (WUS-to-CEUS) = transfer function for converting WUS V/H to CEUS V/H

Given the dearth of CEUS observations of horizontal or vertical ground motions, the NUREG procedure is necessarily approximating in nature. In development and use of the f (rock-to-soil) transfer function, the characterization of “rock” and “soil” ground motions using readily available WUS relationships has often been generic, intended to capture dominant vertical ground motion characteristics that are distinctly different on rock versus weaker material. Current methodologies, however, allow for more explicit distinction in the specification of V_{S30}, as discussed below. The f (WUS-to-CEUS) transfer function is intended to capture the most relevant distinction between WUS and CEUS ground motions. As presented in the NUREG, even the $V/H_{CEUS,rock}$ function entails significant modeling assumptions and approximations, e.g., the dependence of V/H observed on magnitude and distance uses only three discrete bins of rock peak ground acceleration (PGA) values as a proxy for magnitude and distance dependency (Reference 2.5-385, Figure 4-39 and Table 4-5).

For the development of vertical FIRS and GMRS in this section, each of the three elements of the right side of Equation 2.5.2.6-5 are estimated, as appropriate for the Unit 3 site, in order to develop an estimate of an

appropriate V/H for the application of Equation 2.5.2.6-4.

$V/H_{CEUS,rock}$

Figure 2.5.2-314 plots WUS rock and CEUS rock V/H ratios from the NUREG (Reference 2.5-385). The CEUS rock V/H from the NUREG gives the $V/H_{CEUS,rock}$ of Equation 2.5.2.6-5, as a function of the appropriate hard rock PGA. Given the hard rock PSHA results in Table 2.5.2-217, the 10^{-4} and 10^{-5} PGA values are 0.259g and 0.847g, respectively. Applying RG 1.208 DRS Equations 2.5.2.6-1 through 2.5.2.6-3, an equivalent hard rock DRS PGA would be 0.401g. Consequently, the appropriate NUREG CEUS rock V/H function, to be used as $V/H_{CEUS,rock}$, is the middle V/H ratio relationship, specified for $0.2g < PGA \leq 0.5g$.

***f* (rock-to-soil)**

To estimate the transfer function for converting rock V/H to soil V/H, the WUS V/H model of Gülerce and Abrahamson (2011) (Reference 2.5-388), referred to here as the "GA11" model, is used. This model is a function of magnitude, distance, V_{S30}, and various fault parameters, as discussed further, below.

The *f* (rock-to-soil) transfer function takes the following form:

$$f\text{ (rock-to-soil)} = V/H_{WUS,soil}/V/H_{WUS,rock} \qquad (2.5.2.6\text{-}6)$$

where "soil" corresponds to the appropriate V_{S30} for the FIRS/GMRS soil profile horizon of interest, and "rock" is for a V_{S30} of 9,200 ft/s.

The magnitude and distance dependence of the V/H GA11 model is addressed by considering the controlling earthquakes given in Table 2.5.2-218 for high-frequency and low-frequency at MAFE of 10^{-4} and 10^{-5}.

For the purpose of developing the *f* (rock-to-soil) transfer function of Equation 2.5.2.6-6, the fact that the current EPRI (2004) GMPEs are not dependent on most fault parameters, and that the application of V/H considers the PSHA contribution of multiple seismic sources, the fault parameters used with the GA11 model are kept generic: e.g., strike-slip fault, dip 90 degrees, no hanging wall/foot wall.

***f* (WUS-to-CEUS)**

The purpose of this transfer function is to basically adjust the *f* (rock-to-soil) transfer function to be appropriate for CEUS, since what

was developed above from GA11 is based on WUS GMPE data and models. As discussed in the NUREG, as well as EPRI (1993) (Reference 2.5-387), development of such regional transfer functions require significant modeling and analyses to obtain for even generic CEUS transfer functions.

As in other recent SSAR and FSAR documents in the NRC Reading Room that use the NUREG (Reference 2.5-385) procedure, a simplified approach is considered here in estimating the *f* (WUS-to-CEUS) transfer function. Similar to what is seen in ground motions, WUS V/H functions tend to peak at a lower frequency than CEUS V/H functions. This can be seen in Figure 2.5.2-314. As discussed in the NUREG, this high-frequency shift is generally attributed to the lower kappa (κ) values (shallow crustal damping factor) in CEUS than WUS. To affect this frequency shift – similar to considering the peak in WUS rock V/H at ~16 to 17 Hz in Figure 2.5.2-314 shifted to the peak in CEUS rock V/H at ~60 Hz – one needs simply to scale the frequencies of the *f* (rock-to-soil) = $V/H_{WUS,soil}/V/H_{WUS,rock}$ function by the ratio of the peak frequencies in Figure 2.5.2-314. The scaling factor of (62.5/16.7) is used, where the numerator and denominator values are taken at the frequencies (in Hz) of the CEUS and WUS V/H peaks, respectively, as given in the NUREG Tables 4.5 and 4.4, respectively, and shown in Figure 2.5.2-314. Therefore, two of the terms on the right-side of Equation 2.5.2.6-5 become

$$f\text{ (rock-to-soil) x }f\text{ (WUS-to-CEUS)} = (V/H_{WUS,soil}/V/H_{WUS,rock})_{frequency\text{-}shifted} \quad (2.5.2.6\text{-}7)$$

Or, to combine Equations 2.5.2.6-4, 2.5.2.6-5, and 2.5.2.6-7

$$DRS_V(f) = DRS_H(f) \times V/H_{CEUS,rock} \times (V/H_{WUS,soil} / V/H_{WUS,rock})_{frequency\text{-}shifted} \quad (2.5.2.6\text{-}8)$$

$V/H_{CEUS,soil}$

Finally, to implement Equation 2.5.2.6-5, it remains only to multiply the appropriate CEUS rock V/H ($V/H_{CEUS,rock}$) by the frequency-shifted $V/H_{WUS,soil}$ / $V/H_{WUS,rock}$ of Equation 2.5.2.6-7.

2.5.2.6.2.1 RB/FB and CB Vertical FIRS

In the development of the $DRS_V(f)$ from Equation 2.5.2.6-8 for each of these FIRS, the corresponding $DRS_H(f)$ are given as the various horizontal FIRS in Sections 2.5.2.6.1.1 through 2.5.2.6.1.4.

As presented earlier, the appropriate $V/H_{CEUS,rock}$ for all of the FIRS, as well as the GMRS, is the middle CEUS hard rock V/H ratio relationship, specified for $0.2g < PGA \leq 0.5g$, given by the NUREG (Reference 2.5-385).

The remaining term of Equation 2.5.2.6-8 is the frequency-shifted version of the ratio $V/H_{WUS,soil} / V/H_{WUS,rock}$, where the numerator and denominator are given by the GA11 V/H model. In the determination of the "soil" and "rock" V/H_{WUS} ratios, the four magnitude-distance pairs of controlling earthquakes (10^{-4} and 10^{-5}, HF and LF), given in Table 2.5.2-218, are considered. For the denominator $V/H_{WUS,rock}$ the V_{S30} is fixed to 9,200 ft/s. For the numerator $V/H_{WUS,soil}$ the V_{S30} is set to the value corresponding to the FIRS soil column and horizon:

Soil Column	Elev. (ft)	V_{S30}
RB/FB Column	241	6,078 ft/s
RB/FB Column	224	6,783 ft/s
CB Column	241	6,068 ft/s
CB Column	224	7,553 ft/s

One of the aspects of the GA11 model is that for V_{S30} greater than about 5,000 ft/s, the V/H ratio does not change. Therefore, for the RB/FB and CB columns at the elevations above $(V/H_{WUS,soil} / V/H_{WUS,rock})_{frequency\text{-}shifted}$ is simply unity, and the applicable V/H ratio $V/_{HCEUS,soil}$ is just equal to $V/H_{CEUS,rock}$, the middle CEUS hard rock V/H ratio relationship, specified for $0.2g < PGA \leq 0.5g$, given by the NUREG (Reference 2.5-385). See Figure 2.5.2-314.

Upon application of Equation 2.5.2.6-4, the V/H ratios and corresponding $FIRS_V(f)$ for the RB/FB Full Column Outcrop, CB Full Column Outcrop, RB/FB Partial Column Outcrop, and CB Partial Outcrop are tabulated in Table 2.5.2-222, 2.5.2-223, 2.5.2-224, and 2.5.2-225, respectively, and the $FIRS_V(f)$ are shown in Figures 2.5.2-307, 2.5.2-308, 2.5.2-309, and 2.5.2-310, respectively.

2.5.2.6.2.2 Vertical PBSRS for RB/FB and CB

In the development of the $DRS_V(f)$ from Equation 2.5.2.6-8 for the PBSRS for RB/FB and CB, the corresponding $DRS_H(f)$ is given as the horizontal PBSRS in Section 2.5.2.6.1.5.

As presented earlier, the appropriate $V/H_{CEUS,rock}$ for all of the FIRS, as well as the GMRS and PBSRS, is the middle CEUS hard rock V/H ratio relationship, specified for 0.2g < PGA ≤ 0.5g, given by NUREG/CR-6728.

The remaining term of Equation 2.5.2.6-8 is the frequency-shifted version of the ratio $V/H_{WUS,soil}$ /$V/H_{WUS,rock}$, where the numerator and denominator are given by the GA11 V/H model. In the determination of the "soil" and "rock" V/H_{WUS} ratios, the four magnitude-distance pairs of controlling earthquakes (10^{-4} and 10^{-5}, HF and LF), given in Table 2.5.2-218, are considered. For the denominator $V/H_{WUS,rock}$ the V_{S30} is fixed to 5,000 ft/s—equivalent to using V_{S30} fixed to 9,200 ft/s, as discussed earlier. For the numerator $V/H_{WUS,soil}$ the V_{S30} is set to the pair of values corresponding to the soil columns and finished grade horizon considered for the PBSRS:

Soil Column	Elevation (ft)	V_{S30}
RB/FB Column	290 {finished grade}	3,423 ft/s
CB Column	290 {finished grade}	2,439 ft/s

Considering the V_{S30} of 2,439 ft/s, Figure 2.5.2-315 shows the four magnitude-distance versions of the ratio $V/H_{WUS,soil}$ /$V/H_{WUS,rock}$, where they are very similar, with the envelope being given by the **M** 6.2 at a distance of 17 km. Figure 2.5.2-316 shows the four frequency-shifted versions of the ratio $V/H_{WUS,soil}$ /$V/H_{WUS,rock}$.

Shown in Figure 2.5.2-317, the $V/H_{CEUS,rock}$ has been multiplied by each of the four frequency-shifted versions of the ratio $V/H_{WUS,soil}$ / $V/H_{WUS,rock}$ to give V/H ratios considering the V_{S30} of 2,439 ft/s. As a comparison, this figure also shows $V/H_{CEUS,rock}$ and the often-considered V/H ratio from RG 1.60. For frequencies less than about 2.5 Hz, the V/H ratio developed here is slightly greater than that given by RG 1.60. For frequencies above about 3.5 Hz the RG 1.60 V/H ratio is 1.0, while the V/H ratio developed here initially decreases between about 3.5 Hz and 7.5 Hz, then increases to a V/H ratio greater than 1.0 between about 40 and 85 Hz. The high frequency V/H exceedance of 1.0 reflects the character of the $V/H_{CEUS,rock}$ for moderate to high ground motions. The lower value dip in the V/H ratio between about 2 and 20 Hz is addressed further below.

Similar to the process above for determining $V/H_{CEUS,soil}$ ratios for a V_{S30} of 2,439 ft/s (743 m/s) in Figure 2.5.2-317, Figure 2.5.2-318 shows a similar plot of $V/H_{CEUS,soil}$ ratios for the second V_{S30} of 3,423 ft/s (1.043 m/s). This second V/H ratio is equal to or slightly higher than that for the V_{S30} of 2,439 ft/s, except for slightly lower V/H values in the peak range of 35 to 75 Hz.

For the purpose a single V/H ratio for application to the PBSRS $DRS_H(f)$, Figure 2.5.2-319 shows an *initial* $V/H_{CEUS,soil}$ ratio for the PBSRS, based on the envelope of all eight $V/H_{CEUS,soil}$ ratios presented above.

As initially described earlier in this section regarding Figure 2.5.2-317, the initial PBSRS V/H in Figure 2.5.2-319 has a dip in V/H values between 4.5 and 20 Hz, which could be considered an unconservative or WUS-biased character. Analogous to what was done in the NUREG for the CEUS V/H rock ratios, as compared to the WUS V/H rock ratios (see Figure 2.5.2-314) the V/H values in this dip were raised to give the *final* V/H ratio for the PBSRS for RB/FB and CB, shown in Figure 2.5.2-320. As seen in Figure 2.5.2-320, the final $V/H_{CEUS,soil}$ ratio for the PBSRS for RB/FB and CB is very similar to $V/H_{CEUS,rock}$.

Upon application of Equation 2.5.2.6-4, the V/H ratio and corresponding $PBSRS_V(f)$ for the PBSRS for CB/FB and CB are tabulated in Table 2.5.2-226 and the $PBSRS_V(f)$ is shown in Figure 2.5.2-311.

2.5.2.6.2.3 FWSC Geologic Outcrop Vertical FIRS

In the development of the $DRS_V(f)$ from Equation 2.5.2.6-8 for the FWSC FIRS, the corresponding $DRS_H(f)$ is given as the horizontal FIRS in the earlier Section 2.5.2.6.1.6.

As presented in Section 2.5.2.6.2, the appropriate $V/H_{CEUS,rock}$ for all of the FIRS, as well as the GMRS, is the middle CEUS hard rock V/H ratio relationship, specified for 0.2g < PGA ≤ 0.5g, given by NUREG/CR-6728.

The remaining term of Equation 2.5.2.6-8 is the frequency-shifted version of the ratio $V/H_{WUS,soil}/V/H_{WUS,rock}$, where the numerator and denominator are given by the GA11 V/H model. In the determination of the "soil" and "rock" V/H_{WUS} ratios, the four magnitude-distance pairs of controlling earthquakes (10^{-4} and 10^{-5}, HF and LF), given in Table 2.5.2-218, are considered. For the denominator $V/H_{WUS,rock}$ the V_{S30} is fixed to 5,000 ft/s, equivalent to using V_{S30} fixed to 9,200 ft/s, as

discussed earlier. For the numerator $V/H_{WUS,soil}$ the V_{S30} is set to the value corresponding to the FIRS soil column and horizon:

Soil Column	Elev. (ft)	V_{S30}
FWSC Column	282	2,124 ft/s

Following the same procedure as detailed in Section 2.5.2.6.2.2 for the PBSRS, a similar $V/H_{CEUS,soil}$ for the FWSC Geologic Outcrop FIRS was determined, therefore, the final PBSRS $V/H_{CEUS,soil}$ is used for the FWSC Geologic Outcrop FIRS.

Upon application of Equation 2.5.2.6-4, the V/H ratio and corresponding $FIRS_V(f)$ for the FWSC Geologic Outcrop are tabulated in Table 2.5.2-227 and the $FIRS_V(f)$ is shown in Figure 2.5.2-312.

2.5.2.6.2.4 Vertical GMRS

In the development of the $DRS_V(f)$ from Equation 2.5.2.6-8 for the GMRS, the corresponding $DRS_H(f)$ is given as the horizontal GMRS in Section 2.5.2.6.1.7.

As presented in Section 2.5.2.6.2, the appropriate $V/H_{CEUS,rock}$ for all of the FIRS, as well as the GMRS, is the middle CEUS hard rock V/H ratio relationship, specified for 0.2g < PGA ≤ 0.5g, given by NUREG/CR-6728.

The remaining term of Equation 2.5.2.6-8 is the frequency-shifted version of the ratio $V/H_{WUS,soil}/V/H_{WUS,rock}$, where the numerator and denominator are given by the GA11 V/H model. In the determination of the "soil" and "rock" V/H_{WUS} ratios, the four magnitude-distance pairs of controlling earthquakes (10^{-4} and 10^{-5}, HF and LF), given in Table 2.5.2-218, are considered. For the denominator $V/H_{WUS,rock}$ the V_{S30} is fixed to 9,200 ft/s. For the numerator $V/H_{WUS,soil}$ the V_{S30} is set to the pair of values corresponding to the soil columns and horizon considered for the GMRS:

Soil Column	Elev. (ft)	V_{S30}
RB/FB Column	224	6,783 ft/s
CB Column	224	7,553 ft/s

One of the aspects of the GA11 model is that for V_{S30} greater than about 5,000 ft/s, the V/H ratio does not change. Therefore, for the RB/FB and CB columns at the elevation above $(V/H_{WUS,soil}/V/H_{WUS,rock})_{frequency\text{-}shifted}$ is simply unity, and the applicable V/H ratio is just $V/H_{CEUS,rock}$, the middle CEUS hard rock V/H ratio relationship,

BASIS: NEW

specified for 0.2g < PGA ≤ 0.5g, given by NUREG/CR-6728. See Figure 2.5.2-314.

Upon application of Equation 2.5.2.6-4, the V/H ratio and corresponding $GMRS_V(f)$ are tabulated in Table 2.5.2-228 and the $GMRS_V(f)$ is shown in Figure 2.5.2-313.

NAPS COL 2.0-27-A
NAPS ESP VAR 2.0-4

Table 2.5.2-201 Statistics of the Original and Updated CEUS SSC Earthquake Catalog

	All Earthquakes			Mainshock (Independent) Earthquakes		
	CEUS SSC[1]	Update[2]	Total Catalog	CEUS SSC[1]	Update[2]	Total Catalog
ALL (no Dist or M filter)	10,984	3,298	14,282	6,965	946	7,911
E[**M**] ≥ **2.9**	3,298	474	3,772	2,563	200	2,763
Dist ≤ 322 km (200 miles)	398	80	478	312	22	334
E[**M**] ≥ **2.9,** **Dist ≤ 322 km (200 miles)**	159	12	171	135	6	141
Dist ≤ 80 km (50 miles)	73	53	126	62	4	66
E[**M**] ≥ **2.9** **Dist ≤ 80 km (50 miles)**	36	7	43	33	1	34

1. CEUS SSC Report (EPRI et al., 2012) (Reference 2.5-223); See Section 2.5.2.1.1.
2. See Section 2.5.2.1.2.

BASIS: NEW

NAPS COL 2.0-27-A
NAPS ESP VAR 2.0-4

Table 2.5.2-202 Earthquakes Within 322 km (200 miles) from the Updated CEUS SSC Earthquake Catalog for Independent or Mainshock Earthquakes with Magnitudes E[M] ≥ 2.9

	Coordinated Universal Time (UTC)						Epicentral Location									
TID	Year	Month	Day	Hour	Minute	Second	Lat. (+N°)	Long. (+E°)	Depth (km)	ERH (km)	E[M]	N*	sigM	EQNO	FLAG	Dist (km)
TMP00243	1758	3	23	2	58	0.00	37.910	-77.400	0.0	50	4.95	1.390	0.371	91	0	38
TMP00245	1758	4	25	2	30	0.00	38.900	-76.500	0.0	40	3.31	1.872	0.512	92	0	146
TMP00254	1763	10	13	13	0	0.00	40.000	-75.200	0.0	45	3.98	1.877	0.513	97	0	310
TMP00268	1772	4	25	13	0	0.00	39.800	-75.500	0.0	45	3.00	1.385	0.369	107	0	276
TMP00270	1774	2	21	19	0	0.00	37.200	-77.400	0.0	45	4.38	1.057	0.152	108	0	101
TMP00306	1791	1	13	9	0	0.00	37.730	-77.680	0.0	40	3.77	1.390	0.371	126	0	38
TMP00327	1795	2	12	1	0	0.00	37.410	-77.630	0.0	50	3.38	1.390	0.371	140	0	73
TMP00335	1800	11	20	9	45	0.00	40.280	-76.550	0.0	34	4.11	1.390	0.371	145	0	268
TMP00336	1800	11	20	10	5	0.00	40.276	-76.885	0.0	38	2.98	1.877	0.513	146	0	257
TMP00346	1802	8	23	10	0	0.00	37.400	-79.100	0.0	30	3.31	1.872	0.512	152	0	136
TMP00367	1807	5	1	9	0	0.00	37.400	-79.100	0.0	30	3.31	1.872	0.512	164	0	136
TMP00447	1812	2	2	9	30	0.00	37.600	-77.400	0.0	30	3.27	1.371	0.363	172	0	61
TMP00689	1820	8	21	14	35	0.00	40.042	-76.301	0.0	38	3.27	1.371	0.363	198	0	254
TMP00698	1821	5	11	4	0	0.00	39.301	-76.611	0.0	34	3.98	1.877	0.513	206	0	171
TMP00699	1822	5	4	20	30	0.00	40.042	-76.301	0.0	38	3.44	1.371	0.363	207	0	254
TMP00713	1824	7	15	16	20	0.00	39.700	-80.500	0.0	30	4.20	1.107	0.206	214	0	296
TMP00731	1828	3	9	0	0	0.00	37.000	-80.000	0.0	30	4.86	1.058	0.153	225	0	226
TMP00732	1828	3	10	3	0	0.00	38.300	-78.470	0.0	34	5.08	1.175	0.260	226	0	65

BASIS: NEW

NAPS COL 2.0-27-A
NAPS ESP VAR 2.0-4

Table 2.5.2-202 Earthquakes Within 322 km (200 miles) from the Updated CEUS SSC Earthquake Catalog for Independent or Mainshock Earthquakes with Magnitudes E[M] ≥ 2.9

	Coordinated Universal Time (UTC)						Epicentral Location									
TID	Year	Month	Day	Hour	Minute	Second	Lat. (+N°)	Long. (+E°)	Depth (km)	ERH (km)	E[M]	N*	sigM	EQNO	FLAG	Dist (km)
TMP00745	1830	3	29	7	0	0.00	39.650	-77.720	0.0	30	3.42	1.108	0.207	231	0	176
TMP00761	1833	8	27	11	0	0.00	37.700	-78.000	0.0	38	4.37	1.052	0.146	243	0	43
TMP00762	1834	2	5	22	30	0.00	39.850	-76.140	0.0	30	3.70	1.107	0.206	244	0	244
TMP00935	1852	2	16	6	0	0.00	39.330	-76.300	0.0	30	3.49	1.107	0.206	323	0	191
TMP00936	1852	4	29	18	0	0.00	37.360	-80.680	0.0	34	5.21	1.175	0.260	324	0	265
TMP00952	1852	11	2	23	35	0.00	37.600	-78.600	0.0	34	4.18	1.056	0.151	331	0	87
TMP00959	1853	5	2	14	20	0.00	38.470	-80.560	0.0	34	5.16	1.175	0.260	335	0	245
TMP01007	1855	2	2	8	0	0.00	37.000	-78.600	0.0	30	3.78	1.056	0.151	355	0	137
TMP01025	1855	6	28	0	18	0.00	39.070	-76.580	0.0	30	3.75	1.106	0.205	364	0	153
TMP01043	1857	1	1	0	0	0.00	38.642	-79.539	0.0	38	3.31	1.872	0.512	371	0	165
TMP01107	1861	1	20	0	0	0.00	40.042	-76.301	0.0	38	3.31	1.872	0.512	406	0	254
TMP01156	1866	9	3	5	0	0.00	39.000	-76.890	0.0	30	3.09	1.124	0.221	434	0	130
TMP01181	1868	10	11	0	0	0.00	36.910	-80.320	0.0	38	3.31	1.872	0.512	450	0	256
TMP01191	1869	3	30	6	45	0.00	38.140	-78.190	0.0	38	3.31	1.872	0.512	457	0	36
TMP01250	1871	10	9	14	40	0.00	39.700	-75.500	0.0	30	3.42	1.126	0.223	493	0	268
TMP01266	1872	6	5	3	0	0.00	37.700	-78.000	0.0	30	3.66	1.106	0.205	501	0	43
TMP01301	1873	10	3	12	45	0.00	37.200	-78.200	0.0	30	3.56	1.107	0.206	520	0	101
TMP01329	1874	5	14	20	30	0.00	37.200	-77.350	0.0	38	3.31	1.872	0.512	533	0	103

BASIS: NEW

NAPS COL 2.0-27-A
NAPS ESP VAR 2.0-4

Table 2.5.2-202 Earthquakes Within 322 km (200 miles) from the Updated CEUS SSC Earthquake Catalog for Independent or Mainshock Earthquakes with Magnitudes E[M] ≥ 2.9

	Coordinated Universal Time (UTC)						Epicentral Location									
TID	Year	Month	Day	Hour	Minute	Second	Lat. (+N°)	Long. (+E°)	Depth (km)	ERH (km)	E[M]	N*	sigM	EQNO	FLAG	Dist (km)
TMP01362	1875	12	23	4	45	0.00	37.600	-78.500	0.0	34	4.77	1.270	0.316	551	0	80
TMP01441	1879	3	26	0	30	0.00	39.200	-75.500	0.0	30	3.20	1.124	0.221	588	0	235
TMP01463	1880	3	19	0	0	0.00	39.850	-77.750	0.0	38	3.31	1.872	0.512	597	0	198
TMP01573	1883	3	11	23	57	0.00	39.500	-76.400	0.0	30	3.07	1.125	0.222	639	0	200
TMP01641	1885	1	3	2	12	0.00	39.200	-77.500	0.0	30	3.69	1.057	0.152	675	0	129
TMP01668	1885	10	10	4	35	0.00	37.700	-78.800	0.0	30	4.11	1.056	0.151	682	0	96
TMP01924	1886	9	25	2	0	0.00	36.700	-80.050	0.0	30	2.98	1.124	0.221	881	0	249
TMP01939	1886	9	28	0	21	0.00	40.000	-76.400	0.0	38	3.27	1.371	0.363	898	0	246
TMP01949	1886	9	29	4	0	0.00	40.154	-76.599	0.0	38	2.98	1.877	0.513	905	0	253
TMP02151	1887	1	2	22	30	0.00	39.570	-77.000	0.0	30	3.14	1.108	0.207	1090	0	180
TMP02458	1889	3	8	23	40	0.00	40.000	-76.000	0.0	34	3.82	1.048	0.140	1312	0	264
TMP02462	1889	3	30	21	30	0.00	38.562	-76.078	0.0	38	3.31	1.872	0.512	1315	0	159
TMP02482	1889	8	26	0	0	0.00	35.532	-77.031	0.0	38	2.98	1.877	0.513	1330	0	287
TMP02592	1893	1	11	22	15	0.00	39.428	-77.417	0.0	34	3.98	1.877	0.513	1390	0	155
TMP02794	1895	10	7	4	30	0.00	35.900	-77.500	0.0	30	3.31	1.872	0.512	1464	0	240
TMP39333	1895	11	20	3	0	0.00	39.980	-75.750	0.0	30	3.00	1.130	0.226	1478	0	276
TMP02873	1896	11	20	15	0	0.00	39.730	-75.390	0.0	30	3.00	1.130	0.226	1501	0	278
TMP02877	1896	12	8	16	55	0.00	39.980	-79.614	0.0	38	3.65	1.872	0.512	1504	0	264

BASIS: NEW

NAPS COL 2.0-27-A
NAPS ESP VAR 2.0-4

Table 2.5.2-202 Earthquakes Within 322 km (200 miles) from the Updated CEUS SSC Earthquake Catalog for Independent or Mainshock Earthquakes with Magnitudes E[M] ≥ 2.9

	Coordinated Universal Time (UTC)						Epicentral Location									
TID	Year	Month	Day	Hour	Minute	Second	Lat. (+N°)	Long. (+E°)	Depth (km)	ERH (km)	E[M]	N*	sigM	EQNO	FLAG	Dist (km)
TMP02887	1897	2	7	4	30	0.00	39.301	-76.611	0.0	38	3.31	1.872	0.512	1508	0	171
TMP02921	1897	5	31	18	58	0.00	37.300	-80.700	0.0	30	5.91	1.270	0.316	1521	0	268
TMP02953	1897	12	18	23	45	0.00	37.700	-77.500	0.0	30	3.81	1.038	0.125	1538	0	47
TMP03034	1900	4	28	19	7	0.00	39.840	-75.150	0.0	20	3.07	1.125	0.222	1580	0	301
TMP03084	1902	5	18	4	0	0.00	37.300	-80.600	0.0	20	3.31	1.872	0.512	1598	0	260
TMP03231	1906	5	8	17	41	0.00	38.700	-75.700	0.0	20	3.15	1.108	0.207	1652	0	195
TMP03294	1906	12	5	6	0	0.00	38.670	-76.080	0.0	20	2.98	1.131	0.227	1664	0	164
TMP39338	1907	1	26	6	0	0.00	37.270	-81.223	0.0	25	2.98	1.877	0.513	1667	0	313
TMP03309	1907	2	11	13	22	0.00	37.700	-78.300	0.0	22	3.76	1.107	0.206	1671	0	59
TMP03349	1908	8	23	9	30	0.00	37.500	-77.900	0.0	20	3.37	1.115	0.213	1689	0	62
TMP03376	1909	4	2	7	25	0.00	39.400	-78.000	0.0	20	3.47	1.059	0.155	1701	0	149
TMP03401	1909	12	23	0	0	0.00	38.555	-75.573	0.0	22	3.98	1.877	0.513	1719	0	201
TMP03406	1910	2	8	14	0	0.00	38.800	-78.700	0.0	20	3.20	1.117	0.215	1722	0	113
TMP03417	1910	5	8	21	10	0.00	37.700	-78.400	0.0	20	3.47	1.108	0.207	1726	0	66
TMP03455	1912	8	7	20	0	0.00	37.700	-78.400	0.0	20	3.00	1.130	0.226	1752	0	66
TMP03635	1918	4	10	2	9	0.00	38.700	-78.400	0.0	20	4.41	1.107	0.206	1851	0	88
TMP03639	1918	4	19	16	55	0.00	36.800	-76.300	0.0	28	3.14	1.116	0.214	1854	0	191
TMP03675	1919	9	6	2	46	0.00	38.800	-78.200	0.0	20	3.98	1.877	0.513	1880	0	89

BASIS: NEW

NAPS COL 2.0-27-A
NAPS ESP VAR 2.0-4

Table 2.5.2-202 Earthquakes Within 322 km (200 miles) from the Updated CEUS SSC Earthquake Catalog for Independent or Mainshock Earthquakes with Magnitudes E[M] ≥ 2.9

	Coordinated Universal Time (UTC)						Epicentral Location									
TID	Year	Month	Day	Hour	Minute	Second	Lat. (+N°)	Long. (+E°)	Depth (km)	ERH (km)	E[M]	N*	sigM	EQNO	FLAG	Dist (km)
TMP39347	1921	8	7	6	30	0.00	37.800	-78.400	0.0	20	3.61	1.110	0.209	1906	0	60
TMP03813	1924	12	26	4	30	0.00	37.300	-79.900	0.0	20	3.31	1.872	0.512	1959	0	203
TMP03890	1925	5	16	1	30	0.00	37.300	-77.500	0.0	20	3.31	1.872	0.512	1986	0	88
TMP04012	1927	6	10	7	16	0.00	38.000	-79.000	0.0	20	3.49	1.110	0.209	2047	0	105
TMP04089	1928	10	30	11	45	0.00	37.500	-77.500	0.0	20	3.41	1.109	0.208	2086	0	67
TMP04159	1929	12	26	2	56	0.00	38.100	-78.500	0.0	22	3.37	1.062	0.159	2124	0	62
TMP04293	1932	1	5	4	5	0.00	37.600	-78.400	0.0	20	3.17	1.065	0.162	2187	0	73
TMP04555	1937	2	3	1	26	0.00	37.700	-78.700	0.0	20	3.55	1.107	0.206	2294	0	89
TMP04603	1937	12	3	12	15	0.00	38.700	-75.500	0.0	20	2.98	1.877	0.513	2316	0	212
TMP04635	1938	7	15	22	46	12.00	40.680	-78.430	1.0	20	3.09	1.045	0.135	2331	0	295
TMP04814	1939	11	15	2	53	48.70	39.580	-75.050	3.0	39	3.50	1.040	0.128	2382	0	291
TMP04815	1939	11	18	2	33	0.00	39.500	-76.600	0.0	20	3.11	1.123	0.220	2383	0	190
TMP04835	1940	3	25	21	0	0.00	38.800	-78.500	0.0	20	2.94	1.164	0.252	2394	0	102
TMP04980	1942	10	7	2	15	0.00	37.600	-78.400	0.0	20	3.26	1.115	0.213	2488	0	73
TMP05028	1944	1	8	0	0	0.00	39.800	-75.500	0.0	20	3.31	1.872	0.512	2516	0	276
TMP05243	1948	1	4	23	0	0.00	37.600	-78.600	0.0	20	3.29	1.114	0.212	2629	0	87
TMP05297	1949	5	8	11	1	0.00	37.600	-77.600	0.0	20	3.49	1.110	0.209	2657	0	53
TMP05341	1950	11	26	7	45	0.00	37.700	-78.300	0.0	20	3.28	1.119	0.217	2683	0	59

BASIS: NEW

NAPS COL 2.0-27-A
NAPS ESP VAR 2.0-4

Table 2.5.2-202 Earthquakes Within 322 km (200 miles) from the Updated CEUS SSC Earthquake Catalog for Independent or Mainshock Earthquakes with Magnitudes E[M] ≥ 2.9

	Coordinated Universal Time (UTC)						Epicentral Location									
TID	Year	Month	Day	Hour	Minute	Second	Lat. (+N°)	Long. (+E°)	Depth (km)	ERH (km)	E[M]	N*	sigM	EQNO	FLAG	Dist (km)
TMP05346	1951	3	9	7	0	0.00	37.600	-77.600	0.0	20	3.31	1.872	0.512	2686	0	53
TMP05429	1952	9	11	3	15	0.00	38.100	-78.500	0.0	25	3.01	1.130	0.226	2743	0	62
TMP05457	1953	2	7	7	5	0.00	37.700	-78.100	0.0	20	3.29	1.114	0.212	2760	0	48
TMP05496	1954	1	7	7	25	0.00	40.300	-76.000	0.0	20	3.45	1.055	0.149	2791	0	292
TMP05575	1955	1	17	12	37	0.00	37.300	-78.400	0.0	20	3.34	1.111	0.210	2829	0	99
TMP05804	1959	4	23	20	58	39.50	37.390	-80.680	1.0	17	3.51	1.041	0.129	2992	0	264
TMP05813	1959	7	7	23	17	0.00	37.300	-80.700	0.0	28	3.05	1.126	0.223	2999	0	268
TMP05988	1963	1	17	11	40	26.80	37.300	-80.100	0.0	20	3.36	1.040	0.128	3100	0	219
TMP06065	1963	10	10	14	59	52.30	39.655	-78.197	0.0	17	3.33	1.083	0.183	3148	0	180
TMP06076	1963	10	28	22	38	0.30	36.700	-81.000	0.0	20	3.48	1.041	0.129	3157	0	320
TMP06154	1964	5	12	6	45	10.70	40.300	-76.410	1.0	6	3.84	1.066	0.164	3215	0	275
TMP06354	1965	10	8	2	17	27.00	40.080	-79.750	0.0	39	3.21	1.152	0.243	3334	0	280
TMP06511	1966	5	31	6	18	59.50	37.660	-78.130	2.0	17	3.82	1.032	0.114	3387	0	53
TMP06830	1968	3	8	5	38	15.70	37.280	-80.770	8.0	6	3.66	1.030	0.112	3529	0	275
TMP07006	1969	11	20	1	0	9.30	37.450	-80.930	5.0	6	4.50	1.048	0.140	3628	0	283
TMP07011	1969	12	11	23	44	37.40	37.840	-77.670	1.0	39	3.48	1.032	0.114	3629	0	26
TMP07179	1971	9	12	0	6	27.60	38.150	-77.590	5.0	39	3.38	1.033	0.116	3731	0	21
TMP07243	1972	2	11	0	16	0.30	39.700	-75.600	0.0	20	3.21	1.123	0.220	3769	0	262

BASIS: NEW

NAPS COL 2.0-27-A
NAPS ESP VAR 2.0-4

Table 2.5.2-202 Earthquakes Within 322 km (200 miles) from the Updated CEUS SSC Earthquake Catalog for Independent or Mainshock Earthquakes with Magnitudes E[M] ≥ 2.9

	Coordinated Universal Time (UTC)						Epicentral Location									
TID	Year	Month	Day	Hour	Minute	Second	Lat. (+N°)	Long. (+E°)	Depth (km)	ERH (km)	E[M]	N*	sigM	EQNO	FLAG	Dist (km)
TMP07289	1972	9	5	16	0	0.00	37.600	-77.700	0.0	6	3.30	1.043	0.133	3794	0	51
TMP07316	1972	12	8	3	0	33.30	40.140	-76.240	2.0	6	3.33	1.034	0.118	3808	0	266
TMP07350	1973	2	28	8	21	33.20	39.690	-75.430	12.0	17	3.77	1.020	0.092	3820	0	272
TMP07369	1973	4	9	23	11	0.00	37.300	-77.700	0.0	20	3.38	1.110	0.209	3823	0	84
TMP07500	1974	4	28	14	19	0.00	39.800	-75.600	0.0	8	3.28	1.152	0.243	3877	0	270
TMP07510	1974	5	30	21	28	35.30	37.460	-80.540	5.0	6	3.55	1.032	0.115	3882	0	250
TMP08058	1975	11	11	8	10	37.60	37.220	-80.890	1.0	17	3.20	1.041	0.129	4112	0	287
TMP08400	1976	9	13	18	54	38.00	36.620	-80.770	9.0	17	3.74	1.030	0.112	4234	0	307
TMP09059	1978	3	17	18	26	34.80	36.780	-80.740	16.0	4	3.00	1.045	0.136	4491	0	295
TMP09269	1978	7	16	6	39	29.70	39.900	-76.220	0.0	8	3.30	1.027	0.105	4552	0	244
TMP09434	1978	10	6	19	25	47.40	40.080	-76.150	0.0	17	3.34	1.054	0.148	4593	0	264
TMP10865	1981	2	11	13	44	16.40	37.720	-78.440	6.0	1	3.35	1.044	0.134	4980	0	68
TMP13487	1984	4	23	1	36	0.00	39.950	-76.370	4.0	2	4.05	1.018	0.086	5894	0	242
TMP13693	1984	8	17	18	5	46.90	37.868	-78.324	8.0	1	3.88	1.047	0.138	5968	0	51
TMP14236	1985	6	10	12	22	38.30	37.248	-80.485	11.0	1	3.03	1.074	0.173	6165	0	253
TMP14815	1986	3	26	16	36	23.90	37.245	-80.494	12.0	1	3.11	1.152	0.243	6379	0	253
TMP18191	1990	10	23	1	34	48.20	39.512	-75.506	10.0	2	2.99	1.027	0.106	7453	0	255
TMP18460	1991	3	15	6	54	8.20	37.746	-77.916	17.0	1	3.55	1.072	0.170	7544	0	36

BASIS: NEW

NAPS COL 2.0-27-A
NAPS ESP VAR 2.0-4

Table 2.5.2-202 Earthquakes Within 322 km (200 miles) from the Updated CEUS SSC Earthquake Catalog for Independent or Mainshock Earthquakes with Magnitudes E[M] ≥ 2.9

	Coordinated Universal Time (UTC)						Epicentral Location									
TID	Year	Month	Day	Hour	Minute	Second	Lat. (+N°)	Long. (+E°)	Depth (km)	ERH (km)	E[M]	N*	sigM	EQNO	FLAG	Dist (km)
TMP18517	1991	4	22	1	1	20.20	37.941	-80.207	14.0	2	3.40	1.071	0.169	7563	0	211
TMP20103	1994	1	17	4	42	25.60	40.329	-76.023	0.0	2	2.93	1.094	0.194	8082	0	293
TMP20648	1995	1	22	8	24	48.70	37.050	-80.789	9.0	2	2.92	1.036	0.122	8273	0	286
TMP20756	1995	3	11	21	10	16.00	40.100	-76.400	5.0	2	2.94	1.082	0.182	8305	0	255
TMP21206	1995	11	29	18	24	46.00	37.970	-81.350	19.0	2	3.16	1.195	0.273	8428	0	311
TMP23395	1998	10	21	5	56	47.20	37.381	-78.367	13.0	1	3.47	1.050	0.143	8935	0	90
TMP31138	2003	5	5	16	32	32.70	37.755	-78.072	5.0	12	3.53	1.024	0.100	9780	0	41
TMP31784	2003	12	9	20	59	14.10	37.587	-77.903	5.0	2	4.33	1.070	0.168	9896	0	53
TMP39207	2008	12	27	5	4	34.60	40.110	-76.400	4.0	25	3.34	1.152	0.243	10982	0	256
UPD00135	2009	7	1	13	44	43.38	39.644	-75.483	5.0	--	2.97	1.091	0.191	11119	0	265
UPD00476	2010	4	4	9	19	14.00	38.619	-80.909	0.0	--	3.08	1.148	0.240	11460	0	278
UPD00624	2010	6	3	12	25	2.93	40.086	-76.974	1.0	--	2.94	1.055	0.149	11608	0	235
UPD00745	2010	7	16	9	4	46.55	39.184	-77.287	5.0	--	3.37	1.024	0.100	11729	0	132
UPD02754	2011	8	23	17	51	4.59	37.936	-77.933	6.0	--	5.71	1.008	0.058	13738	0	18
UPD02768	2011	8	25	5	59	13.00	37.916	-80.215	12.0	--	2.93	1.161	0.250	13752	0	212

BASIS: NEW

NAPS COL 2.0-27-A
NAPS ESP VAR 2.0-4

Table 2.5.2-202 Earthquakes Within 322 km (200 miles) from the Updated CEUS SSC Earthquake Catalog for Independent or Mainshock Earthquakes with Magnitudes E[M] ≥ 2.9

Notes	
TID	Unique identification number assigned in the project to each earthquake. These values are not necessarily sequential. Sequential numbering of earthquakes in uniform magnitude catalog is provided by the EQNO field.
Year, Month, Day	Date of Earthquake
Hour, Minute, Second	Time of Earthquake. The times are assumed to be UTC times. During assembly of the catalog, UTC time was selected when it was clear that other times were present among the various catalog sources. However, the reported times are based primarily on those reported in the source catalog and no attempt was made to verify that the time was UTC for the individual sources. The master catalog database contains all of the individual catalog entries with their individual times.
Lat., Long.	Location of Earthquake (degrees). The precision of the reported location represents the precision reported for the preferred entry among the source catalogs. Variability in the precision in location among the earthquake entries is not an issue as the earthquake recurrence rates are computed using grid sizes of ¼ or ½ degree longitude and latitude.
Depth	Earthquake Depth (km) or Depth of Focus
ERH	Estimated Horizontal Location Uncertainty (km). This entry provides a measure of the uncertainty in location of the earthquake. The values represent a mixture of reported standard errors in location of instrumentally located earthquakes from various catalog sources and estimates of location uncertainty for locations based on felt effects (shaking intensity). Note: ERH does not appear to be used in specific analyses presented in the CEUS SSC Report, so this parameter was not estimated in the update of the earthquake catalog.
E[**M**]	Expected value of moment magnitude.
N*	Equivalent earthquake count. This value is used to account for the effects of magnitude uncertainty in computing unbiased earthquake recurrence parameters.
sig**M**	Standard deviation in the estimated moment magnitude, E[**M**]. It is used to compute N*
EQNO	Earthquake number in the uniform moment magnitude CEUS SSC Project catalog.
Flag	Flag for dependent earthquakes, where a value of 0 indicates an independent earthquake and a value greater than 0 indicates a dependent earthquake with the value of FLAG indicating the EQNO of the main shock of the cluster.
Dist	Epicentral distance (from epicenter to project site) in kilometers.

NAPS COL 2.0-27-A
NAPS ESP VAR 2.0-4

Table 2.5.2-203 Comparison[1] of Some Reported Moment Magnitudes (M^) in the CEUS SSC Report[2] and Those from the "Preferred" SLU NAMT Catalog[3] (*Mechanism*)

Year	Month	Day	Hour	Minute	Latitude (+N°)	Longitude (+E°)	M^[2]	Mechanism[3]
2002	6	18	17	37	38.100	-87.700	4.50	4.57
2002	11	3	20	41	42.768	-98.896	4.14	4.15
2004	8	19	23	51	33.199	-86.934	3.63	3.62
2005	6	2	11	35	36.140	-89.460	3.89	3.98
2008	4	7	9	51	28.920	-98.040	4.86	3.86
2008	11	15	10	52	47.740	-69.710	3.60	3.57

1 Records are only shown when differences in the magnitudes occur

2 EPRI et al., 2012 ((Reference 2.5-223), Table B-2

3 Saint Louis University (SLU) North America Moment Tensor (NAMT) catalog "Mechanism Files" at http://www.eas.slu.edu/eqc/eqc_mt/MECH.NA/

BASIS: NEW

NAPS COL 2.0-27-A
NAPS ESP VAR 2.0-4

Table 2.5.2-204 Comparison of Double-Couple Focal Mechanisms for the 2011 M 5.8 Mineral, Virginia Earthquake

Source	Mag. (M)	Depth (km)	Strike (NP1/NP2)[1]	Dip (NP1/NP2)	Rake (NP1/NP2)
Horton et al., 2012 [7]	-	-	N28°E	50°SE	113°
USGS[3] W-Phase MTS[2, 6]	5.8	11	30°/177°	37°/57°	117°/71°
USGS/SLU[4] regional MTS[6]	5.7	6	177°/26°	39°/55°	66°/108°
SLU MTS using the frequency band 0.01-0.03 Hz[6]	5.65	6	28°/175°	50°/45°	113°/65°
Global CMT[5] catalog[6]	5.8	12	28°/169°	47°/50°	119°/62°

1 NP = Nodal Planes to identify the fault rupture of earthquake. One of the two nodal planes represents the orientation of the fault plane that generated the earthquakes and the other is the auxiliary plane, a plane perpendicular to the line describing the direction of slip on the fault plane.
2 MTS = Moment Tensor Solution
3 USGS = United States Geological Survey
4 SLU = Saint Louis University
5 CMT = Centroid Moment Tensor
6 Source: SLU (2012) (Reference 2.5-271)
7 Reference 2.5-232

BASIS: NEW

NAPS COL 2.0-27-A
NAPS ESP VAR 2.0-4

Table 2.5.2-205 Peak Ground Motion Data[1] (Distance Order) for the 2011 M 5.8 Mineral, Virginia Earthquake from the Center for Engineering Strong Motion Data (CESMD)

Source[2]	Station Name	Latitude (+N°)	Longitude (+E°)	Dist. (Km)[3]	PGAv1 (g)[4]	PGAv2 (g)[4]	PGV (cm/s)[5]	PGD (cm)[6]
NMSN	VA Charlottesville	38.022	-78.532	53.5	0.121	0.121	1.68	0.2
NEIC	VA Corbin (Fredericksburg Obs)	38.205	-77.373	57.5	0.135	0.135	7.13	1.6
USGS	VA Reston Fire Station 25	38.951	-77.336	124.1	0.109	0.092	3.05	-
USGS	VA Pearisburg - Giles County CH	37.327	-80.735	256.4	0.003	0.003	0.14	0.1
USGS	PA Philadelphia - Drexel Univ.	39.957	-75.192	326.8	0.009	0.009	0.35	0.1
USGS	SC Columbia - VA Hospital	33.975	-80.961	517.5	0.003	0.003	0.18	.0
USGS	NY Buffalo - VA Medical Center	42.952	-78.811	561.9	0.001	0.001	0.18	.0
USGS	SC Summerville - Fire Station	33.025	-80.176	581.6	0.001	0.001	0.12	0.1
USGS	SC Charleston - Cha Pla Hotel	32.781	-79.932	600.1	0.002	0.001	0.13	0.1
USGS	NY Albany - VA Med	42.652	-73.773	631.9	0.007	-	-	-
USGS	MA Northampton VA Medical Ctr	42.350	-72.682	663.7	0.008	0.008	0.74	0.1
USGS	MA Boston - Jamaica Plains	42.328	-71.110	759.0	0.001	0.001	0.09	.0
USGS	MA Bedford - VA Hospital	42.504	-71.273	760.7	0.001	0.001	0.07	.0
USGS	Manchester - VA Medical Center	43.013	-71.442	787.9	0.001	0.001	0.13	.0
USGS	VT White River Junction VAMC	43.649	-72.343	790.6	0.005	0.001	0.11	-

BASIS: NEW

NAPS COL 2.0-27-A
NAPS ESP VAR 2.0-4

Table 2.5.2-205 Peak Ground Motion Data[1] (Distance Order) for the 2011 M 5.8 Mineral, Virginia Earthquake from the Center for Engineering Strong Motion Data (CESMD)

1 CESMD (http://www.strongmotioncenter.org) gives no information of the site conditions of the recording station

2 Source:
NMSN: New Madrid Seismic Network
NEIC: National Earthquake Information Center
USGS: U.S. Geological Survey

3 Dist = Epicentral distance (from epicenter to project site) in kilometers

4 PGA = Peak Ground Acceleration
PGAv1 is Peak Ground Acceleration (Phase 1, Vol. 1) based on the uncorrected accelerations
PGAv2 is Peak Ground Acceleration (Phase 2, Vol. 2) based on instrument and baseline-corrected accelerations

5 PGV = Peak Ground Velocity

6 PGD = Peak Ground Displacement

BASIS: NEW

NAPS COL 2.0-27-A
NAPS ESP VAR 2.0-4

Table 2.5.2-206 Distributed Seismicity Sources

Zone Acronym	Zone Name	Comments
	Mmax Zones	
MESE-N* and MESE-W*	Mesozoic and Younger Extended Crust, narrow and wide geometries	
NMESE-N* and NMESE-W*	Non-Mesozoic and Younger Extended Crust, narrow and wide geometries	NMESE-N is paired with MESE-N, and NMESE-W is paired with MESE-W
Study Region*	CEUS Study Region	Exclusive with MESE and NMESE
	Seismotectonic Source Zones	
AHEX*	Atlantic Highly Extended Crust	
ECC-AM*	Extended Continental Crust—Atlantic Margin	Host zone for North Anna site
ECC-GC	Extended Continental Crust—Gulf Coast	
GHEX	Gulf Coast Highly Extended Crust	
GMH	Great Meteor Hotspot	
IBEB*	Illinois Basin Extended Basement	
MidC-A*, B*, C*, D*	Midcontinent-Craton	Alternative geometries depend on PEZ and RR/RR-RCG
NAP	Northern Appalachian	
OKA	Oklahoma Aulacogen	
PEZ-N* and PEZ-W*	Paleozoic Extended Crust narrow and Paleozoic Extended Crust wise	PEZ-N is modeled either with MidC-A and RR, or MidC-B and RR-RCG. PEZ-W is modeled with MidC-C and RR, or MidC-D and RR-RCG
RR and RR-RCG	Reelfoot Rift, Reelfoot Rift with Rough Creek Graben	RR and RR-RCG are mutually exclusive
SLR*	St. Lawrence Rift, including the Ottawa and Saguenay grabens	

*Source area within 1,000 km included in North Anna hazard calculation

NAPS COL 2.0-27-A
NAPS ESP VAR 2.0-4

Table 2.5.2-207 Alternative Mmax Zonation Models[1]

	Mesozoic Extended Narrow Model		Mesozoic Extended Wide Model	
Mmax Zone	**MESE-N***	**NMESE-N***	**MESE-W***	**NMESE-W***
Corresponding Seismotectonic Zones	AHEX*	MidC-A, -B*	AHEX*	MidC-C, -D*
	ECC-AM*	IBEB*	ECC-AM*	OKA
	ECC-GM	OKA	ECC-GM	
	GHEX		GHEX	
	RR		RR-RCG	
	SLR*		SLR*	
	NAP		NAP	
	GMH		GMH	
	PEZ-N*		PEZ-W*	
			IBEB*	

Notes
1. EPRI et al., 2012 (Reference 2.5-223, Table 6.2-1)
*Source area within 1,000 km included in Unit 3 hazard calculation

NAPS COL 2.0-27-A
NAPS ESP VAR 2.0-4

Table 2.5.2-208 Maximum Magnitude Distributions for Mmax Distributed Seismicity Sources[1]

Weight Assigned to Mmax	Maximum Magnitude for:				
	Study Region	**MESE-N**	**MESE-W**	**NMESE-N**	**NMESE-W**
0.101	6.5	6.4	6.4	6.5	5.7
0.244	6.9	6.8	6.8	6.9	6.1
0.310	7.2	7.2	7.1	7.3	6.6
0.244	7.7	7.7	7.5	7.7	7.2
0.101	8.1	8.1	8.0	8.1	7.9

Notes
1. EPRI et al., 2012 (Reference 2.5-223, Table H-3-3

BASIS: NEW

NAPS COL 2.0-27-A
NAPS ESP VAR 2.0-4

Table 2.5.2-209 Assessment of Default Characteristics of Future Earthquakes in the CEUS[1]

Future Earthquake Characteristic	TI Team Assessments (Relative frequencies or weighted alternatives)	References[2]
Tectonic Stress Regime	Compressional	Hurd (2010) (Reference 2.5-340)
Sense of Slip/Style of Faulting	Treat as aleatory (relative frequency): • 2:1 strike-slip:reverse	Focal mechanisms: New Madrid (Shumway, 2008 (Reference 2.5-341); Horton et al., 2005 (Reference 2.5-342)) Eastern Tennessee (Chapman et al., 1997 (Reference 2.5-343)) Central Virginia (Kim and Chapman, 2005 (Reference 2.5-344)) St. Lawrence (S. Mazzotti, Wksp 2, 2009) (Reference 2.5-345) Southern Great Lakes (Dineva et al., 2004) (Reference 2.5-346) Wabash Valley (Kim, 2003) (Reference 2.5-347) Pennsylvania (Seeber et al., 1998)(Reference 2.5-348) CEUS (Hurd, 2010 (Reference 2.5-340); Heidbach et al., 2008 (Reference 2.5-349); van Lanen and Mooney, 2007 (Reference 2.5-350)) Charleston (P. Talwani, Wksp 2, 2009) (Reference 2.5-351) Zoback (1992) (Reference 2.5-352)
Strike and Dip of Ruptures	Aleatory distribution: • N50W (0.2) • N-S (0.2) • N35E (0.4) • N60E (0.1) • E-W (0.1) Dip is a function of sense of slip: • Strike-slip (90°-60°) (uniform) • Reverse (30°-60°) (uniform) • Either direction (50:50)	van Lanen and Mooney (2007) (Reference 2.5-350) Sibson and Xie (1998) (Reference 2.5-353) Zoback (1992) (Reference 2.5-352) Marshak and Paulsen (1997) (Reference 2.5-354) (NW trends)

BASIS: NEW

NAPS COL 2.0-27-A
NAPS ESP VAR 2.0-4

Table 2.5.2-209 Assessment of Default Characteristics of Future Earthquakes in the CEUS[1]

Future Earthquake Characteristic	TI Team Assessments (Relative frequencies or weighted alternatives)	References[2]
Seismogenic Crustal Thickness	Epistemic distribution: • 13 km (0.4) • 17 km (0.4) • 22 km (0.2)	Sibson (1984, 2007) (Reference 2.5-355 and 2.5-356) van Lanen and Mooney (2007) for ENA (Reference 2.5-350) Mai et al. (2005) (Reference 2.5-357) Atkinson (2004a) (Reference 2.5-258) Sykes et al. (2008) (Reference 2.5-358) P. Talwani (Wksp 2, 2009) (Reference 2.5-351)
Fault Rupture Area	Function of magnitude; Use Somerville et al. relation for ENA	Somerville et al. (2001) (Reference 2.5-359)
Rupture Length-to-Width Aspect Ratio	Function of rupture area: • 1:1 for smaller ruptures • With progressively larger areas, when rupture width equals seismogenic crustal thickness, extend only the length	Wesnousky (2008) (Reference 2.5-360) Toro approach in NAGRA (2004) (Reference 2.5-361)
Relationship of Rupture to Source Zone Boundaries	Epicenter is at center of rupture length (map view) All boundaries are “leaky”; rupture is allowed to extend beyond boundary. (Note: If boundary is “strict,” rupture cannot extend beyond boundary, although epicenter can be near boundary)	

Notes

1. EPRI et al., 2012 (Reference 2.5-223, Table 5.4.-1)
2. References provide insight into the assessment of characteristics; however, they do not uniquely define them for purposes of the CEUS SSC study. Those assessments were made by the TI team.

BASIS: NEW

NAPS COL 2.0-27-A
NAPS ESP VAR 2.0-4

Table 2.5.2-210 Characteristics of Future Earthquakes for RLME and Seismotectonic Sources[1]

Source	Sense of Slip[2]	Rupture Strike[2]	Rupture Dip[2]	Source Boundaries	Seismogenic Crustal Thickness[3]
		RLME Sources			
Charlevoix	Reverse	Uniform 0°–360°	Uniform 40°–60°	Leaky	25 km (0.8) 30 km (0.2)
Charleston —Regional*	Strike-slip	NE parallel to long axis (0.8) NW parallel to short axis (0.2)	90°	Strict	*13 km (0.4)*[5] *17 km (0.4)*[5] *22 km (0.2)*[5]
Charleston —Local*	Strike-slip	NE parallel to long axis	90°	Strict	*13 km (0.4)*[5] *17 km (0.4)*[5] *22 km (0.2)*[5]
Charleston —Narrow*	Strike-slip	NE parallel to long axis	90°	Leaky at ends	*13 km (0.4)*[5] *17 km (0.4)*[5] *22 km (0.2)*[5]
Cheraw	Normal-oblique	On fault trace (NE)	50° NW (0.6) 65° NW (0.4)	Strict	*13 km (0.4)* *17 km (0.4)* *22 km (0.2)*
Commerce	Strike-slip	NE parallel to long axis of zone	90°	Leaky at ends	13 km (0.4) 15 km (0.4) 17 km (0.2)
ERM-N	Strike-slip	NE parallel to long axis of zone	90°	Leaky at ends	13 km (0.4) 15 km (0.4) 17 km (0.2)
ERM-S	Strike-slip	NE parallel to long axis of zone	90°	Leaky at ends	13 km (0.4) 15 km (0.4) 17 km (0.2)
Marianna	Strike-slip	NE 45° (0.5) NE 45° (0.5)	90°	Leaky at ends	13 km (0.4) 15 km (0.4) 17 km (0.2)

BASIS: NEW

NAPS COL 2.0-27-A
NAPS ESP VAR 2.0-4

Table 2.5.2-210 Characteristics of Future Earthquakes for RLME and Seismotectonic Sources[1]

Source	Sense of Slip[2]	Rupture Strike[2]	Rupture Dip[2]	Source Boundaries	Seismogenic Crustal Thickness[3]
Meers—Fault	Strike-slip (0.5) Reverse (0.5)	On fault	Strike-slip 90° Reverse 40° SW	Strict	15 km (0.5) 20 km (0.5)
Meers—Random in OKA	Reverse oblique	Parallel to long axis of zone	Uniform 40°–90°	Strict	15 km (0.5) 20 km (0.5)
NMFS*	NMN, NMS: Strike-slip RMT: reverse	On fault	NMN, NMS: 90°RFT: 40° SW	Strict	13 km (0.4)[6] 15 km (0.4)[6] 17 km (0.2)[6]
Wabash Valley*	*2/3 Strike-slip* *1/3 Reverse*	Strike parallel to the long axis of the zone (0.8) N50W (0.1) N20W (0.1)	2/3 Strike-slip, 90° 1/3 Reverse, 40°–60° Strike-slip, 90° Reverse, 40°	*Leaky*	17 km (0.7) 22 km (0.3)
Seismotectonic Zones					
AHEX*	*2/3 Strike-slip* *1/3 Reverse*	*N50W (0.1)* *N-S (0.1)* *N25E (0.4)* *N60E (0.3)* *E-W (0.1)*	*Strike-slip (90°–60°) (uniform)* *Reverse (30°–60°) (uniform)*	*Leaky*	8 km (0.5) 15 km (0.5)
ECC-AM*	*2/3 Strike-slip* *1/3 Reverse*	*N50W (0.2)* *N-S (0.2)* *N35E (0.4)* *N60E (0.1)* *E-W (0.1)*	*Strike-slip (90°–60°) (uniform)* *Reverse (30°–60°) (uniform)*	*Leaky*	13 km (0.6) 17 km (0.3) 22 km (0.1)

BASIS: NEW

NAPS COL 2.0-27-A
NAPS ESP VAR 2.0-4

Table 2.5.2-210 Characteristics of Future Earthquakes for RLME and Seismotectonic Sources[1]

Source	Sense of Slip[2]	Rupture Strike[2]	Rupture Dip[2]	Source Boundaries	Seismogenic Crustal Thickness[3]
ECC-GC	*2/3 Strike-slip* *1/3 Reverse*	Uniform 0° to 360°	*Strike-slip (90°–60°) (uniform)* *Reverse (30°–60°) (uniform)*	*Leaky*	13 km (0.6) 17 km (0.3) 22 km (0.1)
GHEX	*2/3 Strike-slip* *1/3 Reverse*	Uniform 0° to 360°	*Strike-slip (90°–60°) (uniform)* *Reverse (30°–60°) (uniform)*	*Leaky*	8 km (0.5) 15 km (0.5)
GMH	*4/5 Reverse* *1/5 Strike-slip*	N50W (0.4) N20W (0.4) E-W (0.2)	*Strike-slip (90°–60°) (uniform)* *Reverse (30°–60°) (uniform)*	Leaky	25 km (0.5) 30 km (0.5)
IBEB*	SS (0.1) RO (0.1) R (0.3) SS (0.2) SS (0.3)	N50W (0.1) N20W (0.1) N-S (0.3) E-W (0.2) N40E (0.3)	90° 70 E (0.5), 70 W (0.5) 40 (0.4), 70 (0.3) 90° 90°	Leaky	*13 km (0.4)* *17 km (0.4)* *22 km (0.2)*
PEZ*	*2/3 Strike-slip* *1/3 Reverse*	N50W (0.2) N-S (0.2) N35E (0.4) N60E (0.1) E-W (0.1)	*Strike-slip (90°–60°) (uniform)* *Reverse (30°–60°) (uniform)*	Leaky	*13 km (0.4)* *17 km (0.4)* *22 km (0.2)*
MidC*	*2/3 Strike-slip* *1/3 Reverse*	*N50W (0.2)* *N-S (0.2)* *N35E (0.4)* *N60E (0.1)* *E-W (0.1)*	*Strike-slip (90°–60°) (uniform)* *Reverse (30°–60°) (uniform)*	Strict	*13 km (0.4)* *17 km (0.4)* *22 km (0.2)*

BASIS: NEW

NAPS COL 2.0-27-A
NAPS ESP VAR 2.0-4

Table 2.5.2-210 Characteristics of Future Earthquakes for RLME and Seismotectonic Sources[1]

Source	Sense of Slip[2]	Rupture Strike[2]	Rupture Dip[2]	Source Boundaries	Seismogenic Crustal Thickness[3]
NAP	*1/3 Strike-slip* *2/3 Reverse*	N50W (0.2) N-S (0.2) N35E (0.4) N60E (0.1) E-W (0.1)	*Strike-slip (90°–60°) (uniform)* *Reverse (30°–60°) (uniform)*	Leaky	*13 km (0.4)* *17 km (0.4)* *22 km (0.2)*
OKA	Reverse Oblique	Parallel to long axis of zone	Uniform 45°–75°	*Leaky*	15 km (0.5) 20 km (0.5)
RR and RR-RCG	SS (0.2) R (0.35) SS (0.5) SS (0.2) SS (0.2)	N50W (0.2) N10W(0.35) E-W (0.05) N30E (0.2) N55E (0.2)	90° 70° (0.5), 40° (0.5) 90° 90° 90°	Strict	13 km (0.4) 15 km (0.4) 17 km (0.2)
SLR*	*1/3 Strike-slip* *2/3 Reverse*	N25E (0.2) N40E (0.2) N70E (0.2) N50W (0.15) N70W (0.15) N-S (0.05) E-W (0.05)	*Strike-slip (90°–60°) (uniform* *Reverse (30°–60°) (uniform)*	Leaky	25 km (0.5) 30 km (0.5)

BASIS: NEW

NAPS COL 2.0-27-A
NAPS ESP VAR 2.0-4

Table 2.5.2-210 Characteristics of Future Earthquakes for RLME and Seismotectonic Sources[1]

Source	Sense of Slip[2]	Rupture Strike[2]	Rupture Dip[2]	Source Boundaries	Seismogenic Crustal Thickness[3]

Notes

1. EPRI et al., 2012 (Reference 2.5-223, Table 5.4-2). Charleston source names, ECC-AM seismogenic thickness, and IBEB boundaries corrected from original.
2. Weights reflect aleatory uncertainty (natural randomness); weights are therefore relative frequencies.
3. Weights reflect epistemic uncertainty (scientific uncertainty); weights are therefore relative credibility that the given thickness is correct.
4. Default characteristics (i.e., those listed in Table 2.5.2-209 for the entire CEUS region) are indicated in italics.
5. The Seismogenic Crustal Thicknesses (depths) are those as published in the CEUS SSC Report, Table 5.4-2 and used in the PSHA for this project site. As indicated in the June 27, 2012 Updates file on the CEUS SSC Report web site (http://www.ceus-ssc.org), these values were updated and are consistent with the discussion in published CEUS SSC Report, Section 6.1.2.3 – see Figure 2.5.2-224. With the distance of the Charleston source to the project site, the difference in the PSHA results due to these differences in depths is negligible.
6. The weights on the suite of Seismogenic Crustal Thicknesses (depths) are those as published in the CEUS SSC Report, Table 5.4-2. As indicated in the June 27, 2012 Updates file on the CEUS SSC Report web site (http://www.ceus-ssc.org), these values were updated – see Figure 2.5.2-227. As discussed in the FSAR, a single depth of 15 km was used, the justification of which is appropriate regardless the depth weights.

* Source area within 1,000 km and included Unit 3 hazard calculation

BASIS: NEW

NAPS COL 2.0-27-A
NAPS ESP VAR 2.0-4

Table 2.5.2-211 Maximum Magnitude Distributions for Seismotectonic Distributed Seismicity Sources[1]

	Maximum Magnitude (Mmax) for:												
Weight	**AHEX***	**ECC_AM***	**ECC_GC**	**GHEX**	**GMH**	**IBEB***	**MidC-A*, MidC-B*, MidC-C*, and MidC-D***	**NAP**	**OKA**	**PEZ_N* and PEZ_W***	**RR**	**RR_RCG**	**SLR***
0.101	6.0	6.0**	6.0	6.0	6.0	6.5	5.6	6.1	5.8	5.9	6.2	6.1	6.2
0.244	6.7	6.7	6.7	6.7	6.7	6.9	6.1	6.7	6.4	6.4	6.7	6.6	6.8
0.310	7.2	7.2	7.2	7.2	7.2	7.4	6.6	7.2	6.9	6.8	7.2	7.1	7.3
0.244	7.7	7.7	7.7	7.7	7.7	7.8	7.2	7.7	7.4	7.2	7.7	7.6	7.7
0.101	8.1	8.1	8.1	8.1	8.1	8.1	8.0	8.1	8.0	7.9	8.1	8.1	8.1

Notes

EPRI et al., 2012 (Reference 2.5-223, Table H-4-4)

* 1,000 km included in North Anna hazard calculation

** As discussed in Section 2.5.2.4, consideration of the 2011 Mineral earthquake suggested this minimum magnitude to be raised to 6.1

NAPS COL 2.0-27-A
NAPS ESP VAR 2.0-4

Table 2.5.2-212 Maximum Magnitude Distribution for Charleston RLME Source[1]

Expected Charleston RLME Magnitude (M)	Weight
6.7	0.10
6.9	0.25
7.1	0.30
7.3	0.25
7.5	0.10

Notes
1, EPRI et al., 2012 (Reference 2.5-223, Table H-5.2-1)

NAPS COL 2.0-27-A
NAPS ESP VAR 2.0-4

Table 2.5.2-213 Maximum Magnitude Distribution New Madrid RLME Source

Rupture Set	Expected NMFS RLME Magnitude for: Magnitude for: NMS	RFT	NMN	Weight
1	7.9	7.8	7.6	0.167
2	7.8	7.7	7.5	0.167
3	7.6	7.8	7.5	0.250
4	7.2	7.4	7.2	0.083
5	6.9	7.3	7.0	0.250
6	6.7	7.1	6.8	0.083

Source: EPRI et al., 2012 (Reference 2.5-223, Table H-5.5-1)

NAPS COL 2.0-27-A
NAPS ESP VAR 2.0-4

Table 2.5.2-214 Maximum Magnitude Distribution for Wabash Valley RLME Source

Expected Wabash Valley RLME Magnitude (M)	Weight
6.75	0.05
7.0	0.25
7.25	0.35
7.5	0.35

Source: EPRI et al., 2012 (Reference 2.5-223, Section 6.1.9.3)

NAPS COL 2.0-27-A
NAPS ESP VAR 2.0-4

Table 2.5.2-215 Updated Distribution of Mmax for ECC-AM Source Zone

Probability	Original Magnitude	Updated Magnitude
0.101	6.0	6.1
0.244	6.7	6.7
0.310	7.2	7.2
0.244	7.7	7.7
0.101	8.1	8.1

Notes:
1. From Table 5.3.3-1 of EPRI et al. (2012) (Reference 2.5-223)
2. From Table 7.4.2-1 of EPRI et al. (2012) (Reference 2.5-223)

BASIS: NEW

NAPS COL 2.0-27-A
NAPS ESP VAR 2.0-4

Table 2.5.2-216 Total Mean Rock Hazard for 7 Spectral Frequencies

Horizontal Rock Spectral Acceleration[1], g	0.5 Hz	1 Hz	2.5 Hz	5 Hz	10 Hz	25 Hz	PGA
0.0005	2.62E-02	4.60E-02	7.65E-02	8.57E-02	7.97E-02	6.54E-02	5.52E-02
0.001	1.46E-02	2.73E-02	5.11E-02	5.99E-02	5.60E-02	4.59E-02	3.59E-02
0.005	2.97E-03	6.23E-03	1.41E-02	1.84E-02	1.86E-02	1.71E-02	1.11E-02
0.01	1.24E-03	2.76E-03	7.09E-03	1.01E-02	1.10E-02	1.08E-02	6.25E-03
0.015	6.97E-04	1.58E-03	4.47E-03	6.86E-03	7.89E-03	8.14E-03	4.33E-03
0.03	2.33E-04	5.42E-04	1.82E-03	3.28E-03	4.27E-03	4.90E-03	2.14E-03
0.05	9.76E-05	2.25E-04	8.68E-04	1.77E-03	2.56E-03	3.20E-03	1.17E-03
0.075	4.61E-05	1.06E-04	4.61E-04	1.04E-03	1.61E-03	2.18E-03	6.87E-04
0.1	2.56E-05	6.02E-05	2.88E-04	6.95E-04	1.13E-03	1.61E-03	4.61E-04
0.15	1.03E-05	2.63E-05	1.43E-04	3.79E-04	6.58E-04	1.00E-03	2.55E-04
0.3	1.83E-06	5.98E-06	3.96E-05	1.23E-04	2.37E-04	4.00E-04	8.51E-05
0.5	4.90E-07	1.88E-06	1.41E-05	4.93E-05	1.04E-04	1.87E-04	3.48E-05
0.75	1.66E-07	6.96E-07	5.77E-06	2.23E-05	5.08E-05	9.78E-05	1.58E-05
1	7.41E-08	3.25E-07	2.92E-06	1.21E-05	2.94E-05	6.01E-05	8.54E-06
1.5	2.19E-08	1.01E-07	1.03E-06	4.77E-06	1.28E-05	2.89E-05	3.24E-06
3	2.07E-09	1.00E-08	1.31E-07	7.54E-07	2.41E-06	7.14E-06	4.33E-07
5	2.79E-10	1.39E-09	2.18E-08	1.52E-07	5.53E-07	2.15E-06	6.84E-08
7.5	4.77E-11	2.42E-10	4.36E-09	3.59E-08	1.46E-07	7.29E-07	1.23E-08
10	1.23E-11	6.34E-11	1.26E-09	1.17E-08	5.11E-08	3.10E-07	3.15E-09

1. 5% critical damping

NAPS COL 2.0-27-A
NAPS ESP VAR 2.0-4

Table 2.5.2-217 Horizontal Rock Spectral Accelerations from the PSHA for MAFEs of 10^{-4}, 10^{-5}, and 10^{-6}

5% Critically-Damped Spectral Acceleration, g			
Spectral Frequency	**10^{-4}**	**10^{-5}**	**10^{-6}**
PGA (100 Hz)	0.271	0.929	2.25
25 Hz	0.740	2.54	6.66
10 Hz	0.510	1.66	4.07
5.0 Hz	0.337	1.09	2.70
2.5 Hz	0.182	0.584	1.52
1.0 Hz	0.0772	0.236	0.647
0.5 Hz	0.0493	0.152	0.379

MAFE: mean annual frequency of exceedance
UHRS: uniform hazard response spectrum

NAPS COL 2.0-27-A
NAPS ESP VAR 2.0-4

Table 2.5.2-218 Mean Magnitude and Distance for LF and HF Response Spectra for Three MAFEs

MAFE >	**10^{-4}**	**10^{-5}**	**10^{-6}**
Low Frequency **M**	7.4	7.5	6.8
Low Frequency R (km)	540	480	18
High Frequency **M**	5.9	6.2	6.5
High Frequency R (km)	21	15	14

LF: low frequency, 1 to 2.5 Hz
HF: high frequency, 5 to 10 Hz
MAFE: mean annual frequency of exceedance
M: moment magnitude
R: distance (kilometers)

BASIS: NEW

NAPS COL 2.0-27-A
NAPS ESP VAR 2.0-4

Table 2.5.2-219 Horizontal Rock UHRS (g) for MAFEs of 10^{-4}, 10^{-5}, and 10^{-6}

Spectral Frequency, Hz	10^{-4} HF	10^{-4} LF	10^{-5} HF	10^{-5} LF	10^{-6} HF	10^{-6} LF
100	2.71E-01	1.57E-01	9.29E-01	5.02E-01	2.25E+00	2.02E+00
90	3.00E-01	1.71E-01	1.03E+00	5.45E-01	2.50E+00	2.19E+00
80	3.48E-01	1.95E-01	1.19E+00	6.21E-01	2.93E+00	2.50E+00
70	4.21E-01	2.31E-01	1.44E+00	7.36E-01	3.58E+00	2.96E+00
60	5.16E-01	2.76E-01	1.77E+00	8.80E-01	4.42E+00	3.54E+00
50	6.12E-01	3.19E-01	2.10E+00	1.02E+00	5.30E+00	4.09E+00
45	6.54E-01	3.35E-01	2.24E+00	1.07E+00	5.69E+00	4.30E+00
40	6.88E-01	3.47E-01	2.36E+00	1.11E+00	6.03E+00	4.45E+00
35	7.14E-01	3.55E-01	2.45E+00	1.13E+00	6.31E+00	4.54E+00
30	7.32E-01	3.58E-01	2.51E+00	1.14E+00	6.52E+00	4.56E+00
25	7.40E-01	3.58E-01	2.54E+00	1.14E+00	6.66E+00	4.52E+00
20	7.04E-01	3.53E-01	2.38E+00	1.13E+00	6.15E+00	4.37E+00
15	6.35E-01	3.42E-01	2.11E+00	1.09E+00	5.33E+00	4.05E+00
12.5	5.81E-01	3.32E-01	1.91E+00	1.06E+00	4.77E+00	3.80E+00
10	5.10E-01	3.17E-01	1.66E+00	1.01E+00	4.07E+00	3.45E+00
9	4.83E-01	3.09E-01	1.57E+00	9.82E-01	3.85E+00	3.27E+00
8	4.52E-01	2.99E-01	1.46E+00	9.51E-01	3.60E+00	3.08E+00

BASIS: NEW

NAPS COL 2.0-27-A
NAPS ESP VAR 2.0-4

Table 2.5.2-219 Horizontal Rock UHRS (g) for MAFEs of 10^{-4}, 10^{-5}, and 10^{-6}

Spectral Frequency, Hz	10^{-4} HF	10^{-4} LF	10^{-5} HF	10^{-5} LF	10^{-6} HF	10^{-6} LF
7	4.18E-01	2.88E-01	1.35E+00	9.15E-01	3.33E+00	2.87E+00
6	3.80E-01	2.74E-01	1.23E+00	8.71E-01	3.03E+00	2.63E+00
5	3.37E-01	2.57E-01	1.09E+00	8.16E-01	2.70E+00	2.37E+00
4	2.81E-01	2.34E-01	9.03E-01	7.45E-01	2.27E+00	2.07E+00
3	2.18E-01	2.03E-01	6.99E-01	6.48E-01	1.79E+00	1.72E+00
2.5	1.82E-01	1.82E-01	5.84E-01	5.84E-01	1.52E+00	1.52E+00
2	1.43E-01	1.56E-01	4.70E-01	4.95E-01	1.25E+00	1.29E+00
1.5	9.98E-02	1.21E-01	3.38E-01	3.79E-01	9.24E-01	1.01E+00
1.25	7.77E-02	1.00E-01	2.68E-01	3.10E-01	7.43E-01	8.35E-01
1	5.63E-02	7.72E-02	1.97E-01	2.36E-01	5.57E-01	6.47E-01
0.9	4.82E-02	7.32E-02	1.70E-01	2.24E-01	4.82E-01	6.09E-01
0.8	4.03E-02	6.84E-02	1.43E-01	2.10E-01	4.10E-01	5.63E-01
0.7	3.28E-02	6.29E-02	1.17E-01	1.93E-01	3.39E-01	5.09E-01
0.6	2.58E-02	5.65E-02	9.31E-02	1.73E-01	2.71E-01	4.48E-01
0.5	1.93E-02	4.93E-02	7.03E-02	1.52E-01	2.07E-01	3.79E-01
0.4	1.54E-02	3.94E-02	5.62E-02	1.21E-01	1.66E-01	3.04E-01
0.3	1.16E-02	2.96E-02	4.22E-02	9.09E-02	1.24E-01	2.28E-01

BASIS: NEW

NAPS COL 2.0-27-A
NAPS ESP VAR 2.0-4

Table 2.5.2-219 Horizontal Rock UHRS (g) for MAFEs of 10^{-4}, 10^{-5}, and 10^{-6}

Spectral Frequency, Hz	10^{-4} HF	10^{-4} LF	10^{-5} HF	10^{-5} LF	10^{-6} HF	10^{-6} LF
0.2	7.70E-03	1.97E-02	2.81E-02	6.06E-02	8.28E-02	1.52E-01
0.167	6.43E-03	1.65E-02	2.35E-02	5.06E-02	6.92E-02	1.27E-01
0.125	4.82E-03	1.23E-02	1.76E-02	3.79E-02	5.18E-02	9.49E-02
0.1	3.85E-03	9.86E-03	1.41E-02	3.03E-02	4.14E-02	7.59E-02

LF: low frequency, 1 to 2.5 Hz
HF: high frequency, 5 to 10 Hz
MAFE: mean annual frequency of exceedance
UHRS: uniform hazard response spectrum

NAPS COL 2.0-27-A

Table 2.5.2-220 V_{S30} Values[1] for RB/FB, CB, and FWSC Soil Columns

V_{S30} (fps)	RB/FB Soil Column	CB Soil Column	FWSC Soil Column
Elevation 290 ft (Finished Grade)	3,423	2,439	
Elevation 282 ft (FIRS elevation for FWSC)			2,124
Elevation 241 ft (FIRS elevation for CB)	6,078	6,068	
Elevation 224 ft (FIRS elevation for RB/FB)	6,783	7,553	

1 V_{S30}: Travel-time averaged shear-wave velocity in the top 30 meters of the soil column

NAPS COL 2.0-27-A
NAPS ESP VAR 2.0-4

Table 2.5.2-221 Input Hard Rock Motions and Associated Parameters

Rock Motion	Magnitude (M)	Distance (R, km)	Duration (sec)	Effective Strain Ratio
LF 10^{-4}	7.4	540	26.3	0.64
HF 10^{-4}	5.9	21	2.4	0.49
LF 10^{-5}	7.5	480	26.3	0.65
HF 10^{-5}	6.2	15	5.1	0.52

NAPS COL 2.0-27-A
NAPS DEP 3.7-1

Table 2.5.2-222 Horizontal and Vertical RB/FB Full Column Outcrop FIRS

Frequency (Hz)	$FIRS_H(f)$ (g)	$V/H(f)$	$FIRS_V(f)$ (g)
100	0.671	1.000	0.671
90	0.702	1.038	0.729
80	0.774	1.090	0.844
70	0.920	1.128	1.037
60	1.135	1.137	1.291
50	1.348	1.124	1.515
45	1.425	1.102	1.571
40	1.506	1.042	1.570
35	1.563	0.981	1.533
30	1.641	0.937	1.537
25	1.636	0.880	1.440
20	1.530	0.826	1.263
15	1.428	0.788	1.125
12.5	1.367	0.771	1.053
10	1.226	0.750	0.920
9	1.159	0.750	0.869
8	1.076	0.750	0.807
7	0.967	0.750	0.725
6	0.829	0.750	0.621
5	0.700	0.750	0.525
4	0.534	0.750	0.400
3	0.382	0.750	0.286
2.5	0.308	0.750	0.231
2	0.249	0.750	0.187
1.5	0.187	0.750	0.141

NAPS COL 2.0-27-A
NAPS DEP 3.7-1

Table 2.5.2-222 Horizontal and Vertical RB/FB Full Column Outcrop FIRS

Frequency (Hz)	$FIRS_H(f)$ (g)	$V/H(f)$	$FIRS_V(f)$ (g)
1.25	0.152	0.750	0.114
1	0.116	0.750	0.0870
0.9	0.109	0.750	0.0821
0.8	0.102	0.750	0.0767
0.7	0.0939	0.750	0.0704
0.6	0.0844	0.750	0.0633
0.5	0.0735	0.750	0.0551
0.4	0.0588	0.750	0.0441
0.3	0.0441	0.750	0.0331
0.2	0.0294	0.750	0.0220
0.167	0.0245	0.750	0.0184
0.125	0.0184	0.750	0.0138
0.1	0.0147	0.750	0.0110

NAPS COL 2.0-27-A
NAPS DEP 3.7-1

Table 2.5.2-223 Horizontal and Vertical CB Full Column Outcrop FIRS

Frequency (Hz)	$FIRS_H(f)$ (g)	V/H(*f*)	$FIRS_V(f)$ (g)
100	0.895	1.000	0.895
90	0.936	1.038	0.972
80	1.027	1.090	1.119
70	1.210	1.128	1.365
60	1.498	1.137	1.704
50	1.756	1.124	1.975
45	1.862	1.102	2.052
40	1.947	1.042	2.030
35	2.054	0.981	2.014
30	2.158	0.937	2.021
25	2.143	0.880	1.887
20	1.990	0.826	1.643
15	1.867	0.788	1.472
12.5	1.803	0.771	1.390
10	1.621	0.750	1.216
9	1.544	0.750	1.158
8	1.430	0.750	1.073
7	1.280	0.750	0.960
6	1.087	0.750	0.815
5	0.885	0.750	0.664
4	0.638	0.750	0.479
3	0.435	0.750	0.327
2.5	0.346	0.750	0.259
2	0.270	0.750	0.202
1.5	0.197	0.750	0.148
1.25	0.158	0.750	0.119

NAPS COL 2.0-27-A
NAPS DEP 3.7-1

Table 2.5.2-223 Horizontal and Vertical CB Full Column Outcrop FIRS

Frequency (Hz)	$FIRS_H(f)$ (g)	V/H(*f*)	$FIRS_V(f)$ (g)
1	0.119	0.750	0.0895
0.9	0.112	0.750	0.0843
0.8	0.105	0.750	0.0785
0.7	0.0959	0.750	0.0719
0.6	0.0860	0.750	0.0645
0.5	0.0749	0.750	0.0561
0.4	0.0598	0.750	0.0449
0.3	0.0448	0.750	0.0336
0.2	0.0298	0.750	0.0223
0.167	0.0249	0.750	0.0187
0.125	0.0186	0.750	0.0140
0.1	0.0149	0.750	0.0112

NAPS COL 2.0-27-A
NAPS DEP 3.7-1

Table 2.5.2-224 Horizontal and Vertical RB/FB Partial Column Outcrop FIRS

Frequency (Hz)	$FIRS_H(f)$ (g)	V/H(*f*)	$FIRS_V(f)$ (g)
100	0.699	1.000	0.699
90	0.732	1.038	0.760
80	0.808	1.090	0.880
70	0.952	1.128	1.074
60	1.181	1.137	1.343
50	1.393	1.124	1.566
45	1.492	1.102	1.644
40	1.555	1.042	1.621
35	1.615	0.981	1.584
30	1.634	0.937	1.530
25	1.641	0.880	1.444
20	1.575	0.826	1.301
15	1.535	0.788	1.210
12.5	1.471	0.771	1.134
10	1.279	0.750	0.959
9	1.169	0.750	0.877
8	1.046	0.750	0.785
7	0.902	0.750	0.676
6	0.756	0.750	0.567
5	0.624	0.750	0.468
4	0.490	0.750	0.367
3	0.363	0.750	0.272
2.5	0.298	0.750	0.224
2	0.245	0.750	0.183
1.5	0.186	0.750	0.139

NAPS COL 2.0-27-A
NAPS DEP 3.7-1

Table 2.5.2-224 Horizontal and Vertical RB/FB Partial Column Outcrop FIRS

Frequency (Hz)	$FIRS_H(f)$ (g)	V/H(*f*)	$FIRS_V(f)$ (g)
1.25	0.151	0.750	0.113
1	0.115	0.750	0.0866
0.9	0.109	0.750	0.0818
0.8	0.102	0.750	0.0764
0.7	0.0936	0.750	0.0702
0.6	0.0841	0.750	0.0631
0.5	0.0733	0.750	0.0550
0.4	0.0587	0.750	0.0440
0.3	0.0440	0.750	0.0330
0.2	0.0293	0.750	0.0220
0.167	0.0245	0.750	0.0183
0.125	0.0183	0.750	0.0137
0.1	0.0147	0.750	0.0110

NAPS COL 2.0-27-A
NAPS DEP 3.7-1

Table 2.5.2-225 Horizontal and Vertical CB Partial Column Outcrop FIRS

Frequency (Hz)	$FIRS_H(f)$ (g)	V/H(*f*)	$FIRS_V(f)$ (g)
100	0.941	1.000	0.941
90	0.986	1.038	1.023
80	1.082	1.090	1.180
70	1.260	1.128	1.421
60	1.586	1.137	1.803
50	1.863	1.124	2.094
45	1.975	1.102	2.177
40	2.096	1.042	2.185
35	2.175	0.981	2.133
30	2.098	0.937	1.966
25	2.093	0.880	1.842
20	2.136	0.826	1.763
15	2.199	0.788	1.733
12.5	2.104	0.771	1.622
10	1.709	0.750	1.282
9	1.463	0.750	1.098
8	1.203	0.750	0.902
7	0.974	0.750	0.730
6	0.793	0.750	0.595
5	0.647	0.750	0.485
4	0.505	0.750	0.378
3	0.373	0.750	0.279
2.5	0.306	0.750	0.230
2	0.247	0.750	0.185
1.5	0.187	0.750	0.140

NAPS COL 2.0-27-A
NAPS DEP 3.7-1

Table 2.5.2-225 Horizontal and Vertical CB Partial Column Outcrop FIRS

Frequency (Hz)	$FIRS_H(f)$ (g)	V/H(*f*)	$FIRS_V(f)$ (g)
1.25	0.152	0.750	0.114
1	0.116	0.750	0.0872
0.9	0.110	0.750	0.0823
0.8	0.103	0.750	0.0769
0.7	0.0942	0.750	0.0706
0.6	0.0846	0.750	0.0635
0.5	0.0738	0.750	0.0553
0.4	0.0590	0.750	0.0443
0.3	0.0442	0.750	0.0332
0.2	0.0295	0.750	0.0221
0.167	0.0246	0.750	0.0184
0.125	0.0184	0.750	0.0138
0.1	0.0147	0.750	0.0111

NAPS COL 2.0-27-A
NAPS DEP 3.7-1

Table 2.5.2-226 Horizontal and Vertical PBSRS for RB/FB and CB

Frequency (Hz)	$PBSRS_H(f)$ (g)	V/H(*f*)	$PBSRS_V(f)$ (g)
100	1.044	0.965	1.008
90	1.083	1.009	1.093
80	1.168	1.073	1.254
70	1.332	1.122	1.495
60	1.578	1.142	1.803
50	1.831	1.141	2.090
45	2.016	1.103	2.224
40	2.232	1.036	2.312
35	2.333	0.981	2.288
30	2.421	0.937	2.268
25	2.443	0.880	2.150
20	2.378	0.826	1.964
15	2.376	0.788	1.872
12.5	2.375	0.771	1.831
10	2.235	0.750	1.676
9	2.147	0.750	1.610
8	1.996	0.750	1.497
7	1.794	0.750	1.346
6	1.544	0.750	1.158
5	1.272	0.750	0.954
4	0.909	0.750	0.682
3	0.564	0.750	0.423
2.5	0.419	0.750	0.314
2	0.302	0.750	0.226
1.5	0.212	0.750	0.159
1.25	0.167	0.750	0.126

NAPS COL 2.0-27-A
NAPS DEP 3.7-1

Table 2.5.2-226 Horizontal and Vertical PBSRS for RB/FB and CB

Frequency (Hz)	$PBSRS_H(f)$ (g)	V/H(*f*)	$PBSRS_V(f)$ (g)
1	0.125	0.750	0.0936
0.9	0.117	0.750	0.0877
0.8	0.109	0.750	0.0814
0.7	0.0992	0.750	0.0744
0.6	0.0887	0.750	0.0665
0.5	0.0771	0.750	0.0578
0.4	0.0615	0.750	0.0461
0.3	0.0459	0.750	0.0344
0.2	0.0306	0.750	0.0229
0.167	0.0255	0.750	0.0191
0.125	0.0191	0.750	0.0144
0.1	0.0154	0.750	0.0115

NAPS COL 2.0-27-A
NAPS DEP 3.7-1

Table 2.5.2-227 Horizontal and Vertical FWSC Geologic Outcrop FIRS

Frequency (Hz)	$FIRS_H(f)$ (g)	V/H(*f*)	$FIRS_V(f)$ (g)
100	0.800	0.965	0.772
90	0.811	1.009	0.819
80	0.834	1.073	0.895
70	0.879	1.122	0.986
60	0.955	1.142	1.091
50	1.078	1.141	1.231
45	1.168	1.103	1.288
40	1.284	1.036	1.330
35	1.418	0.981	1.391
30	1.593	0.937	1.493
25	1.787	0.880	1.573
20	1.914	0.826	1.580
15	1.924	0.788	1.516
12.5	1.846	0.771	1.423
10	1.751	0.750	1.313
9	1.753	0.750	1.315
8	1.725	0.750	1.293
7	1.628	0.750	1.221
6	1.459	0.750	1.094
5	1.249	0.750	0.936
4	0.973	0.750	0.730
3	0.670	0.750	0.502
2.5	0.512	0.750	0.384
2	0.377	0.750	0.283
1.5	0.244	0.750	0.183
1.25	0.184	0.750	0.138

NAPS COL 2.0-27-A
NAPS DEP 3.7-1

Table 2.5.2-227 Horizontal and Vertical FWSC Geologic Outcrop FIRS

Frequency (Hz)	$FIRS_H(f)$ (g)	V/H(*f*)	$FIRS_V(f)$ (g)
1	0.132	0.750	0.0994
0.9	0.123	0.750	0.0920
0.8	0.113	0.750	0.0846
0.7	0.102	0.750	0.0767
0.6	0.0909	0.750	0.0682
0.5	0.0786	0.750	0.0589
0.4	0.0624	0.750	0.0468
0.3	0.0465	0.750	0.0349
0.2	0.0309	0.750	0.0232
0.167	0.0258	0.750	0.0194
0.125	0.0194	0.750	0.0145
0.1	0.0156	0.750	0.0117

NAPS COL 2.0-27-A
NAPS ESP VAR 2.0-4

Table 2.5.2-228 Horizontal and Vertical GMRS

Frequency (Hz)	$GMRS_H(f)$ (g)	V/H(*f*)	$GMRS_V(f)$ (g)
100	0.658	1.000	0.658
90	0.692	1.038	0.718
80	0.769	1.090	0.838
70	0.930	1.128	1.048
60	1.169	1.137	1.329
50	1.408	1.124	1.583
45	1.505	1.102	1.659
40	1.570	1.042	1.636
35	1.608	0.981	1.577
30	1.629	0.937	1.526
25	1.648	0.880	1.451
20	1.560	0.826	1.288
15	1.352	0.788	1.065
12.5	1.169	0.771	0.901
10	0.943	0.750	0.707
9	0.863	0.750	0.647
8	0.783	0.750	0.587
7	0.705	0.750	0.529
6	0.626	0.750	0.469
5	0.545	0.750	0.409
4	0.447	0.750	0.335
3	0.342	0.750	0.257
2.5	0.285	0.750	0.214
2	0.238	0.750	0.179
1.5	0.182	0.750	0.137
1.25	0.149	0.750	0.112

NAPS COL 2.0-27-A
NAPS ESP VAR 2.0-4

Table 2.5.2-228 Horizontal and Vertical GMRS

Frequency (Hz)	$GMRS_H(f)$ (g)	V/H(*f*)	$GMRS_V(f)$ (g)
1	0.114	0.750	0.0856
0.9	0.108	0.750	0.0809
0.8	0.101	0.750	0.0757
0.7	0.0928	0.750	0.0696
0.6	0.0834	0.750	0.0626
0.5	0.0728	0.750	0.0546
0.4	0.0583	0.750	0.0437
0.3	0.0437	0.750	0.0328
0.2	0.0291	0.750	0.0218
0.167	0.0243	0.750	0.0182
0.125	0.0182	0.750	0.0136
0.1	0.0146	0.750	0.0109

BASIS: NEW

NAPS COL 2.0-27-A
NAPS ESP VAR 2.0-4

Figure 2.5.2-201 Plot of Regional Seismicity from the CEUS SSC Earthquake Catalog

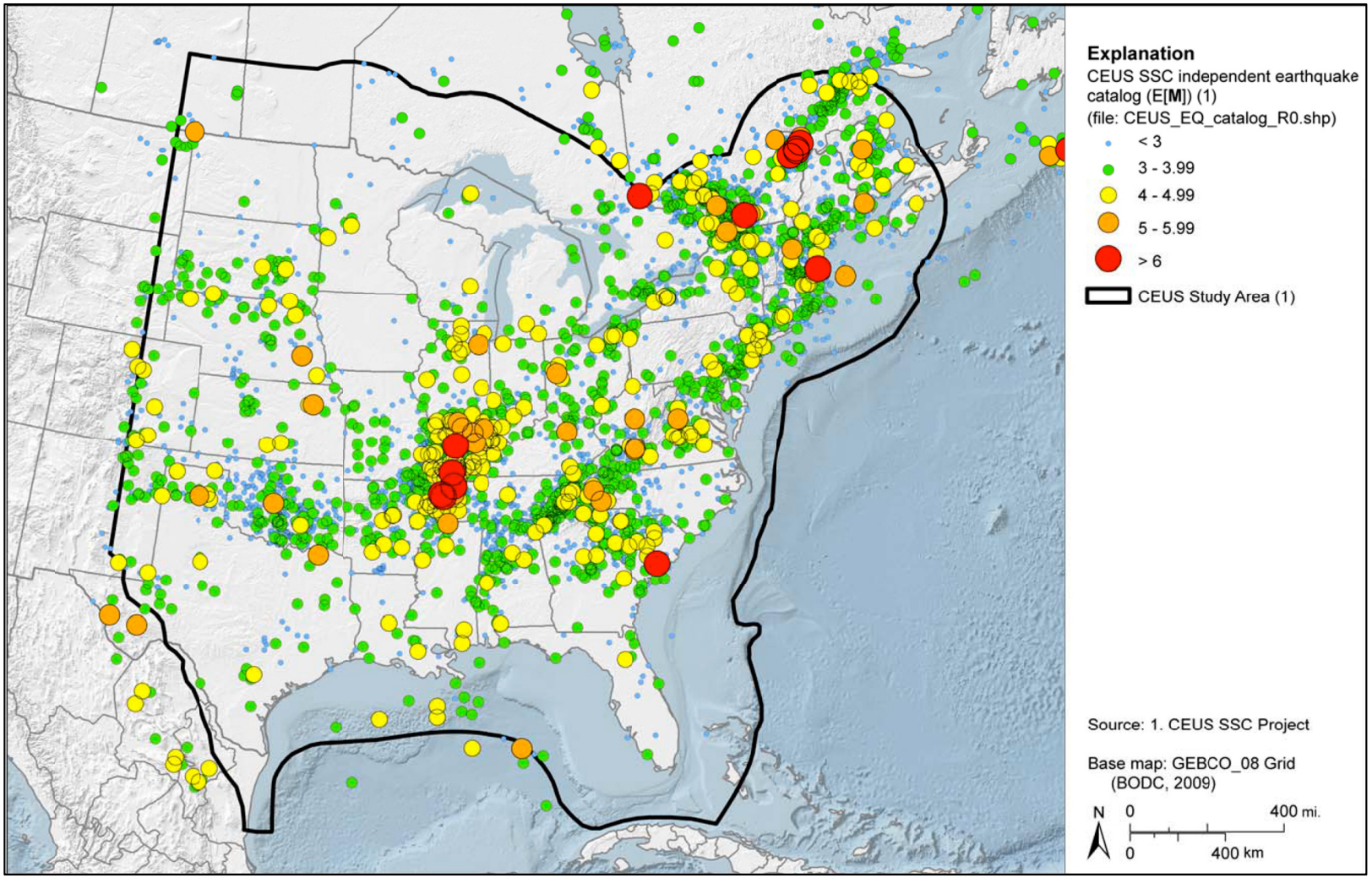

NOTE: Earthquakes shown are independent or mainshock earthquakes with E[**M**] ≥ 2.2. Black line is the spatial coverage of the CEUS SSC study area.
Source: EPRI et al., 2012 (Reference 2.5-223, Figure A-2)

BASIS: NEW

NAPS COL 2.0-27-A
NAPS ESP VAR 2.0-4

Figure 2.5.2-202 Plot of Regional Seismicity

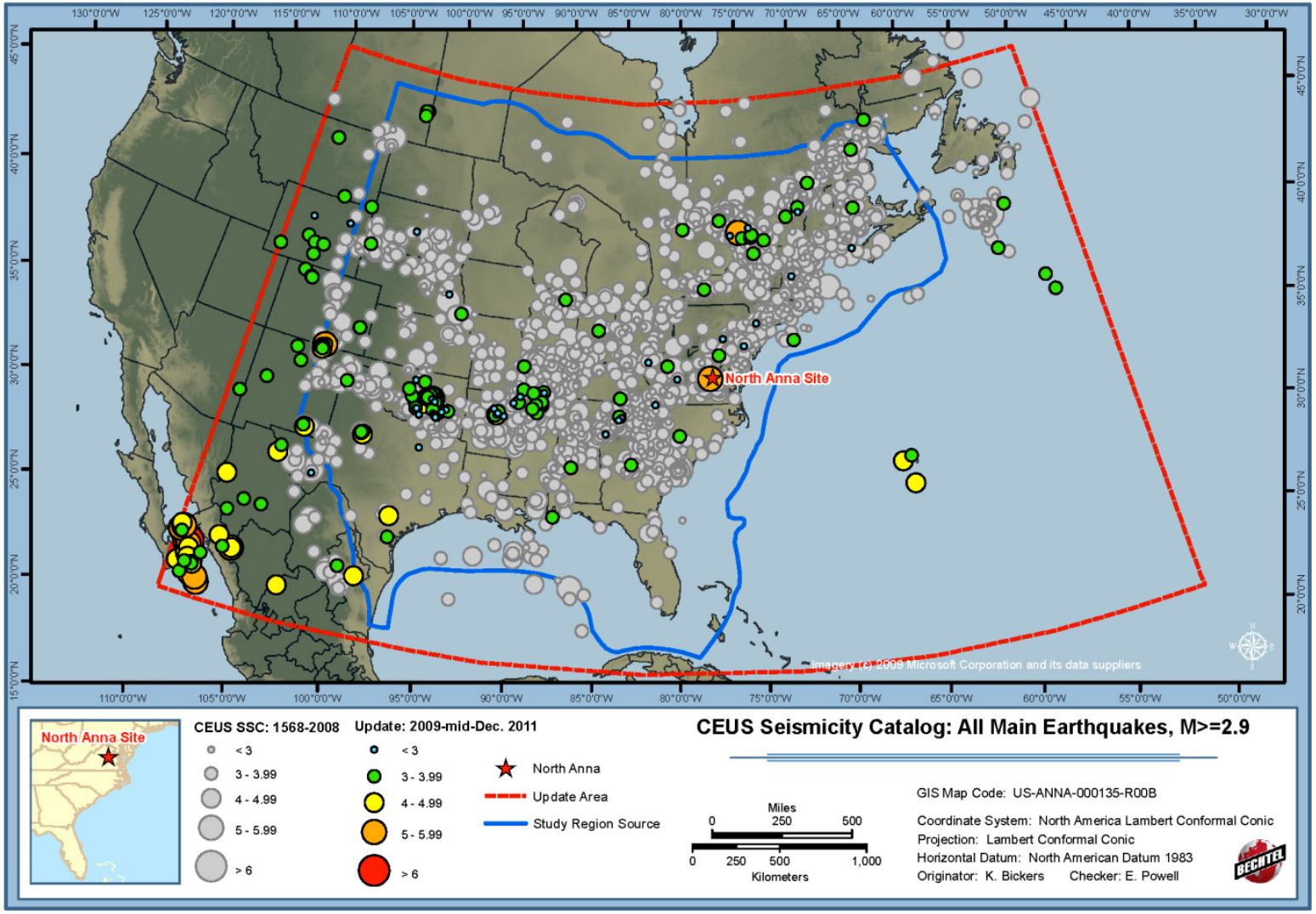

NOTE: Earthquakes shown are from the updated CEUS SSC earthquake catalog for independent or mainshock earthquakes with E[**M**] ≥ 2.9.

BASIS: NEW

NAPS COL 2.0-27-A
NAPS ESP VAR 2.0-4

Figure 2.5.2-203 Plot of Seismicity Within 322 km (200 miles) of the Project Site

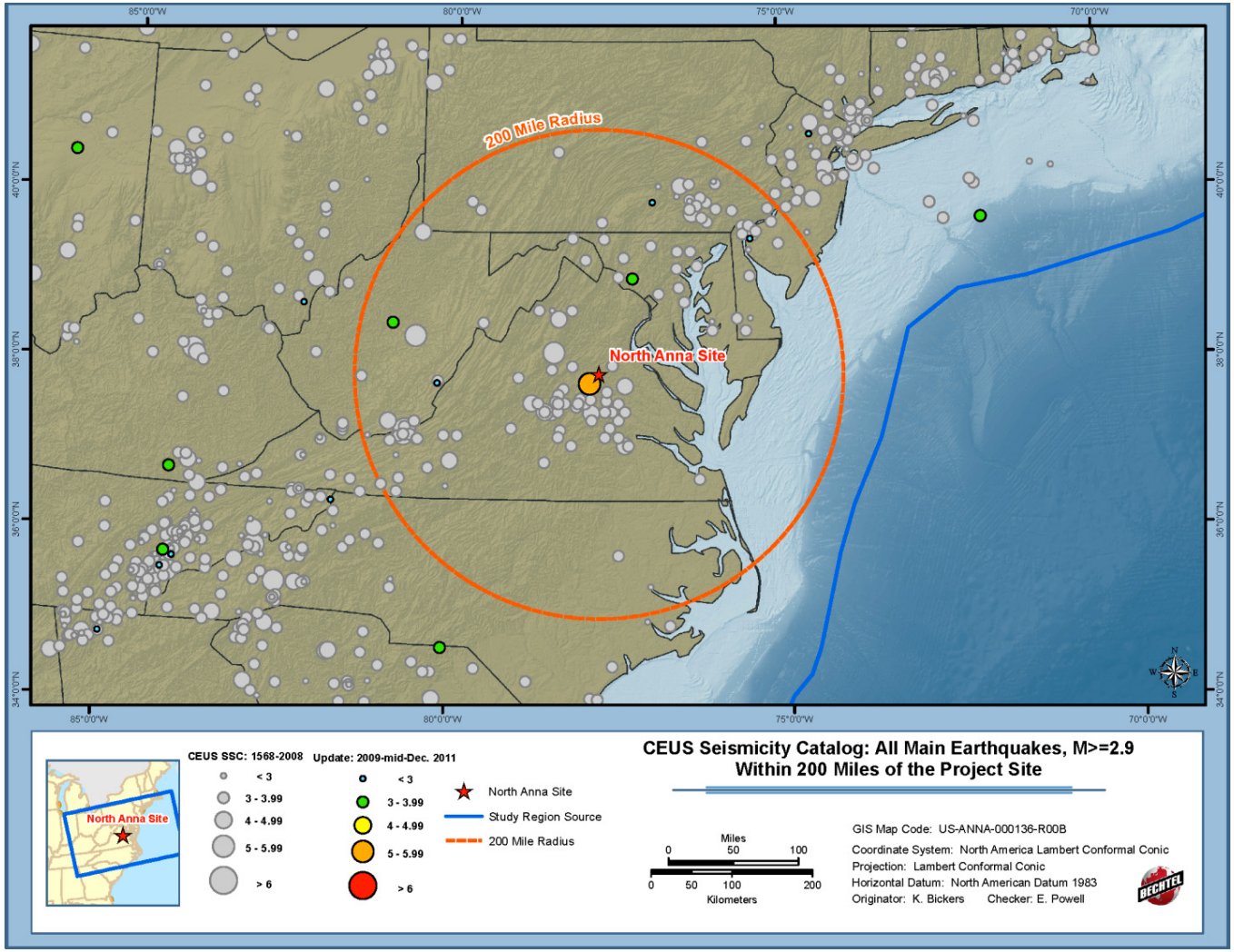

NOTE: Earthquakes shown are from the updated CEUS SSC earthquake catalog for independent or mainshock earthquakes with E[**M**] ≥ 2.9. The red epicenter nearest the project site is that of the 2011 Mineral, Virginia earthquake.

BASIS: NEW

NAPS COL 2.0-27-A
NAPS ESP VAR 2.0-4

Figure 2.5.2-204 Plot of Seismicity Within 80 km (50 miles) of the Project Site

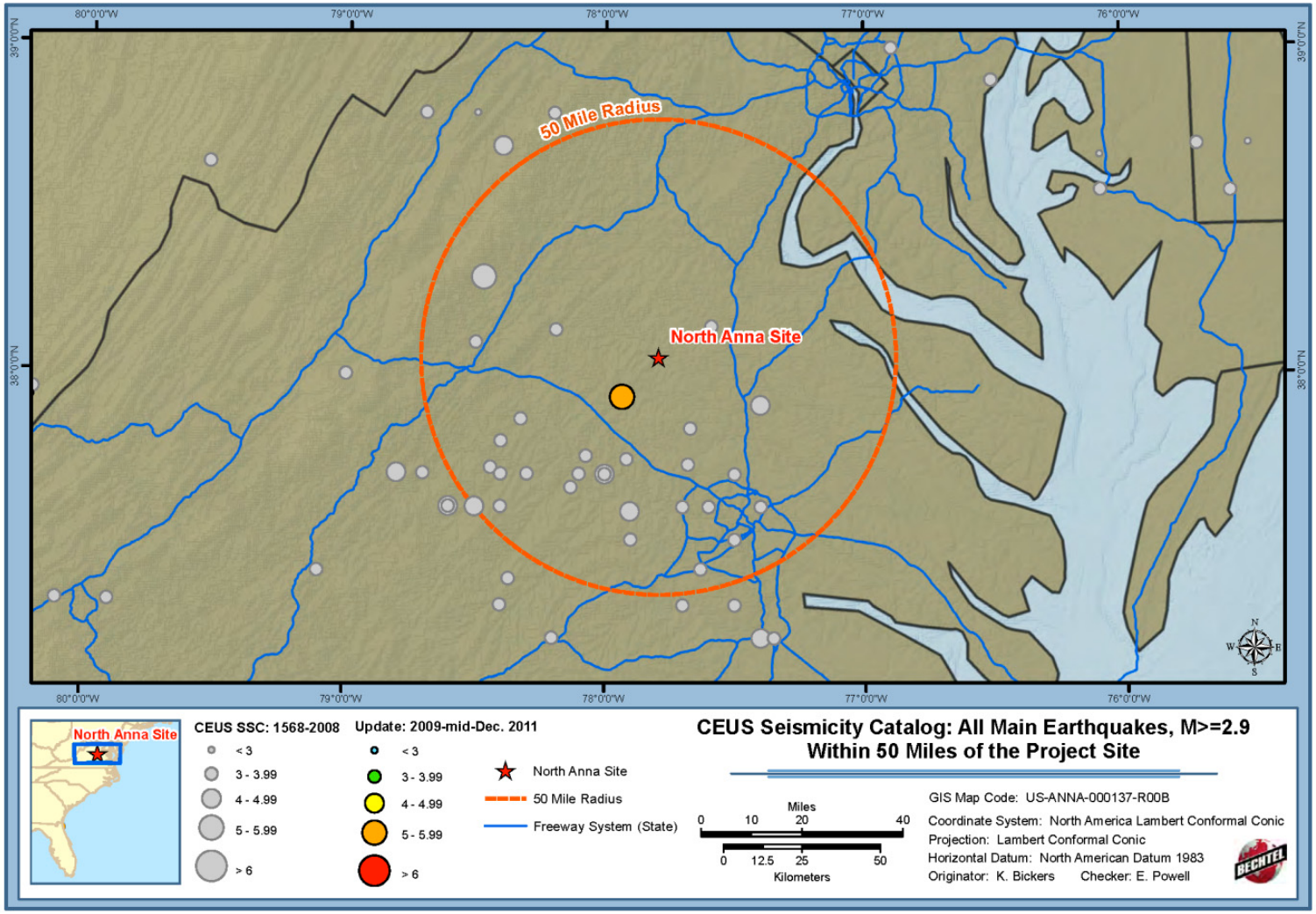

NOTE: Earthquakes shown are from the updated CEUS SSC earthquake catalog for independent or mainshock earthquakes with E[**M**] ≥ 2.9. The red epicenter nearest the project site is that of the 2011 Mineral, Virginia earthquake

NAPS COL 2.0-27-A
NAPS ESP VAR 2.0-4

Figure 2.5.2-205 Processed Acceleration, Velocity, and Displacement Time Histories for the M 5.8 Mineral Earthquake from the Unit 1 Containment Mat Foundation Station (CW026) for Channel 1, L(ongitudinal)-Component

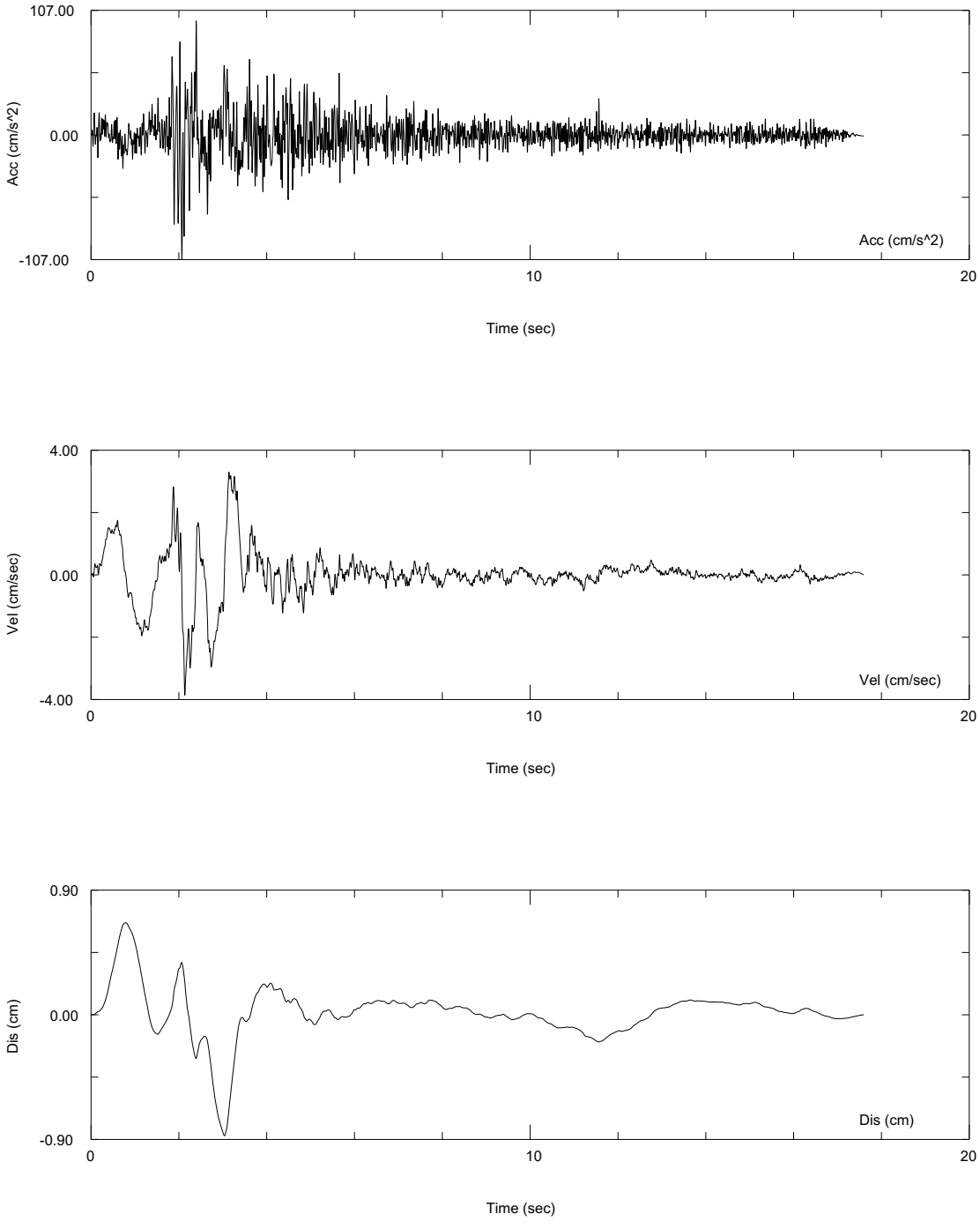

Source: adapted from Kinemetrics (2011) (Reference 2.5-279)

NAPS COL 2.0-27-A
NAPS ESP VAR 2.0-4

Figure 2.5.2-206 Acceleration, Velocity, and Displacement Time Histories for the M5.8 Mineral Earthquake from the Unit 1 from the Containment Mat Foundation Station (CW026) for Channel 2, V(ertical)-Component

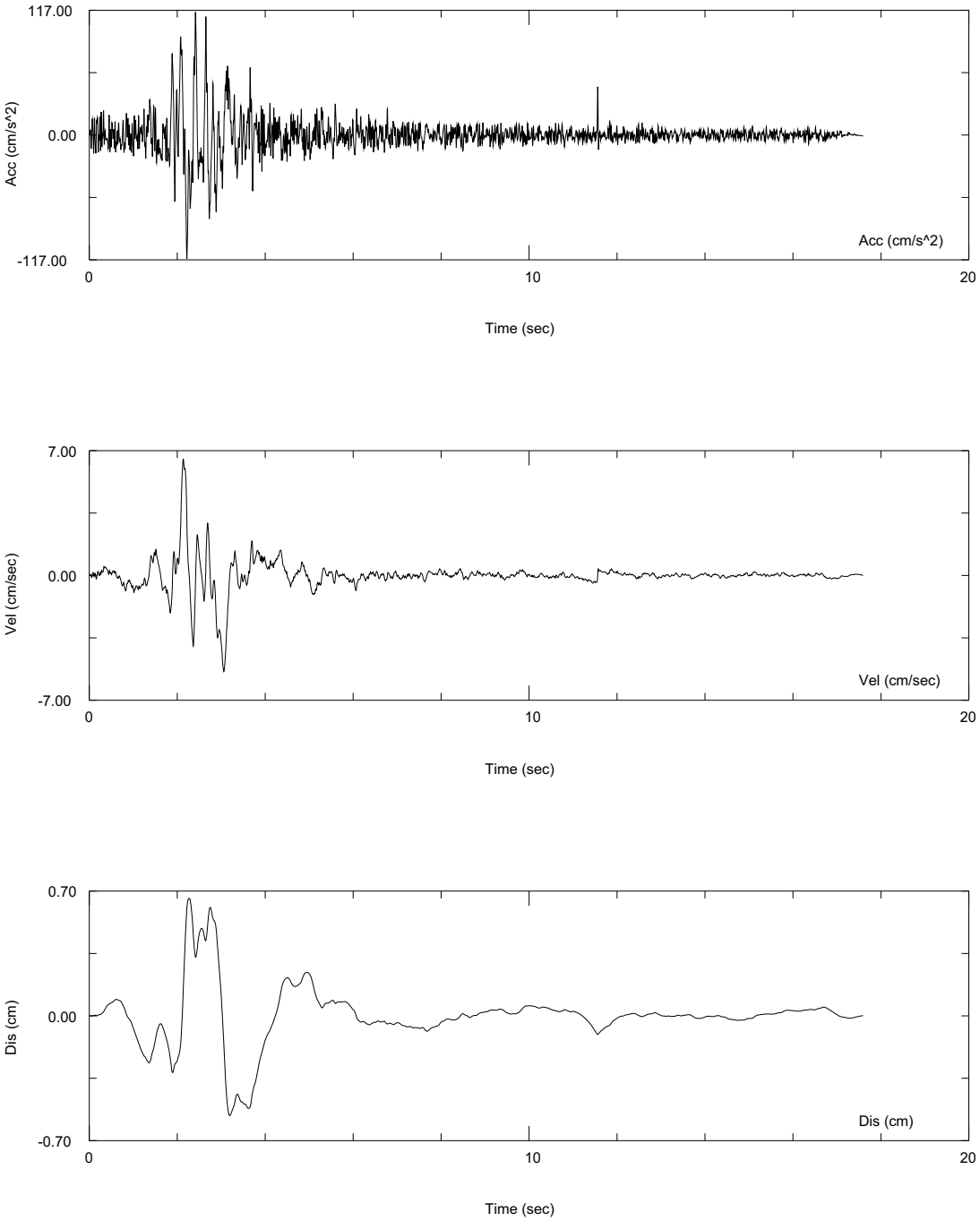

Source: adapted from Kinemetrics (2011) (Reference 2.5-279)

NAPS COL 2.0-27-A
NAPS ESP VAR 2.0-4

Figure 2.5.2-207 Processed Acceleration, Velocity, and Displacement Time Histories for the M 5.8 Mineral Earthquake from the Unit 1 from the Containment Mat Foundation Station (CW026) for Channel 3, T(ransverse)-Component

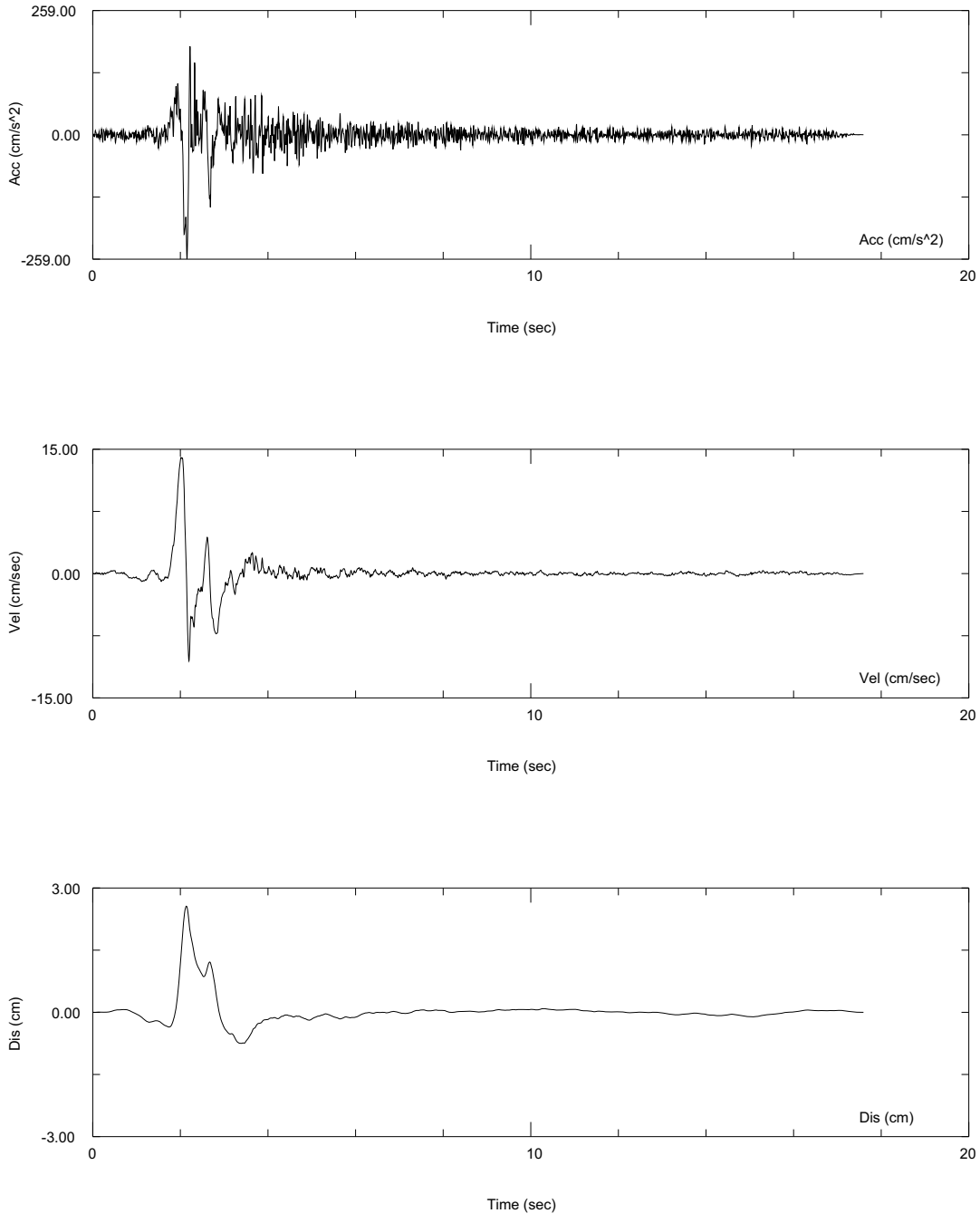

Source: adapted from Kinemetrics (2011)(Reference 2.5-279)

NAPS COL 2.0-27-A
NAPS ESP VAR 2.0-4

Figure 2.5.2-208 Processed Acceleration, Velocity, and Displacement Time Histories for the M5.8 Mineral Earthquake from the Unit 1 from Containment Operating Deck Station (CW018) for Channel 1, L(ongitudinal)-Component

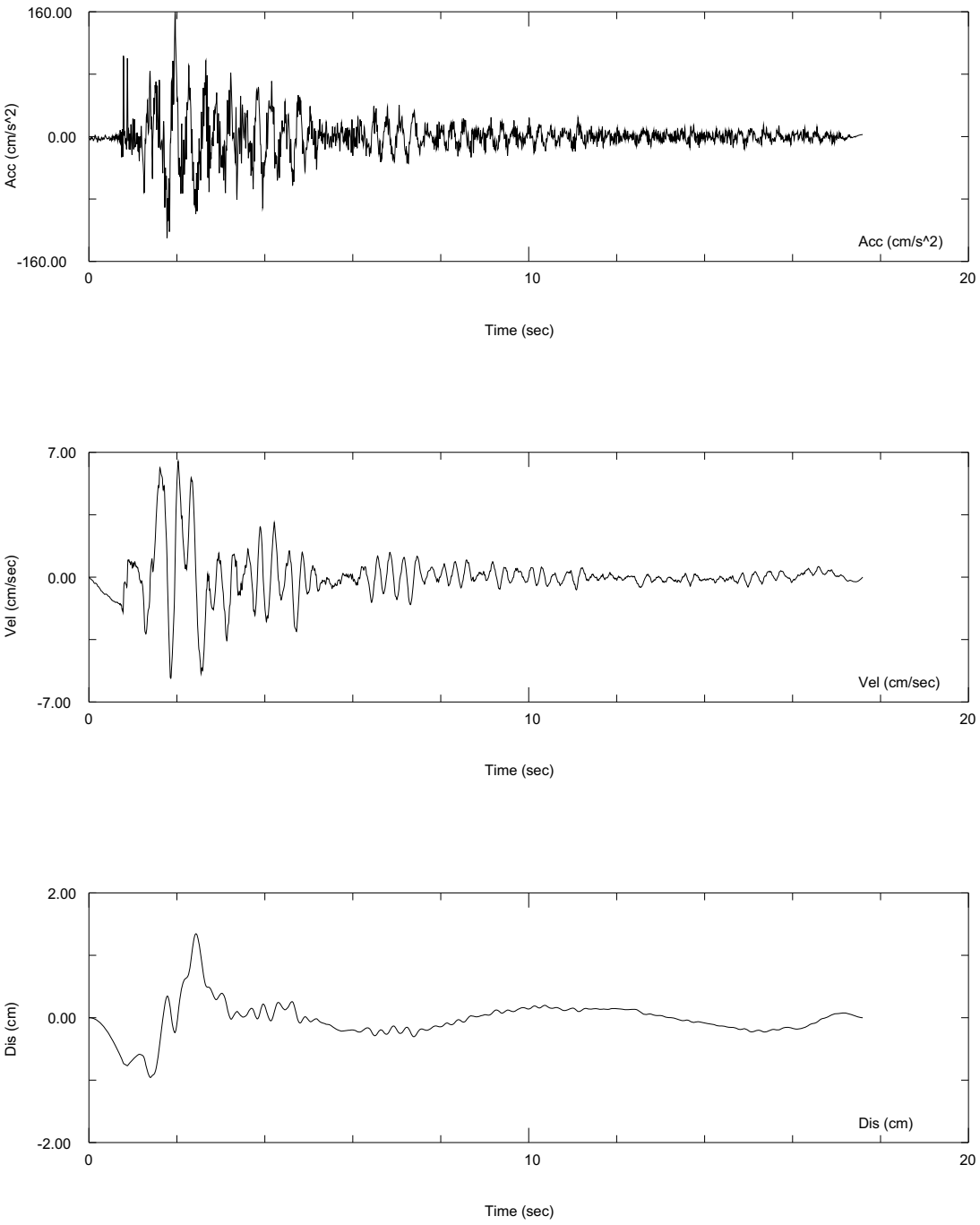

Source: adapted from Kinemetrics (2011)(Reference 2.5-279)

NAPS COL 2.0-27-A
NAPS ESP VAR 2.0-4

Figure 2.5.2-209 Processed Acceleration, Velocity, and Displacement Time Histories for the M 5.8 Mineral earthquake from the Unit 1 from Containment Operating Deck Station (CW018) for Channel 2, V(ertical)-Component

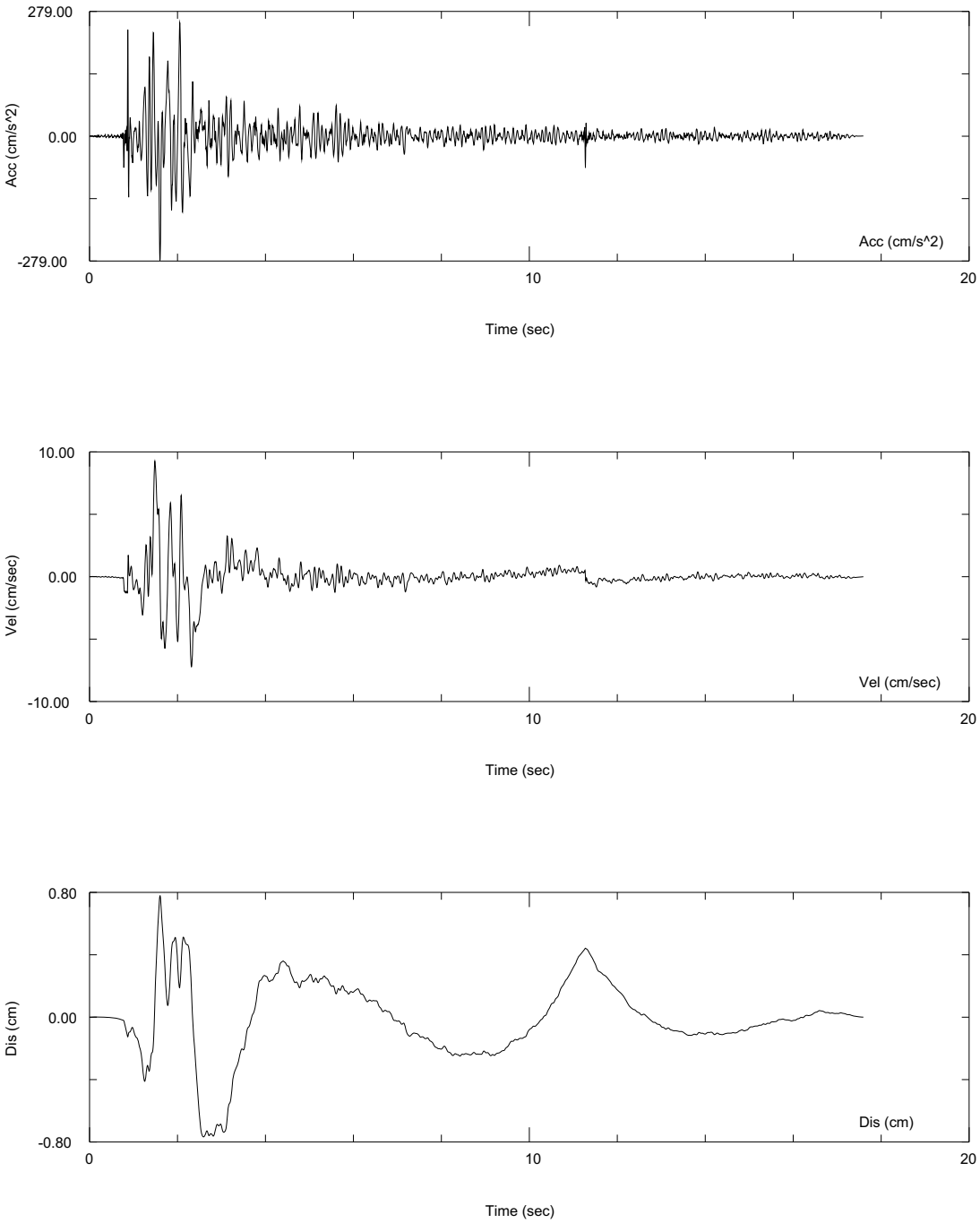

Source: adapted from Kinemetrics (2011)(Reference 2.5-279)

NAPS COL 2.0-27-A
NAPS ESP VAR 2.0-4

Figure 2.5.2-210 Processed Acceleration, Velocity, and Displacement Time Histories for the M5.8 Mineral Earthquake from the Unit 1 from Containment Operating Deck Station (CW018) for Channel 3, T(ransverse)-Component

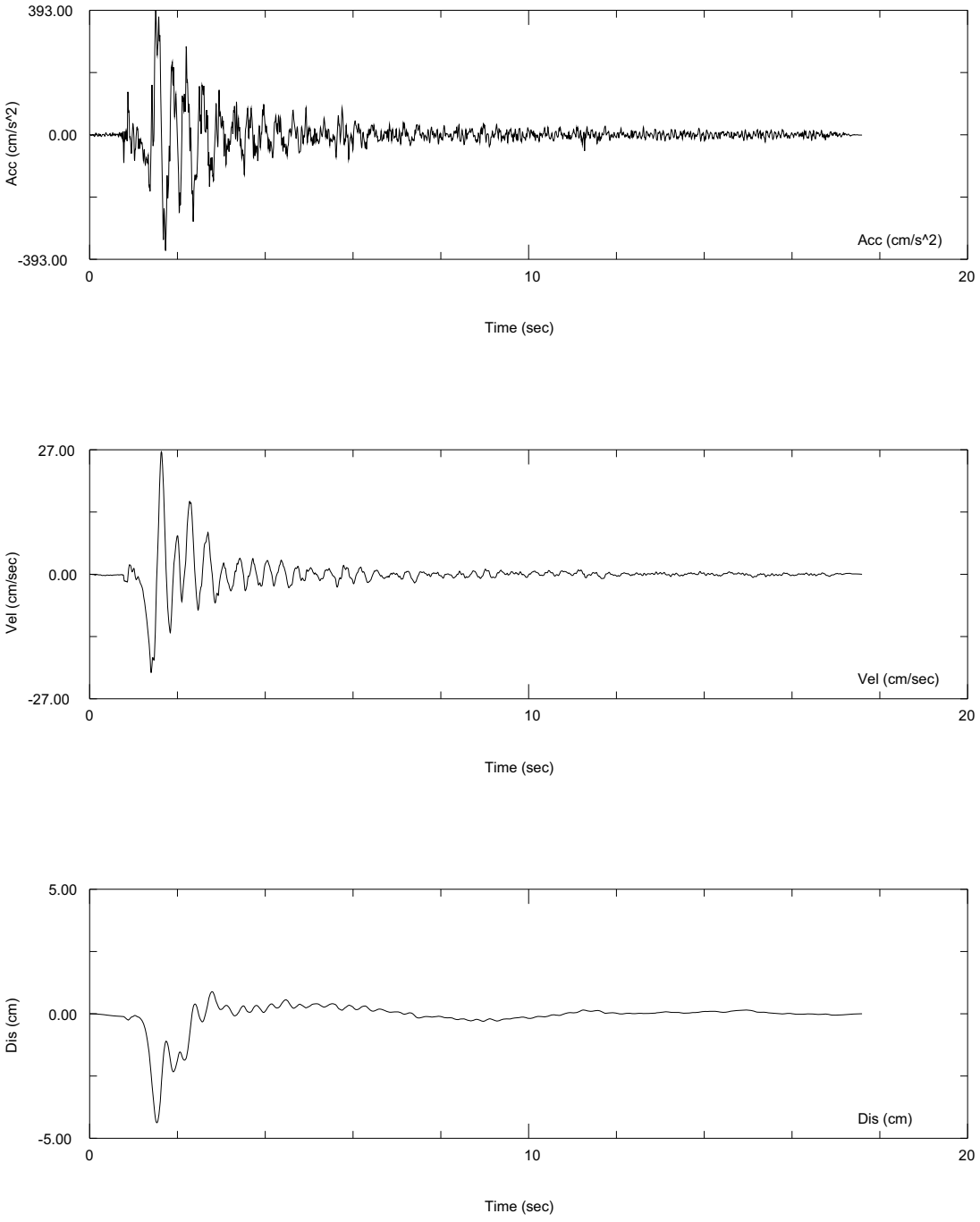

Source: adapted from Kinemetrics (2011)(Reference 2.5-279)

NAPS COL 2.0-27-A
NAPS ESP VAR 2.0-4

Figure 2.5.2-211 Master Logic Tree for the Conceptual Approach of the CEUS SSC Model, Taken from Figure H-2-1 of the CEUS SSC Report (Reference 2.5-223)

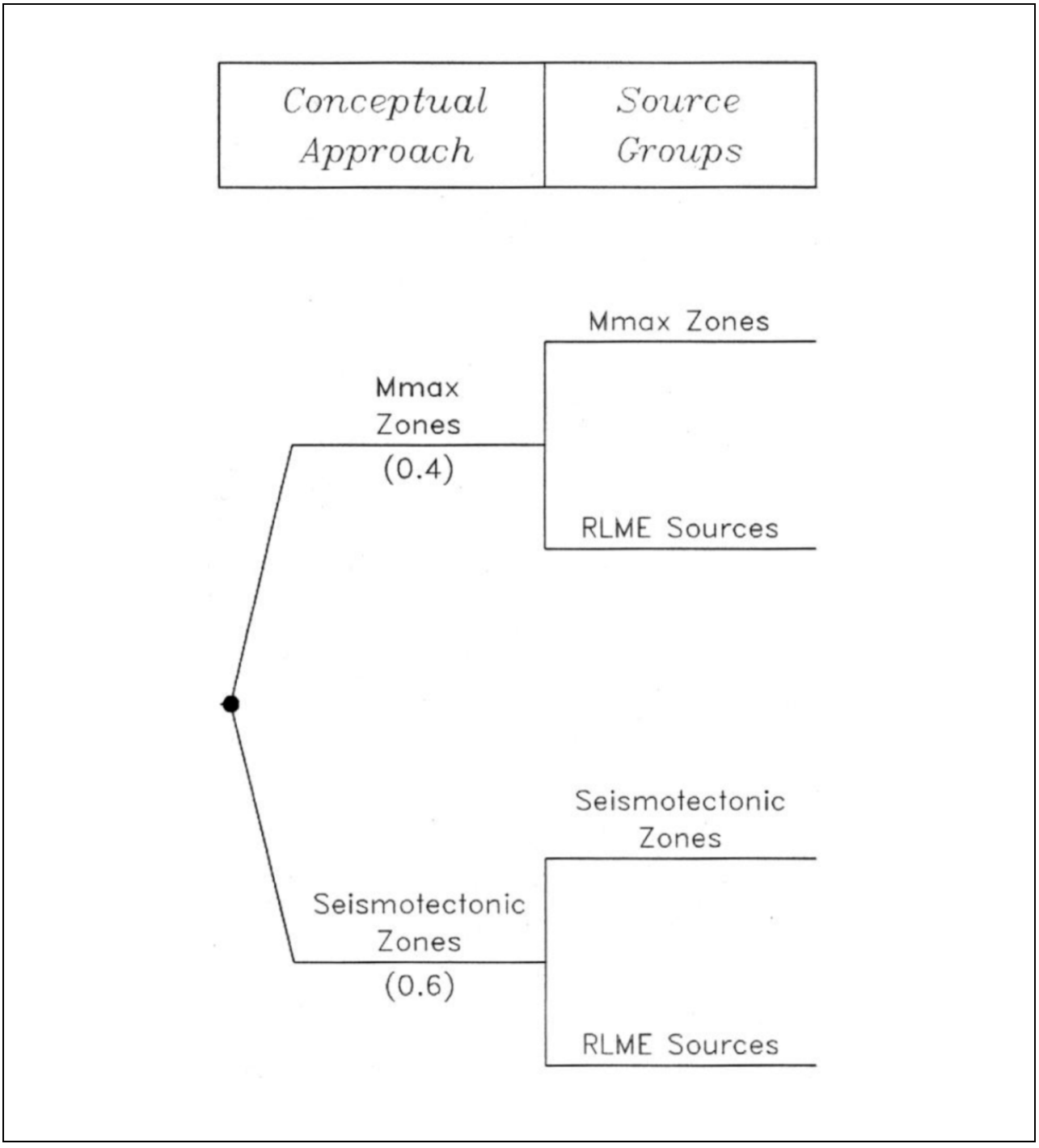

BASIS: NEW

NAPS COL 2.0-27-A
NAPS ESP VAR 2.0-4

Figure 2.5.2-212 CEUS SSC Mmax Zones

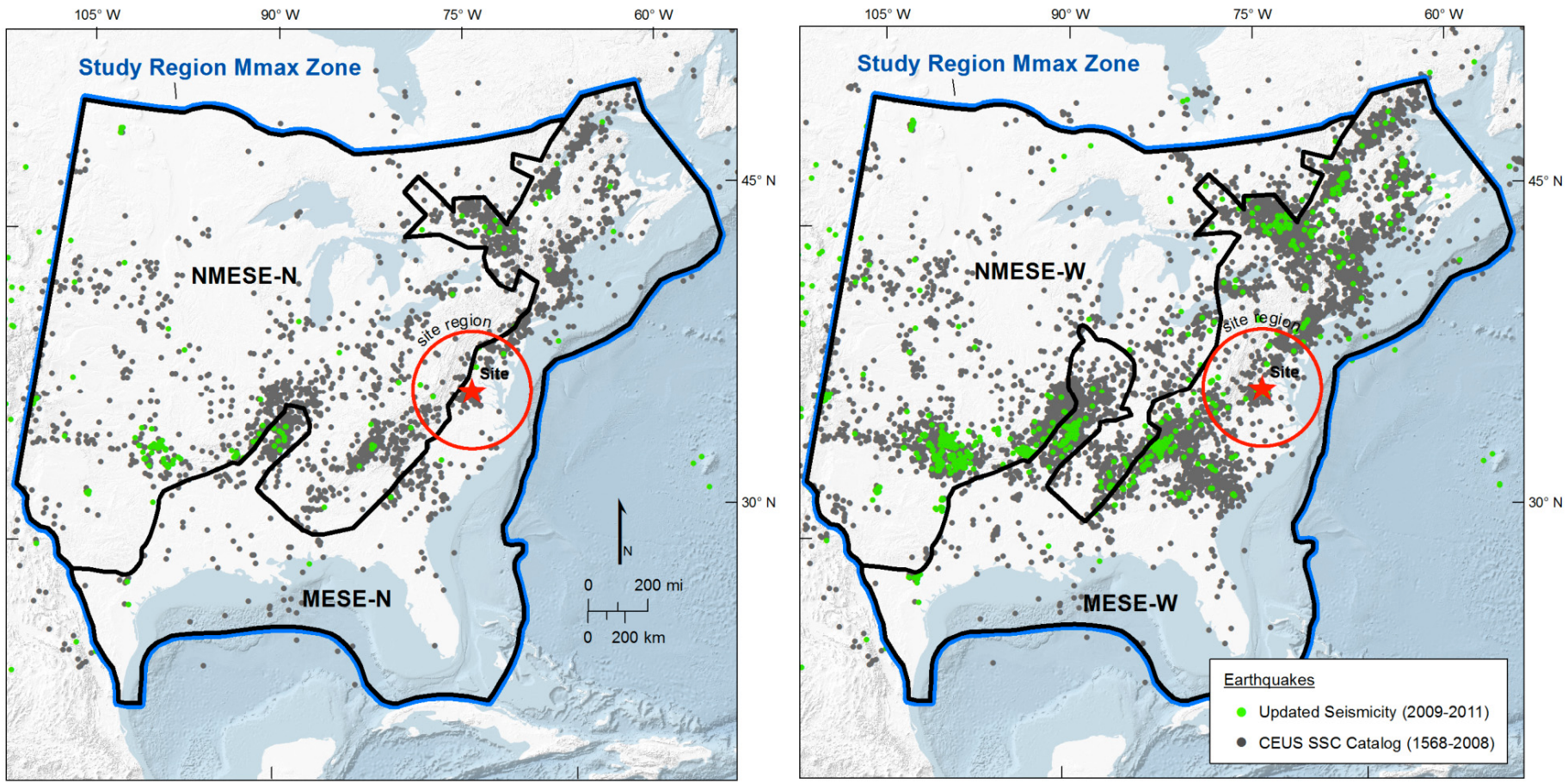

NOTE: MESE-N and NMESE-N geometries (left panel) modified after Figure 6.2-1 of the CEUS SSC Report (Reference 2.5-223). MESE-W and NMESE-W geometries (right panel) modified after Figure 6.2-2 of the CEUS SSC Report (Reference 2.5-223). The Study Region Mmax zone encompasses both the MESE and NMESE zones. Earthquake locations from the CEUS SSC earthquake catalog (Reference 2.5-223) and the North Anna 3 project catalog update. Mmax zone definitions are provided in Table 2.5.2-206 and discussed in Section 2.5.2.2.2. Independent events of E[**M**] ≥ 2.9 are plotted in the left panel, mainshocks and dependent events of E[**M**] ≥ 2.2 are in the right panel.

BASIS: NEW

NAPS COL 2.0-27-A
NAPS ESP VAR 2.0-4

Figure 2.5.2-213 CEUS SSC Logic Tree Showing the Full Characterization of Mmax Zones, Modified After Figure H-3-1 of the CEUS SSC Report

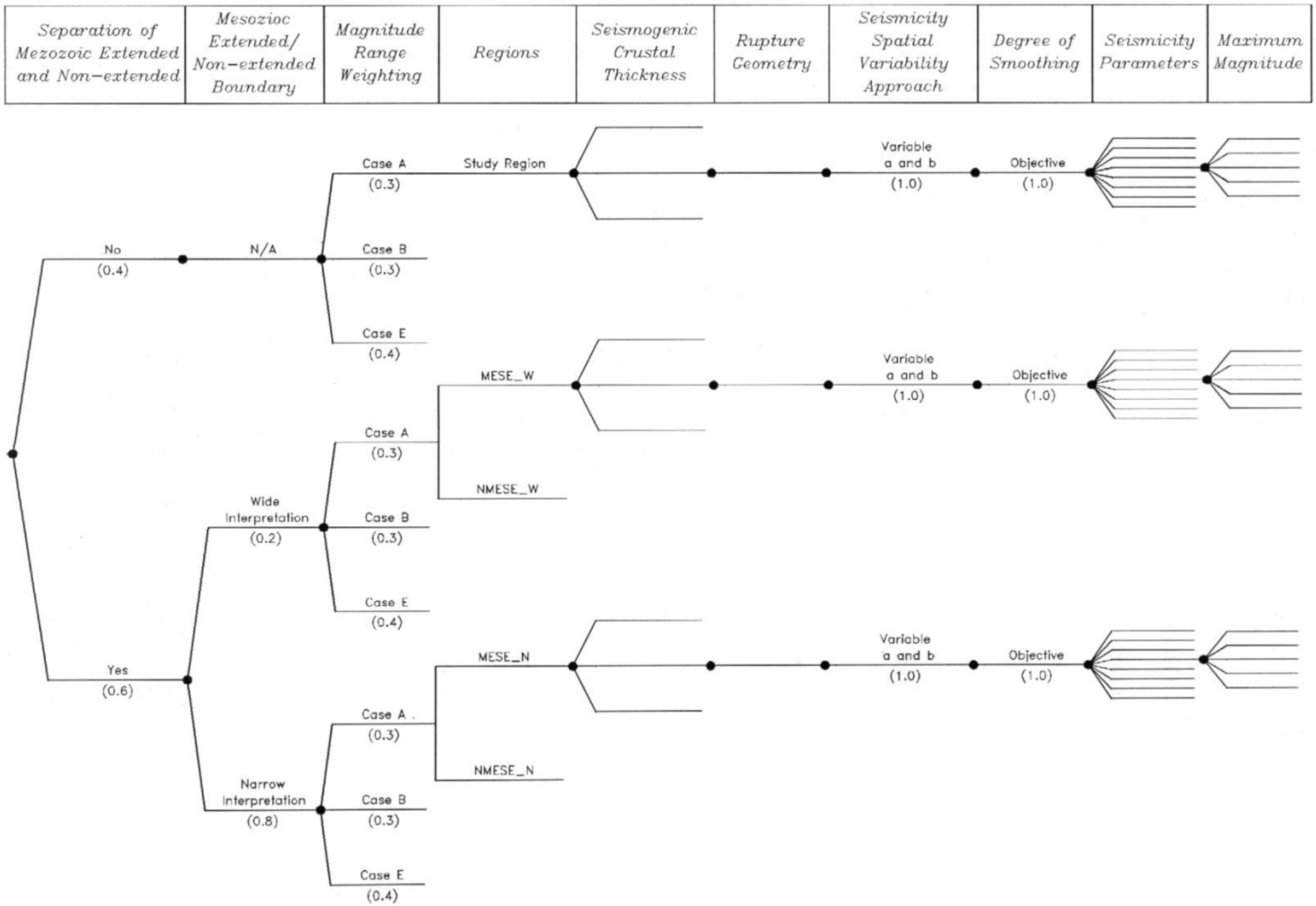

BASIS: NEW

NAPS COL 2.0-27-A
NAPS ESP VAR 2.0-4

Figure 2.5.2-214 CEUS SSC Seismotectonic Zones – "Narrow" Versions

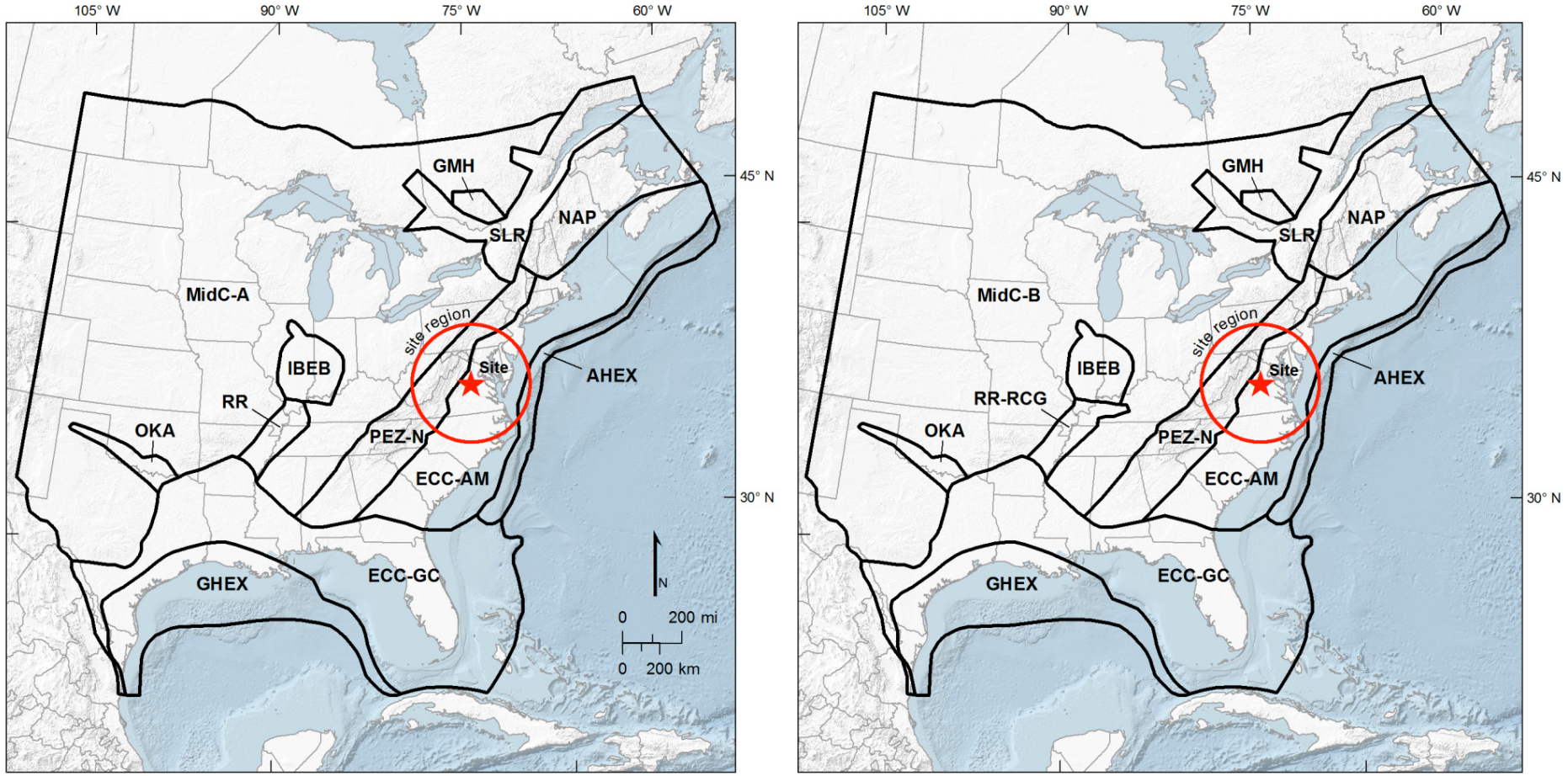

NOTE: Depiction of PEZ-N with MidC-A and Reelfoot Rift (RR) in left panel modified after Figure 7.1-1 of the CEUS SSC Report (Reference 2.5-223). Depiction of PEZ-N with MidC-B and Rough Creek Graben (RR-RCG) in right panel modified after Figure 7.1-2 of the CEUS SSC Report (Reference 2.5-223).

BASIS: NEW

NAPS COL 2.0-27-A
NAPS ESP VAR 2.0-4

Figure 2.5.2-215 CEUS SSC Seismotectonic Zones – "Wide" Versions

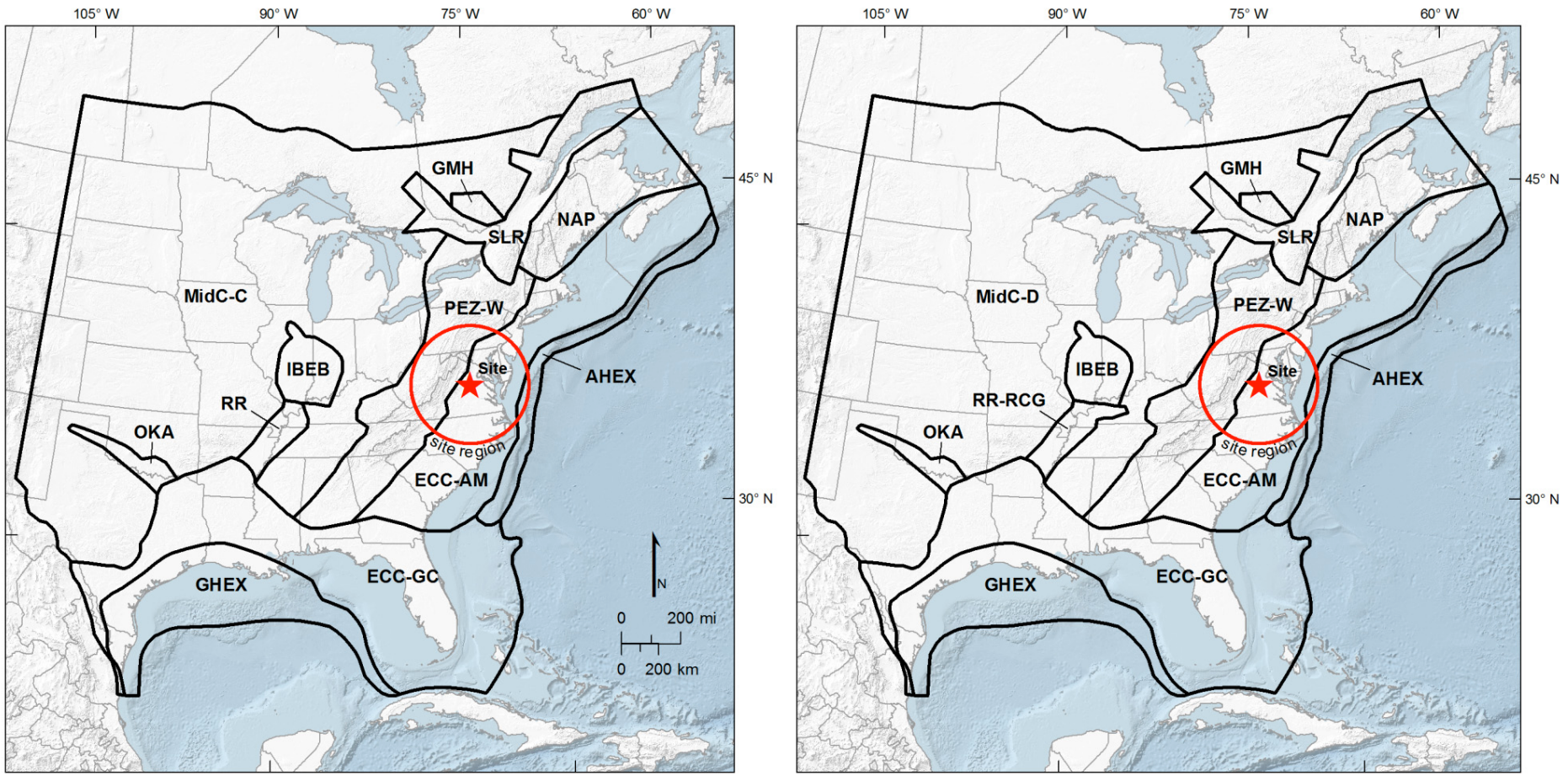

NOTE: Depiction of PEZ-W with MidC-C and Reelfoot Rift (RR) in left panel modified after Figure 7.1-3 of the CEUS SSC Report (Reference 2.5-223). Depiction of PEZ-W with MidC-D and Rough Creek Graben (RR-RCG) in right panel modified after Figure 7.1-4 of the CEUS SSC Report (Reference 2.5-223).

BASIS: NEW

NAPS COL 2.0-27-A
NAPS ESP VAR 2.0-4

Figure 2.5.2-216 CEUS SSC Logic Tree Showing the Characterization of Seismotectonic Zones (continued in Figure 2.5.2-217), Modified After Figure H-4-1(a) of the CEUS SSC Report

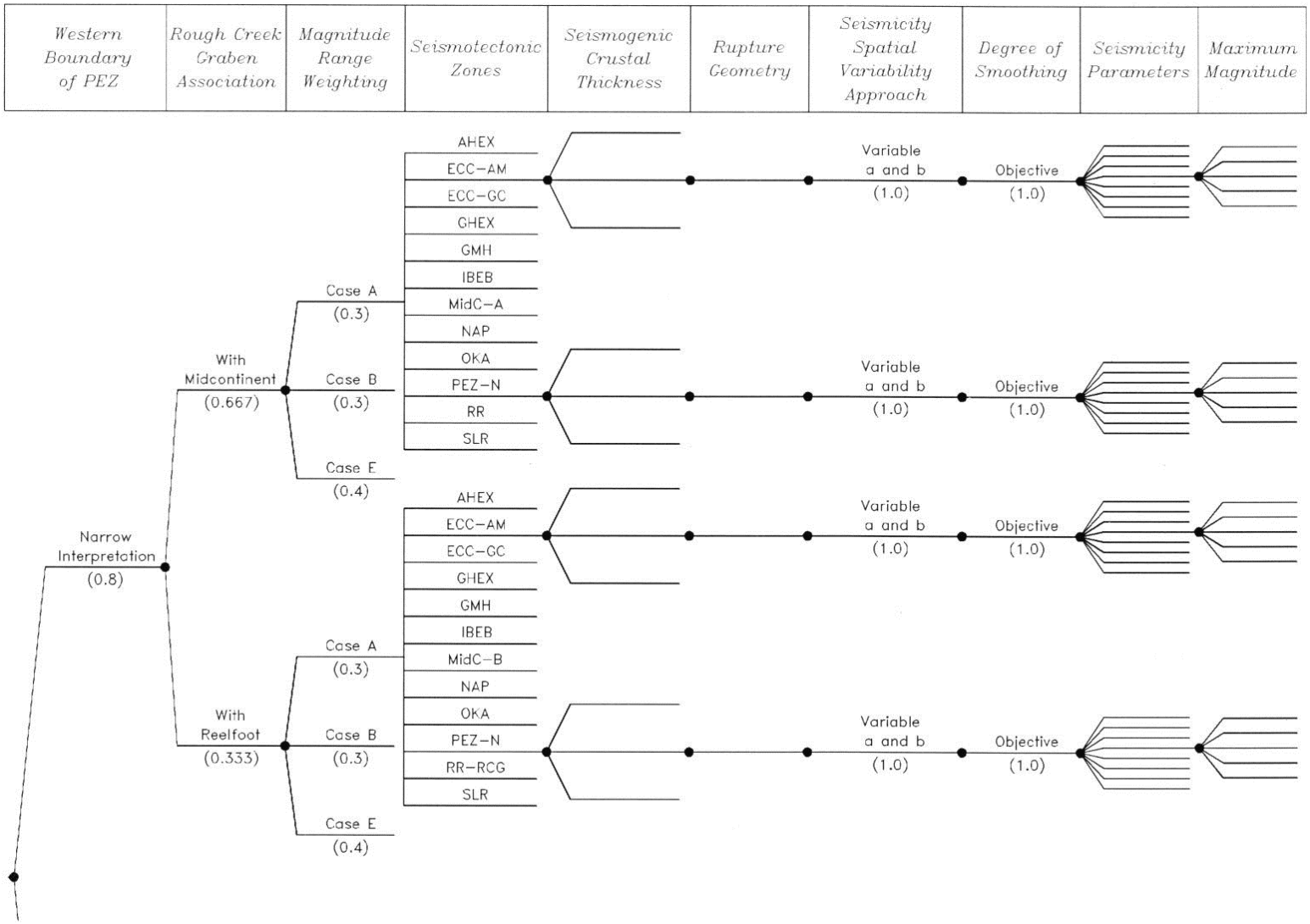

BASIS: NEW

NAPS COL 2.0-27-A
NAPS ESP VAR 2.0-4

Figure 2.5.2-217 CEUS SSC logic tree showing the characterization of seismotectonic zones (continued from Figure 2.5.2-216), modified after Figure H-4-1(b) of the CEUS SSC Report

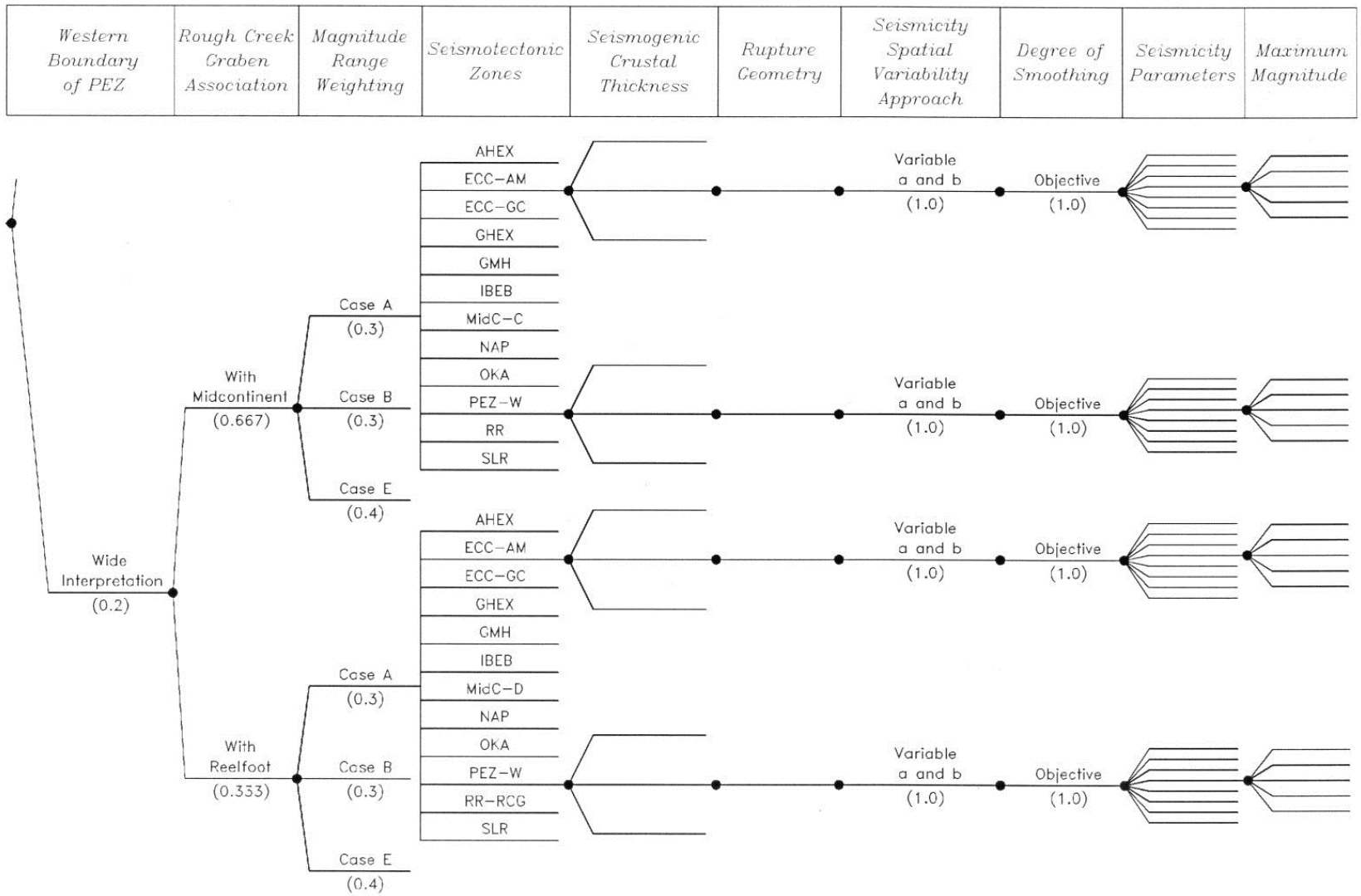

BASIS: NEW

NAPS COL 2.0-27-A
NAPS ESP VAR 2.0-4

Figure 2.5.2-218 RLME Sources Defined in the CEUS SSC Model, Modified After Figure 6.1-1 of the CEUS SSC Report

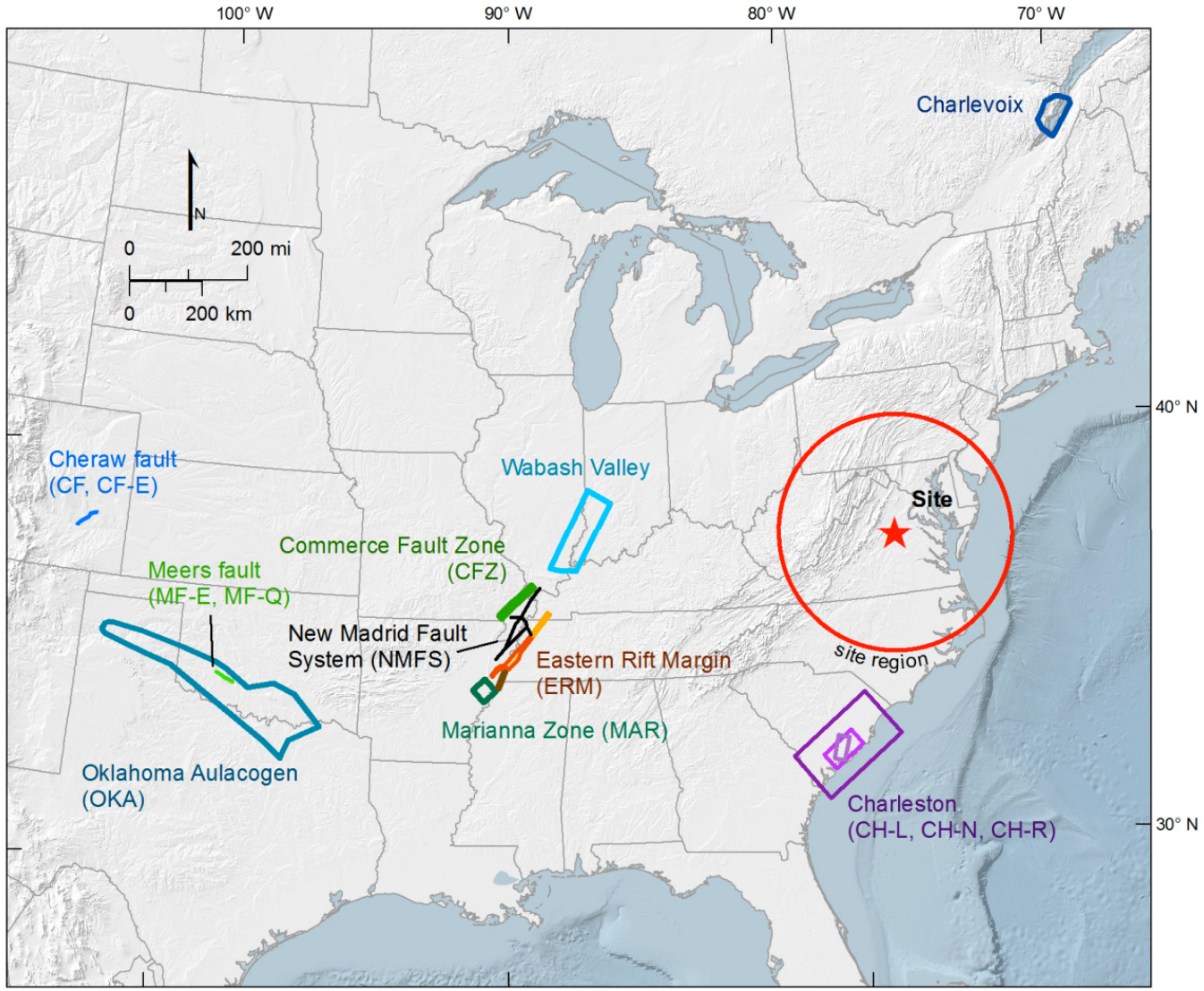

BASIS: NEW

NAPS COL 2.0-27-A
NAPS ESP VAR 2.0-4

Figure 2.5.2-219 CEUS SSC Model Mmax Zones in the Region of the North Anna Site

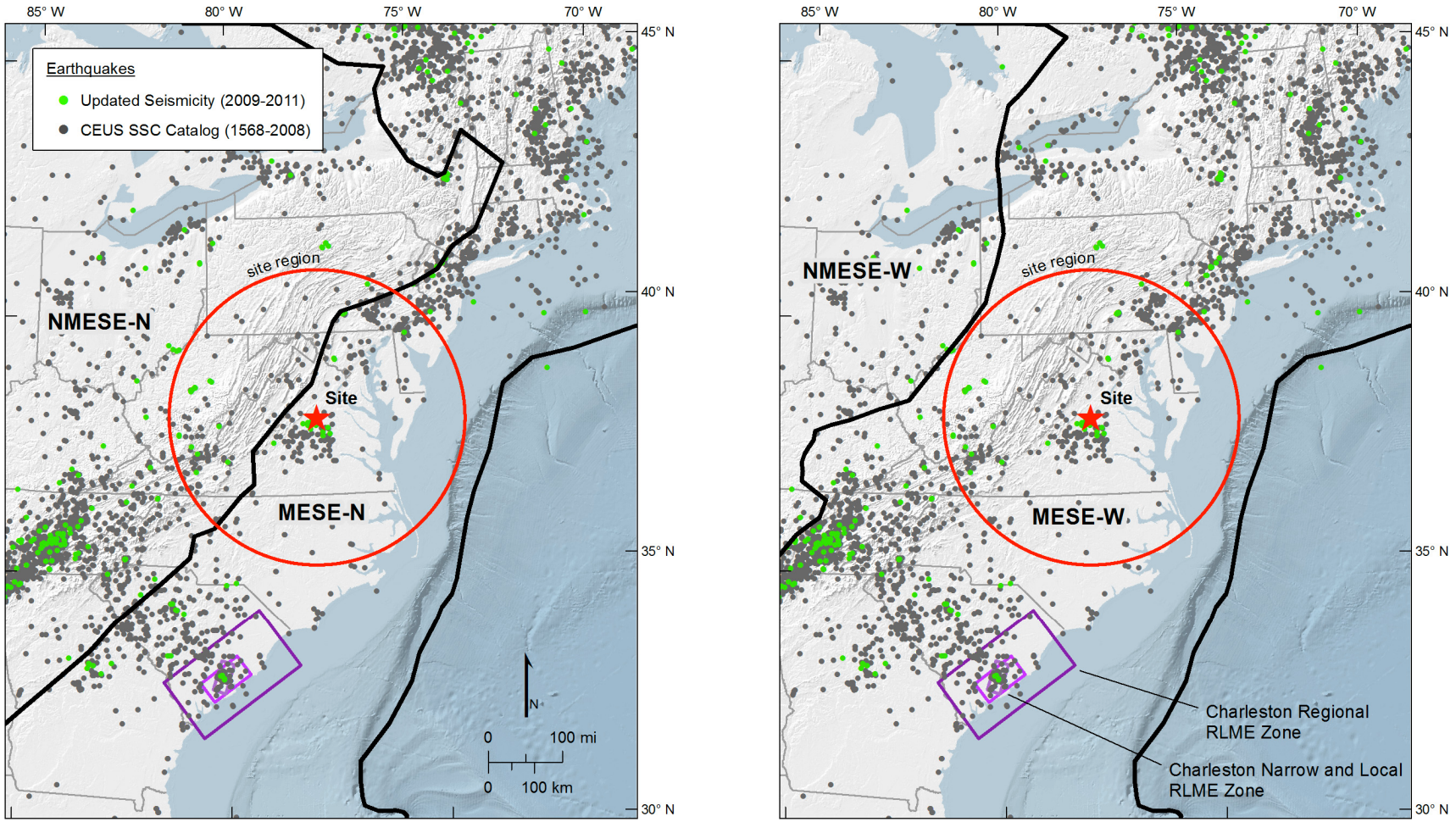

NOTE: MESE-N and NMESE-N geometries (left panel) modified after Figure 6.2-1 of the CEUS SSC Report (Reference 2.5-223). MESE-W and NMESE-W geometries (right panel) modified after Figure 6.2-2 of the CEUS SSC Report (Reference 2.5-223). The Study Region Mmax zone encompasses the both the MESE and NMESE zones. Earthquakes from the CEUS SSC earthquake catalog (Reference 2.5-223) and the North Anna 3 project catalog update include mainshocks and dependent events of E[**M**] ≥ 2.2.

BASIS: NEW

NAPS COL 2.0-27-A
NAPS ESP VAR 2.0-4

Figure 2.5.2-220 The CEUS SSC Model Seismotectonic Zones in the Region of the North Anna Site

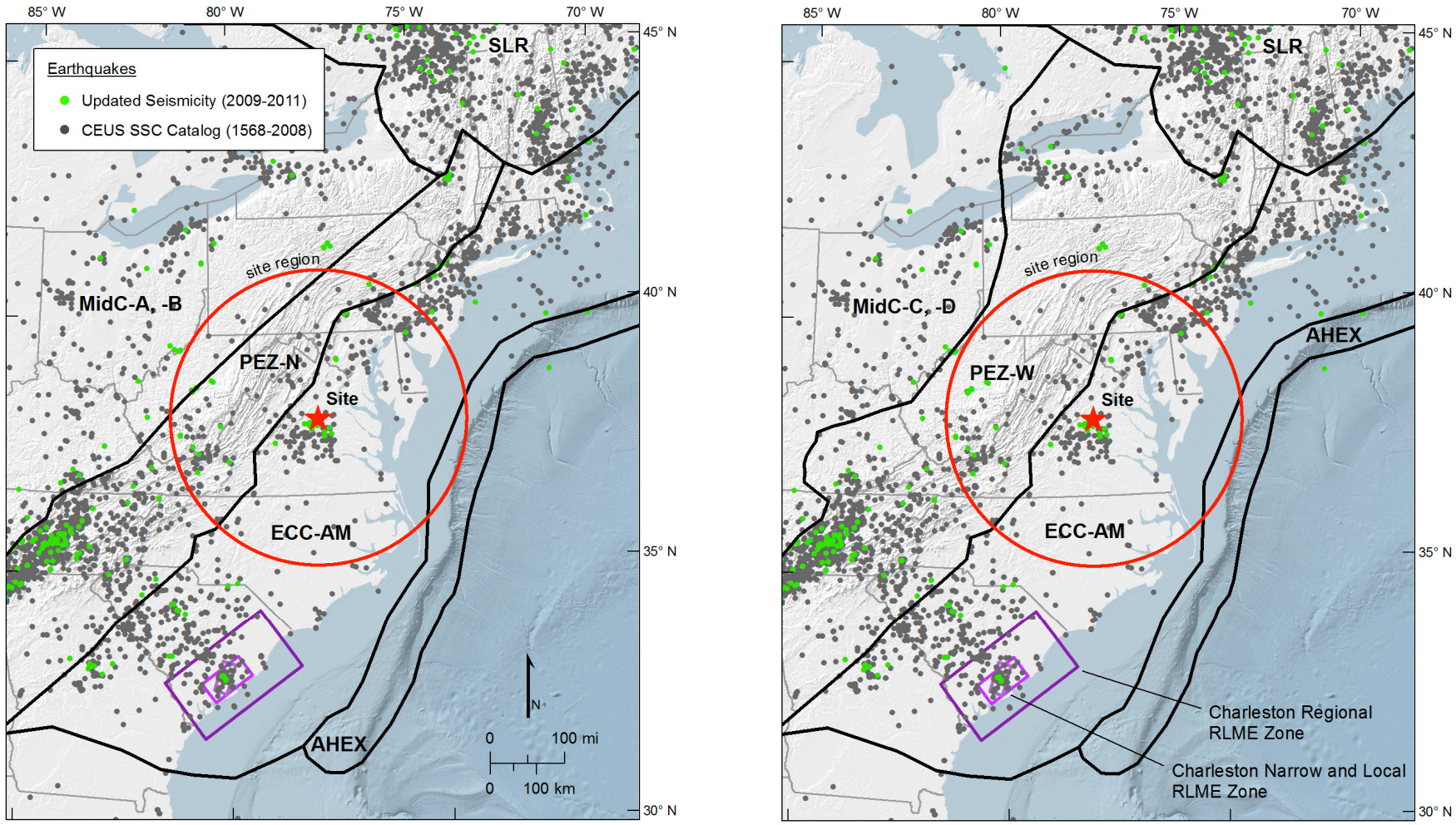

NOTE: Depiction of PEZ-N with MidC in left panel modified after Figure 7.1-1 of the CEUS SSC Report (Reference 2.5-223); PEZ-W with MidC in right panel modified after Figure 7.1-3 of the CEUS SSC Report (Reference 2.5-223). Earthquakes from the CEUS SSC earthquake catalog (Reference 2.5-223) and the North Anna 3 project catalog update include mainshocks and dependent events of E[**M**] ≥ 2.2.

BASIS: NEW

NAPS COL 2.0-27-A
NAPS ESP VAR 2.0-4

Figure 2.5.2-221 Bouguer Gravity (Left Panel) and Magnetic (Right Panel) Anomalies of the Eastern United States, Taken from the GIS Database of the CEUS SSC Report

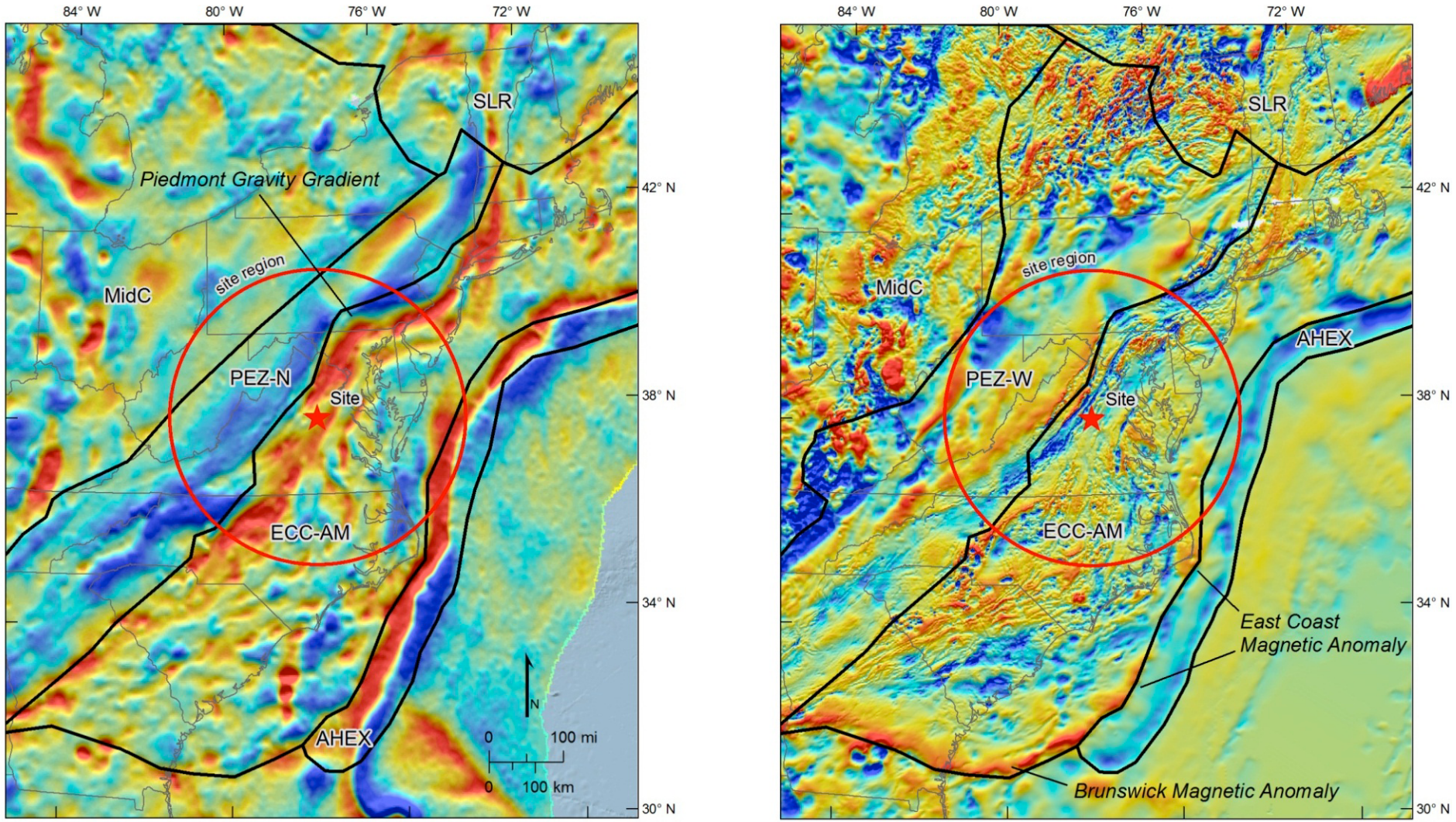

BASIS: NEW

NAPS COL 2.0-27-A
NAPS ESP VAR 2.0-4

Figure 2.5.2-222 Seismic Zones Within or Near the 200-Mile Project Site Region

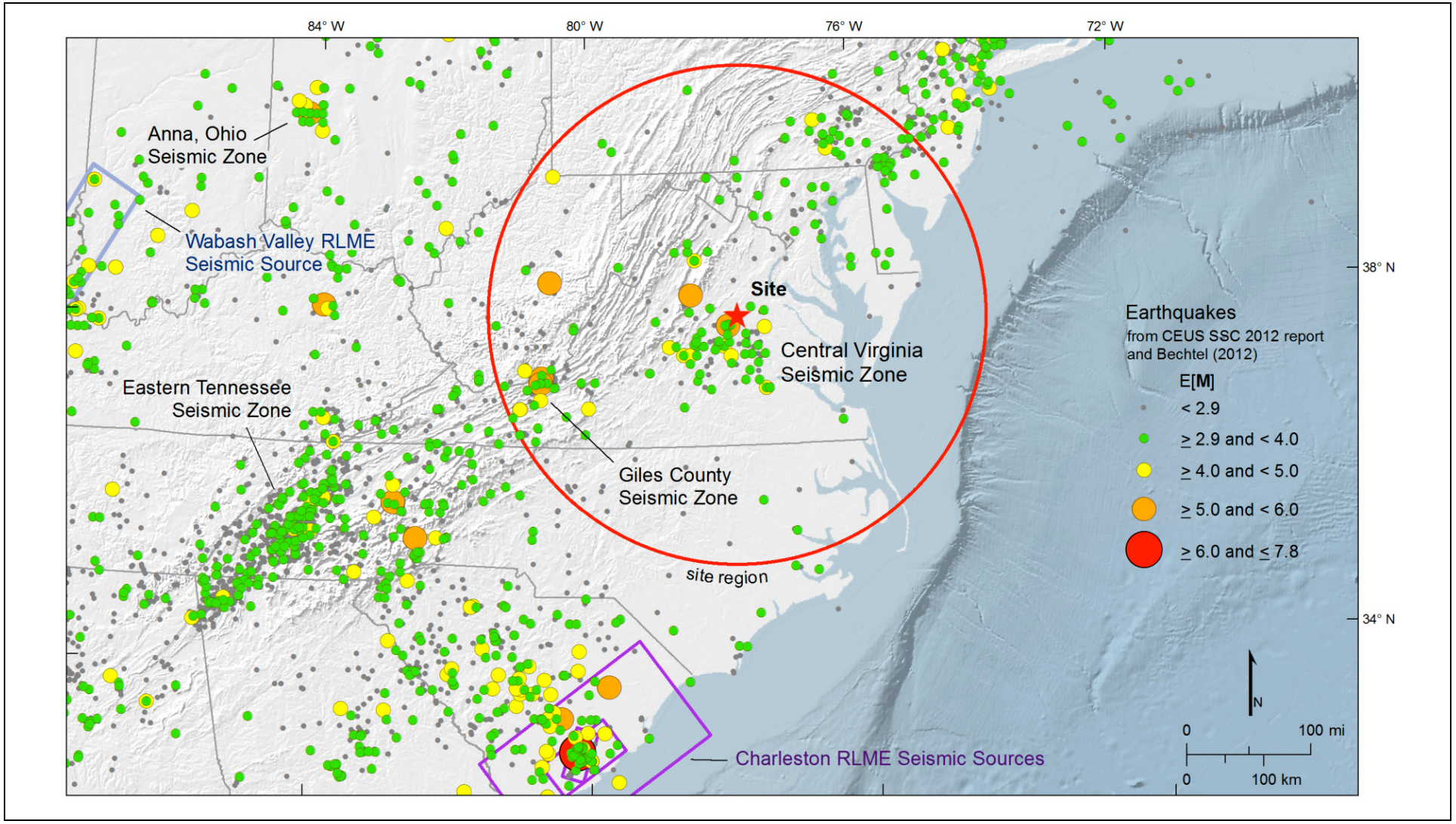

NOTE: Seismicity from the project earthquake catalog, including mainshocks and dependent events of E[**M**] ≥ 2.2, scaled by color and size according to magnitude (E[**M**]). The Charleston and Wabash Valley seismic zones are also shown for reference (Reference 2.5-223).

BASIS: NEW

NAPS COL 2.0-27-A
NAPS ESP VAR 2.0-4

Figure 2.5.2-223 Alternative Source Geometries of the New Madrid Fault System (NMFS) RLME (Left Panel, from Figure 6.1-2b of Reference 2.5-223) and Charleston RLME (Right Panel, from Figure 6.1.2-5a of Reference 2.5-223)

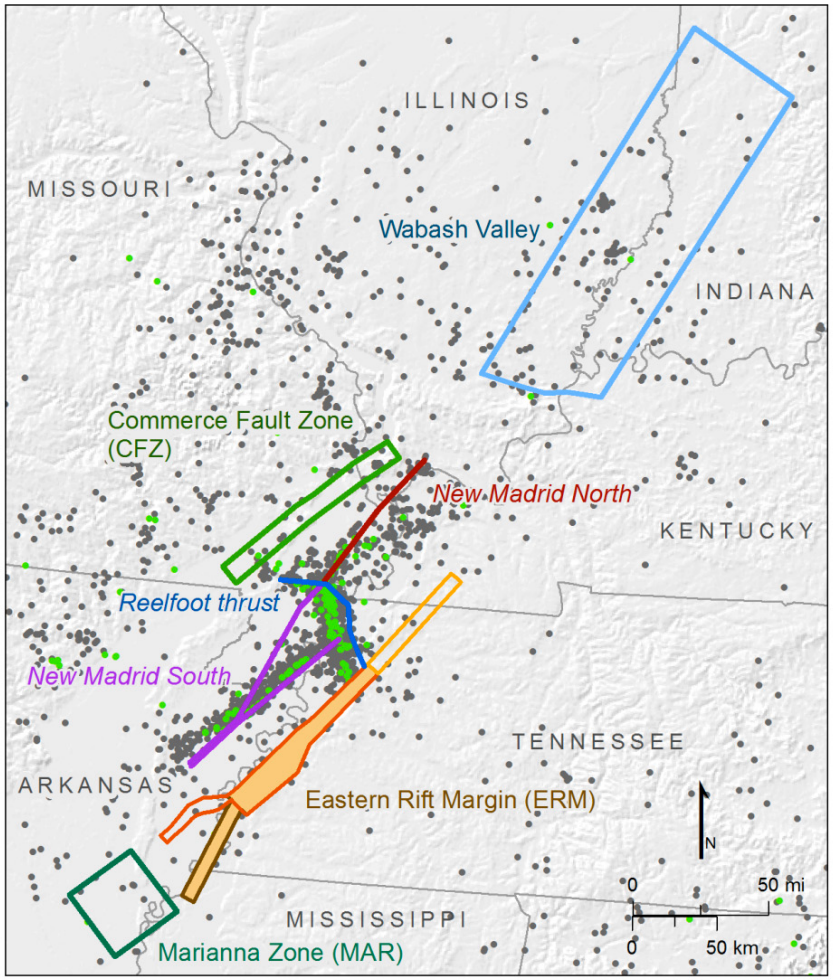

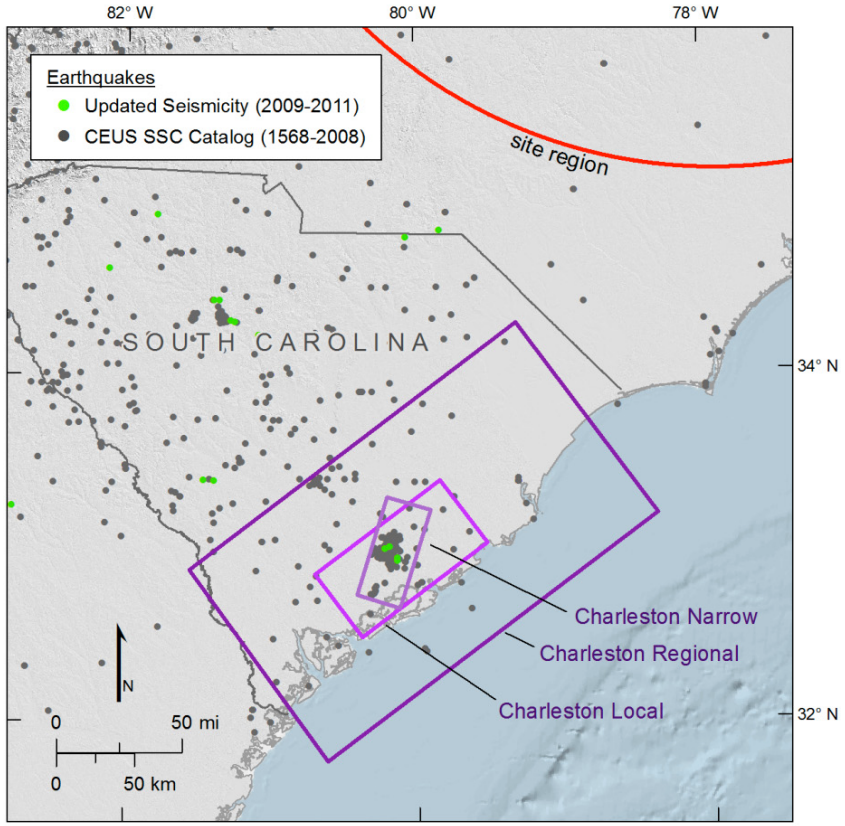

NOTE: Seismicity includes mainshocks and dependent events of E[**M**] ≥ 2.2. The CFZ, ERM, and MAR sources (left panel) are not significant contributors to hazard for the North Anna site and are not included in the hazard calculation.

NAPS COL 2.0-27-A
NAPS ESP VAR 2.0-4

Figure 2.5.2-224 CEUS SSC Logic Tree Showing the Full Characterization of the Charleston RLME Source, Modified After Figure H-5.2-1(a) of the CEUS SSC Report

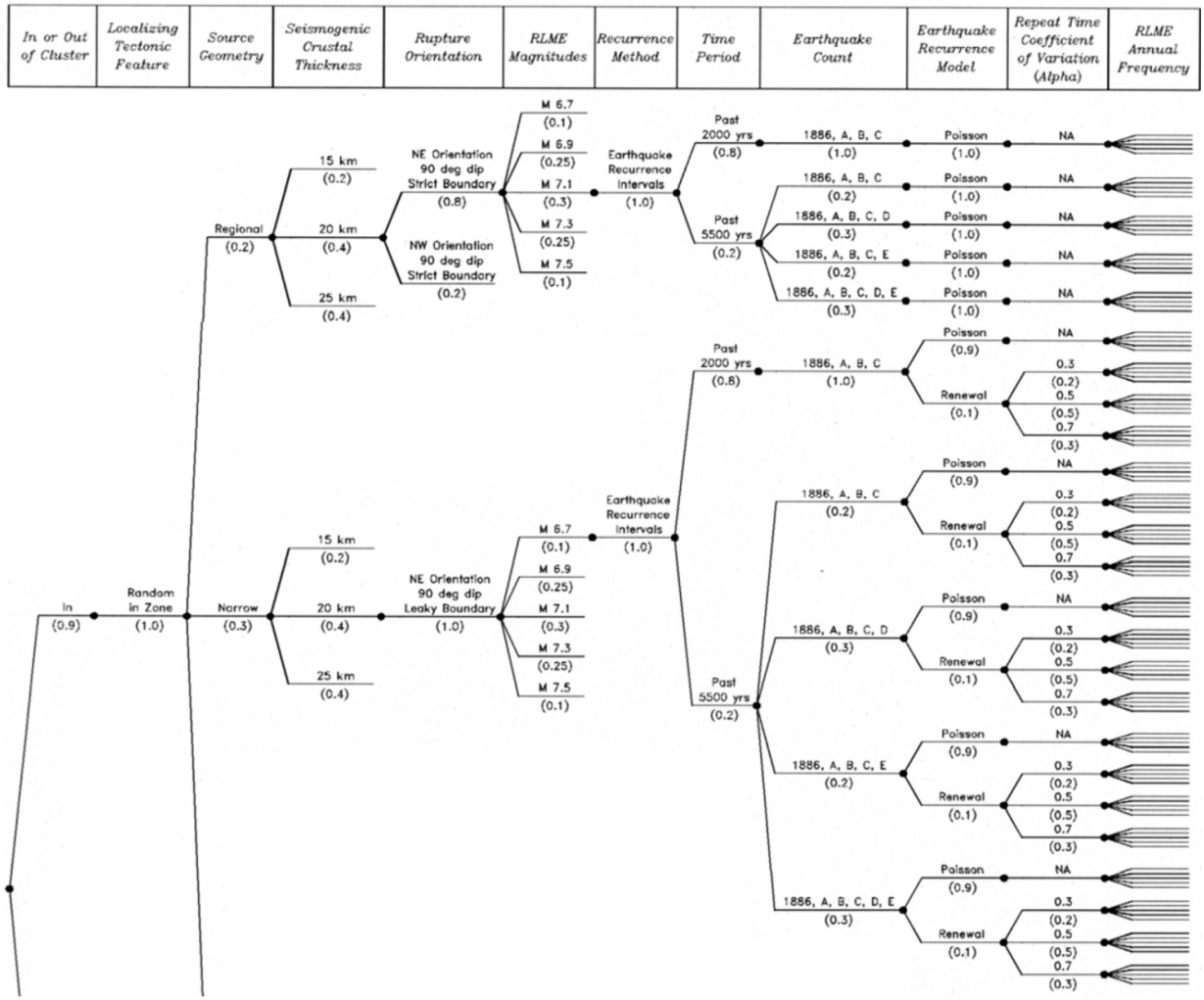

NOTES: For RLME annual frequency information, see Tables H-5.2-2 through H-5.2-21 from the CEUS SSC Report.

The Seismogenic Crustal Thicknesses (depths) are updated values from what was published in the CEUS SSC Report, as indicated in the June 27, 2012 Updates file on the CEUS SSC Report web site (http://www.ceus-ssc.org). While these values are consistent with the discussion in published CEUS SSC Report, Section 6.1.2.3, they differ slightly from the values in the published CEUS SSC Report, Table 5.4-2, shown in Table 2.5.2-210. The depth values in Table 2.5.2-210 were used in the PSHA for this project site. With the distance of the Charleston source to the project site, the difference in the PSHA results due to these differences in depths is negligible.

BASIS: NEW

NAPS COL 2.0-27-A
NAPS ESP VAR 2.0-4

Figure 2.5.2-225 CEUS SSC Logic Tree Showing the Full Characterization of the Charleston RLME Source, Modified After Figure H-5.2-1(b) of the CEUS SSC Report

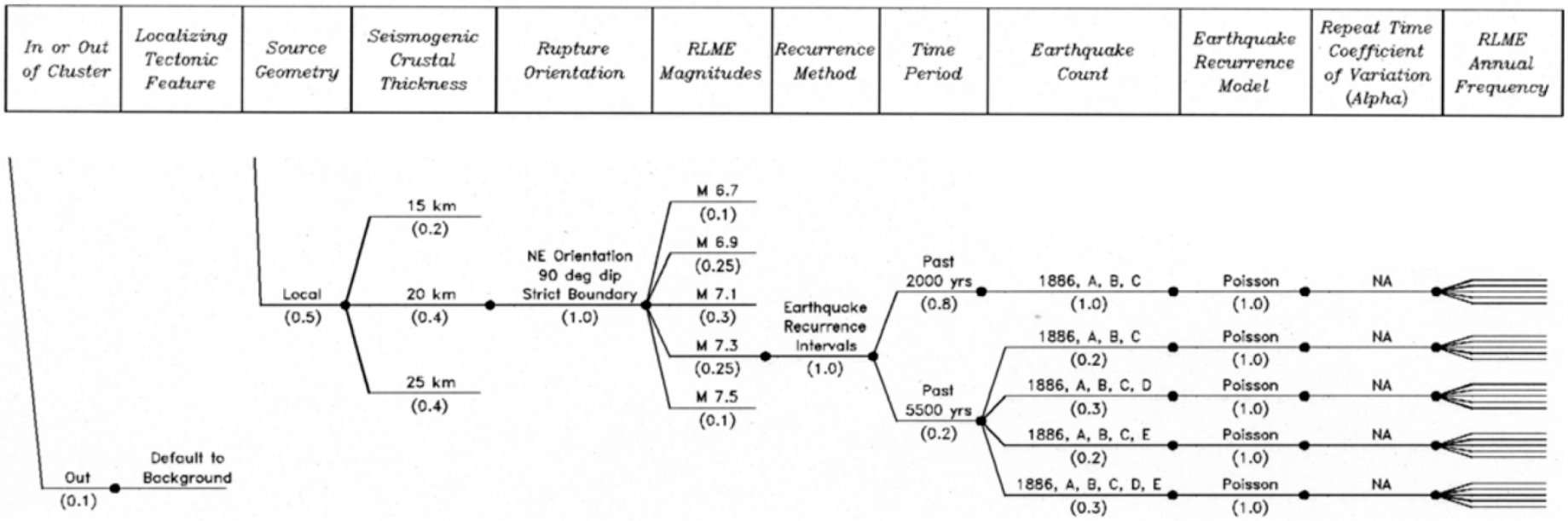

NOTE: For RLME annual frequency information, see Tables H-5.2-2 through H-5.2-21 from the CEUS SSC Report.
See NOTES for Figure 2.5.2-224.